Geo-Multiphysics Models for Gas Energy Extraction/Storage: The Role of Microbial Activities

By

Qi Gao

B. Eng. & M. Eng.

This thesis is presented for the degree of

Doctor of Philosophy

of

The University of Western Australia

School of Engineering

Oil and Gas Engineering

2024

Thesis Declaration

I, Qi Gao, certify that:

This thesis has been substantially accomplished during enrolment in this degree.

This thesis is my own work and does not contain any material previously published or written by another person, except where due reference has been made in the text or Authorship Declaration.

This thesis does not contain material which has been submitted for the award of any other degree or diploma in my name, in any university or other tertiary institution.

In the future, no part of this thesis will be used in a submission in my name, for any other degree or diploma in any university or other tertiary institution without the prior approval of The University of Western Australia and where applicable, any partner institution responsible for the joint-award of this degree.

This thesis does not violate or infringe any copyright, trademark, patent, or other rights whatsoever of any person.

Signature: 

Date: 03/09/2024

Abstract

Most subsurface formations are not life-free environments and harbor a variety of microbial species. When nutrients/substrates are added into these formations during gas energy extraction/storage operations, microbial growth and associated activities can be stimulated. The growth of microbes and their activities not only can influence the transport properties of the formations through occupying a fraction of pore space, but also can catalyze a series of biochemical reactions within the hosting rock. How the changes induced by microbes affect gas energy extraction/storage depends on the complex interactions among hydraulic, mechanical, chemical and biological processes. In this study, the coupled hydraulic-mechanical-chemical-biological processes are defined as "geo-multiphysics". Therefore, the goal of this research is to advance the understanding on geo-multiphysics for gas energy extraction/storage in subsurface formations with a focus on the role of microbial activities. In the following, the achievements of this research are summarized:

(1) **Development of a Generic Geo-Multiphysics Model for Gas Energy Extraction/Storage**. In this model, various processes including rock deformation, fluid flow, reactive transport and microbial activities are captured. These hydraulic-mechanical-chemical-biological processes are linked together through rock porosity and permeability models. According to our review papers published in Fuel (Gao et al., 2022) and Energy & Fuels (Gao et al., 2023), these porosity and permeability models are commonly defined as a function of effective stress and gas sorption-induced strains while in this research they are extended to include the effects of various microbe-induced changes like pore/fracture bioclogging and minerals dissolution/precipitation. Integrating the generic geo-multiphysics model

with porosity and permeability models as well as initial and boundary conditions, the role of microbial activities on gas energy extraction/storage can be quantified.

(2) **Geo-Multiphysics Model for Biogenic Methane Generation and Extraction from Coal Seams**. The generic geo-multiphysics model is tailored to the case of biogenic methane generation and extraction from coal seams and this work has been published in Geoenergy Science and Engineering (Gao et al., 2023). In this work, the specific porosity and permeability models that consider the impacts of effective stress, fracture bioclogging and coal solubilization are integrated with the modified geo-multiphysics model. This integration provides the basis for quantifying the role of microbial activities on biogenic methane generation and extraction. Applying this model and through numerical simulation, it can be found that microbial degradation of organic components in coal not only can aid the generation of additional biogenic methane in coal seams, but also in the long term can greatly enhance the magnitude of coal permeability which in turn further improves biogenic methane extraction performance.

(3) **Geo-Multiphysics Model for Underground Hydrogen Storage in Aquifers**. The generic geo-multiphysics model is tailored to the case of underground hydrogen storage in aquifers and this work has been published in International Journal of Hydrogen Energy (Gao et al., 2024). In this work, the specific porosity and permeability models that consider the impacts of effective stress, pore bioclogging and minerals dissolution/precipitation are integrated with the modified geo-multiphysics model. This integration provides the basis for quantifying the role of microbial activities during hydrogen injection and withdrawal in aquifers. Applying this model and through numerical simulation, it can be found that the existence of iron-reduction bacteria can lead to the degradation of hydrogen recovery efficiency

but only the initial few circles of hydrogen injection and withdrawal are negatively influenced mainly because microbial impacts gradually diminish with the dissolution of the mineral Fe_2O_3 in the hosting rock.

Table of Contents

List of Figures

List of Tables

Acknowledgements

It would be impossible to complete this thesis without the following help over the past four years.

First, I would like to express my sincere gratitude to my supervisor, Prof. Jishan Liu, for his support and encouragement during my study at the University of Western Australia (UWA). His approachable nature and professional supervision have made my study at UWA a fruitful and joyful journey. Many of the ideas in this thesis would not be shaped without his guidance.

Then, many thanks to my colleagues at UWA, including Dr. Jie Zeng, Dr. Jianwei Tian, Dr. Wai Li, Dr. Yifan Huang, Dr. Yide Guo, Mr. Chuanzhong Jiang and Mrs. Haiting Huang, for their friendship, generous help and valuable suggestions during my study. The time spent with them at UWA will always be a cherished memory in my life.

I would also like to thank the financial support provided by the Scholarship for International Research Fees China (IRFSC), UWA-CSC HDR Top-Up Scholarship and Overseas Travel Award. It was their support that made my study at UWA possible.

Finally, I would like to thank my parents, Shengguang Gao and Dongling Ma, for their deep understanding and endless love. I would also like to extend my special gratitude to my fiancee, Huiqi Lin, for her trust, encouragement, and unwavering support throughout this journey.

Declaration for Published Works and Works Prepared for Publication

This thesis contains published works and/or works prepared for publication, some of which have been co-authored. The bibliographic details of these works are outlined below:

1. **Gao, Q.** (60%), Liu, J.S. (15%), Huang, Y.F. (5%), Li, W. (5%), Shi, R. (5%), Leong, Y.K. (5%), & Elsworth, D. (5%). A critical review of coal permeability models. Fuel, 2022, 326: 125124. (Appeared in Chapter 2)
2. **Gao, Q.** (75%), Liu, J.S. (15%), Leong, Y.K. (5%), & Elsworth, D. (5%). A review of swelling effect on shale permeability: Assessments and perspectives. Energy & Fuels, 2023, 37(5): 3488-3500. (Appeared in Chapter 2)
3. **Gao, Q.** (65%)**,** Liu, J.S. (15%), Zhao, Y.Y. (5%), Wei, M.Y. (5%), Leong, Y.K. (5%), & Elsworth, D. (5%). A multiphysics model for biogenic gas extraction from coal seams. Geoenergy Science and Engineering, 2023, 228: 212045. (Appeared in Chapter 3)
4. **Gao, Q.** (80%)**,** Liu, J.S. (15%), & Elsworth, D. (5%). Phenomenal study of microbial impact on hydrogen storage in aquifers: A coupled multiphysics modelling. International Journal of Hydrogen Energy, 2024, 79: 883-900. (Appeared in Chapter 4)
5. **Gao, Q.** (70%), Liu, J.S. (15%), Huang, Y.F. (5%), Leong, Y.K. (5%), & Elsworth, D. (5%). A multiphysics model for biogenic gas extraction: The role of bioconversion processes. In: 3rd International Conference on Coupled Processes in Fractured Geological Media: Observation, Modeling and Application. Berkeley, USA, 2022. (Appeared in Chapter 3)
6. **Gao, Q.** (80%)**,** Liu, J.S. (15%), & Elsworth, D. (5%). Impact of microbial clogging on biogenic coalbed methane generation and extraction: A coupled hydraulic-mechanical-chemical-biological modeling. (Ready to submit to Rock Mechanics and Rock Engineering) (Appeared in Chapter 3)

Student signature: [redacted]

Date: 18/09/2024

I, Jishan Liu certify that the student's statements regarding their contribution to each of the works listed above are correct.

As all co-authors' signatures could not be obtained, I hereby authorise inclusion of the co-authored work in the thesis.

Coordinating supervisor signature: [redacted]

Date: 1/10/2024

Nomenclature

a	fracture-matrix transfer shape factor
c	Kozeny constant
c_f	fracture compressibility
c_m	matrix compressibility
c_p	pore compressibility
C_i	concentration of a given dissolved species in water phase
C_m	concentration of microbes in water phase
C_n	concentration of nutrients/substrates in water phase
C_p	concentration of metabolic products in water phase
C_{H_2}	concentration of hydrogen in water phase
$C_{Fe_2O_3}$	concentration of Fe_2O_3 in porous rock
$C_{Fe_3O_4}$	concentration of Fe_3O_4 in porous rock
C_j^s	concentration of a given mineral phase in the rock
d_1	microbial decay rate
D^0	molecular diffusion coefficient of dissolved species in free water
D_i	hydrodynamic dispersion coefficient of a given dissolved species in water phase
D_m	hydrodynamic dispersion coefficient of microbes
D_n	hydrodynamic dispersion coefficient of nutrients
D_p	hydrodynamic dispersion coefficient of metabolic products

D_{H_2}	hydrodynamic dispersion coefficients of dissolved hydrogen
D_i^{dif}	molecular diffusion coefficient of a given dissolved species in water phase
D_i^{dis}	mechanical dispersion coefficient of a given dissolved species in water phase
E	elastic modulus
f_i	body force component
g	net microbial growth rate
g_1	microbial growth rate
g_{1max}	the maximum microbial growth rate
G	shear modulus
H_c	the corrected Henry's constant
k_+	coal solubilization rate constant
k_1	reversible microbial adsorption rate on pore surface
k_2	microbial desorption rate on pore surface
k_3	irreversible microbial adsorption rate on pore surface
k_f	fracture permeability
k_m	matrix permeability
k_{rg}	relative permeability of gas
k_{rw}	relative permeability of water
K	bulk modulus of rock
K_f	bulk modulus of fracture

K_m	bulk modulus of matrix
K_p	bulk modulus of pores
K_s	bulk modulus of grains
K_{fs}	bulk modulus of solid skeleton of fracture
K_{ms}	bulk modulus of solid skeleton of matrix
$K_{m/s}$	microbial concentration at which iron reduction reaction rate reaches half of its maximum value
$K_{n/s}$	nutrients concentration at which microbial growth rate reaches half of its maximum value
$K_{bc/s}$	bioclogged fraction of porosity at which coal solubilization rate reaches half of its maximum value
$K_{H_2/s}$	hydrogen concentration at which microbial growth rate reaches half of its maximum value
$K_{Fe_2O_3/s}$	Fe_2O_3 concentration at which microbial growth rate reaches half of its maximum value
$L_x,\ L_y,\ L_z$	fracture spacing in three orthogonal directions
m_{mg}	gas mass content in coal matrix
M_{H_2}	molar mass of hydrogen
M_{H_2O}	molar mass of water
$M_{Fe_2O_3}$	molar mass of Fe_2O_3
$M_{Fe_3O_4}$	molar mass of Fe_3O_4
p	pore pressure
p_b	pressure of the entire rock
p_c	capillary pressure
p_e	entry capillary pressure

p_f	fracture pressure
p_m	matrix pressure
p_{fg}	gas pressure in fracture
p_{fw}	water pressure in fracture
P_L	Langmuir pressure constant
Q_g	source/sink term of gas phase
Q_w	source/sink term of water phase
Q_{fm}	source/sink term representing gas mass transfer from fracture to matrix
R_i	reaction source/sink term of a given dissolved species in water phase
R_j	reaction source/sink term of a given mineral phase
R_m	reaction source/sink term of microbes
R_n	reaction source/sink term of nutrients
R_p	reaction source/sink term of metabolic products
R_{H_2}	reaction source/sink term of dissolved hydrogen
$R_{Fe_2O_3}$	reaction source/sink term of Fe_2O_3
$R_{Fe_3O_4}$	reaction source/sink term of Fe_3O_4
S	concentration of rate-limiting nutrients/substrates
S_g	gas saturation
S_p	pore surface area per unit rock volume
S_w	water saturation

S_{gr}	residual gas saturation
S_{wi}	irreducible water saturation
S_g^*	effective saturation of gas phase
S_w^*	effective saturation of water phase
u_i	displacement component
v	Poisson's ratio
v_w	water flow velocity
V	bulk volume of rock
V_f	fracture volume in rock
V_L	Langmuir volume constant
V_p	pore volume
V_s	solid volume of rock
V_{bg}	volume of biogenic methane that can be generated per unit mass of coal
Y_s	microbial growth yield coefficient representing nutrients consumption rate
Y_w	reaction yield coefficient representing water production rate
α	Biot's coefficient
α_f	effective Biot's coefficient of fracture
α_m	effective Biot's coefficient of matrix
α_L	longitudinal dispersivity
$\bar{\alpha}_f$	Biot's coefficient of fracture

$\bar{\alpha}_m$	Biot's coefficient of matrix
γ_f	percentage of fracture volume over total rock volume
γ_m	percentage of matrix volume over total rock volume
δ_{ij}	Kronecker delta
ε_L	Langmuir strain constant
ε_s	gas sorption induced strain
ε_{ij}	strain tensor component
λ	coefficient related to pore size distribution
μ_g	gas viscosity
μ_p	metabolic products generation rate
μ_w	water viscosity
ν	average linear velocity of the water phase
ξ	hydrogen mass transfer rate from gaseous phase to water phase
ρ_c	coal density
ρ_m	microbe density
ρ_w	water density
ρ_{ga}	gas density at the standard condition
ρ_{gf}	gas density in fracture
ρ_{gm}	gas density in matrix
ρ_{rock}	rock density

$\bar{\sigma}$	mean compressive stress
σ_{ij}	stress tensor component
τ	porous media tortuosity factor
$\emptyset$	rock porosity
$\emptyset_1$	porosity occupied by microbes adsorbed reversibly on pore surface
$\emptyset_2$	porosity occupied by microbes adsorbed irreversibly on pore surface
$\emptyset_d$	porosity change induced by mineral dissolution
$\emptyset_f$	fracture porosity
$\emptyset_m$	matrix porosity
$\emptyset_p$	porosity change induced by mineral precipitation
$\emptyset_s$	degradable fraction of coal that can be converted into biogenic methane
$\emptyset_{bc}$	fraction of porosity occupied by microbes adsorbed on pore surface
$\emptyset_{ns}$	fraction of coal that cannot be converted

Chapter 1 Introduction

1.1 Background

Over the last 150 years, human activities are responsible for almost all the greenhouse gas emissions in the atmosphere (Stocker et al., 2014). As can be seen from Fig. 1-1, these greenhouse gas emissions can be broken down by the economic sectors that lead to their production. Almost all these economic sectors excluding agriculture and forestry involve the emission of greenhouse gas CO_2 into the atmosphere through the burning of fossil fuels. The accumulated CO_2 in the atmosphere can act like the blanket wrapping the earth and thereby trapping the heat from the sun and raising the temperature. As a result of these emissions, the earth is now already about 1.1°C warmer than it was in the late 1800s.

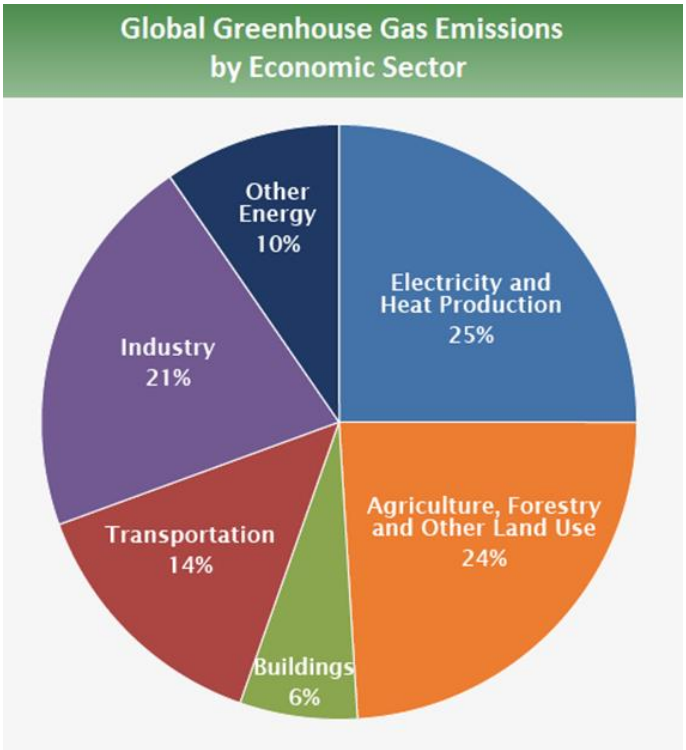

Fig. 1-1 Primary sources of global greenhouse gas emissions (IPCC Climate Change, 2014).

In order to mitigate climate change, the Paris Agreement has been reached (Paris Agreement, 2015). It calls for the international cooperation to limit global temperature increase to 1.5°C above pre-industrial levels. To reach this goal, emissions need to be reduced by 45% by 2030 and reach net zero by 2050. Now, more than 140 countries across the world including the United States, the European Union, China and India have set the net-zero target to cutdown the emissions.

For the energy-related industries, lowering greenhouse gas emissions can be achieved through the use of low-carbon energies. In fossil fuels, natural gas is a type of low-carbon energy when compared with coal and oil as much less CO_2 is released when burning natural gas. Specifically, burning natural gas only releases around 50% and 70% of the CO_2 emissions in comparison to coal and oil, respectively. Meanwhile, burning natural gas also results in much lower emissions of CO, NOx, SOx, particulates and mercury (Das et al., 2000; Sharma et al., 2018). Thus, energy transition from coal and oil to natural gas is considered as an inevitable trend in the context of decarbonization and reaching the net-zero target. In recent years, unconventional natural gas resources have gained great interests worldwide due to the rapid development of horizontal well drilling and hydraulic fracturing techniques (Yu et al., 2015; Cao et al., 2016). As a typical type of unconventional natural gas resource, coalbed methane is playing a significant role in the global energy market (Tan et al., 2019) and it is believed to play a significant role in energy transition as well. Apartment from coalbed methane, another type of clean gas energy, i.e., hydrogen, is also attracting great attention across the world as burning hydrogen only produces water and does not release CO_2 and other harmful substances. The need of hydrogen is considerably increasing and has multiplied three times since 1975, and it will keep increasing in the future as the technology for hydrogen production and its end-use is developing fast nowadays (Dopffel et al., 2021;

Aftab et al., 2022).

Coalbed methane can be categorized into thermogenic methane and biogenic methane according to its origin. For biogenic methane, it is generated through microbial degradation of organic components in coal over time (Rice and Claypool, 1981; Davis and Gerlach, 2018; Lupton et al., 2020). Studies have suggested that around 20% of the global natural gas resources, including coalbed methane, could be microbial in origin. Taking cue from the oil industry that microbial-enhanced oil recovery technique can be applied to stimulate oil production, Scott (1999) introduced the technique of microbially enhanced coalbed methane. This technique involves the injection of nutrients solution into coal seams to stimulate metabolism of the introduced or naturally occurring microbes to convert coal to methane gas. Therefore, microbial activities play a key role in generating and extracting biogenic methane from coal seams. Similarly, underground hydrogen storage in porous media can be influenced by microbial activities as well. This is mainly because most subsurface formations are not life-free environments and can harbor a variety of microbial species. The activities of these microbes could negatively impact the technique feasibility of underground hydrogen storage operations in various forms such as microbial clogging of the pore space and microbial consumption of hydrogen (Dopffel et al., 2021; Heinemann et al., 2021; Aftab et al., 2022). At this point, it can be concluded that both gas energy extraction and storage in subsurface formations can be influenced by microbial activities.

1.2 Microbiology in subsurface formations

About 30 years ago, the Deep Sea Drilling Program first reported the discovery of active microbes in the subsurface formation. This discovery identifies the existence of microbial activities in the depth of about 150 m (Tarafa et al., 1987; Whelan et al., 1986).

After that, microbial activities in continental sedimentary rocks were found to be at the depth of up to 2800 m (Pedersen, 2000). Studies also suggested that there are significant amounts of microbes in subsurface formations and the number of these microbes could be one-tenth or even up to one-third of the total living biomass in the world. Normally, the microbes in subsurface can be categorized into two groups, i.e., bacteria and archaea, both of which are responsible for many geochemical and biochemical reactions in subsurface formations (Hoehler and Jørgensen, 2013).

1.2.1 Microbial species related to gas energy extraction/storage

For biogenic coalbed methane generation and extraction, a collection of different microbes is involved including hydrolytic bacteria, fermentative bacteria, acetogenic bacteria, and methanogenic archaea (Ritter et al., 2015; Park and Liang, 2016; Ponnudurai et al., 2022a). First, hydrolytic bacteria are responsible for degrading the complex organic components in coal into water-soluble monomers and oligomers. Then, fermentative bacteria further degrade these water-soluble intermediates into short-chain volatile organic acids. After that, acetogenic bacteria produce acetate, methanol, hydrogen and carbon dioxide from the earlier fermentation products. In the end, substrates such as acetate, methanol, hydrogen, and carbon dioxide are utilized by methanogenic archaea to generate biogenic methane. Eqs. (1-1) to (1-3) illustrate these three main methanogenic pathways through which biogenic methane can be formed:

$$CH_3COOH \rightarrow CH_4 + CO_2 \quad (1\text{-}1)$$

$$4CH_3OH \rightarrow 3CH_4 + CO_2 + 2H_2O \quad (1\text{-}2)$$

$$CO_2 + 4H_2 \rightarrow CH_4 + 2H_2O \quad (1\text{-}3)$$

For underground hydrogen storage in subsurface formations, the operations could be negatively impacted by a number of classes of microbes such as methanogenic archaea,

acetogenic bacteria, sulphate reduction bacteria, sulfur reduction bacteria, iron reduction bacteria, and denitrification bacteria (Dopffel et al., 2021; Heinemann et al., 2021; Aftab et al., 2022; Kumari and Ranjith, 2023; Fernandez et al., 2024). When methanogenic archaea present in the formation, biochemical reaction between the stored hydrogen and the CO_2 in the formation can be catalyzed and as a result methane is produced:

$$4H_2 + CO_2 \rightarrow CH_4 + 2H_2O \quad (1\text{-}4)$$

When acetogenic bacteria present in the formation, biochemical reaction between the stored hydrogen and the CO_2 in the formation can be catalyzed and as a result acetic acid is produced:

$$4H_2 + 2CO_2 \rightarrow CH_3COOH + 2H_2O \quad (1\text{-}5)$$

When sulphate reduction bacteria or sulfur reduction bacteria present in the formation, biochemical reaction between sulphate/sulfur content and the stored hydrogen can be catalyzed and as a result H_2S is produced:

$$\frac{1}{2}SO_4^{2-} + H_2 + \frac{1}{2}H^+ \rightarrow \frac{1}{2}HS^- + H_2O \quad (1\text{-}6)$$

$$S + H_2 \rightarrow H_2S \quad (1\text{-}7)$$

When iron reduction bacteria present in the formation, biochemical reaction between the stored hydrogen and the mineral content Fe_2O_3 in the rock can be catalyzed and as a result a new mineral Fe_3O_4 is produced:

$$3Fe_2O_3 + H_2 \rightarrow 2Fe_3O_4 + H_2O \quad (1\text{-}8)$$

When denitrification bacteria present in the formation, biochemical reaction between the stored hydrogen and nitrate content can be catalyzed and as a result N_2 is formed:

$$\frac{2}{5}NO_3^- + H_2 + \frac{2}{5}H^+ \rightarrow \frac{1}{5}N_2 + \frac{6}{5}H_2O \quad (1\text{-}9)$$

From the above introduction, it can be known that the presence of microbes can induce permanent loss of a certain amount of hydrogen as well as many other problems like other gases formation, acid formation, mineral dissolution/precipitation, pore-clogging and etc.

1.2.2 Microbial size, structure and growth

The size of a single microbe is typically in the range of 0.5 to 1 μm in diameter and 1 to 3 μm in length (Maier et al., 2009; Ritter et al., 2015). Thus, microbes usually inhabit in the cleats/fractures or large pores (with size greater than 3 μm) in the subsurface formations.

Many microbes have their unique features, but they also share the common characteristics. All these microbes are made of the fundamental units called cells. Each microbial cell is surrounded by the cell membrane, which controls the movement of materials like nutrients in and out of the cell. Some are also surrounded by a cell wall, which provides a structure to enclose the components inside. Within the cell, each contains the DNA encoding its genome (Hagemann, 2018).

Microbial growth refers to the growth of cell numbers instead of the growth of cell size. The most common mechanism of cell growth in microbes is the process called binary fission (Parker et al., 2016), which is shown in Fig. 1-2. The process consists of a few steps. First, the original cell duplicates its DNA and meanwhile generates additional materials to build the membrane and wall for the two cells. In this step, the size of the original cell slightly increases to accommodate the generated materials. Then, the original cell starts to contract at the middle. This contraction process continues until the original cell is split into two individual cells. The created two cells are called daughter

cells. Cell duplication in this way can lead to rapid growth of cell numbers as each daughter cell can duplicate this process by acting as the original cell.

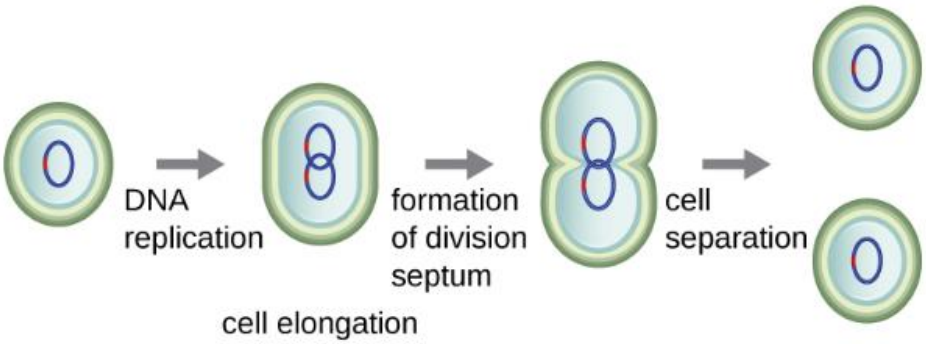

Fig. 1-2 Duplication of a microbial cell (Parker et al., 2016).

The growth of microbes could be influenced by many factors such as nutrients, temperature and pH value. To keep active, microbes need certain nutrients for life including minerals, organic nitrogen source, vitamin solution and a variety of trace elements (Park and Liang, 2016). The temperature limits for microbial activities are usually from -15 ℃ to 120 ℃. In this temperature range, there would exist the optimum temperature at which maximum microbial growth rate occurs (Ratkowsky et al., 1983). Studies have suggested that the optimum temperature for microbial growth should be around 20 ℃ to 40 ℃ (Zhang et al., 2016a). pH value for microbial growth lies between 0 to 11. When pH value ranges between 6 to 7, the diversity and density of microbes should be the highest (Dopffel et al., 2021). Other factors like salinity, water activity, radiation, rock permeability and concentrations of toxic chemicals also can have significant impacts on microbial growth (Jagger 1983; Halim et al., 2014; Payler et al., 2019; Dopffel et al., 2021).

The growth behavior of microbes has been studied in the laboratory. In the study, microbes are placed into the closed reactor that contains all the necessary nutrients for growth. Then, a typical microbial growth curve as shown in Fig. 1-3 can be obtained

through analyzing microbial population variation in the reactor. From this figure, it can be known that microbial growth consists of four typical phases including the lag phase, the log phase, the stationary phase, and the decline phase. In the lag phase, microbial population does not change but the size of microbe grows. The duration of this phase is determined by many factors like the composition of the medium and the species and genetic make-up of the microbial cells. In the log phase, microbial population increases in a logarithmic manner. In this phase, microbial cells actively split and the cell number doubles after each generation. The duration of the log phase is determined by the nutrients concentration and it stops when nutrients are consumed. In the stationary phase, microbial population reaches a plateau. In this phase, the number of created new microbial cells is equivalent to the number of cells dying and thus microbial population remains unchanged. In the decline phase, microbial decay outcompetes microbial growth and thus the microbial population shows an exponential decrease trend.

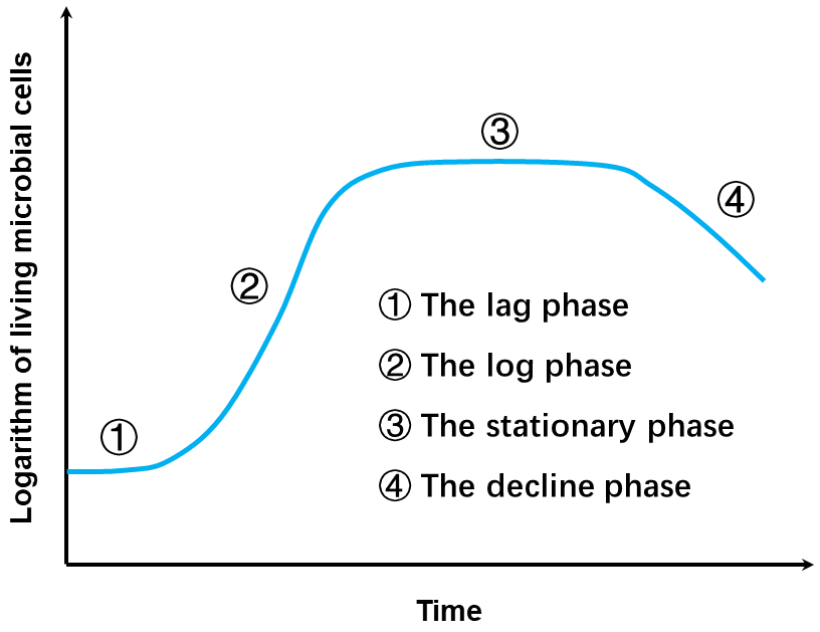

Fig. 1-3 Typical microbial growth curve (modified from Hagemann et al., 2016).

Some empirical equations have been proposed for modelling microbial growth. The mathematical model that is most frequently used to describe microbial growth is the

Monod equation which was proposed by Jacques Monod in 1949 (Jeong et al., 2019):

$$g_1 = g_{1max} \frac{S}{K_{n/s} + S} \tag{1-10}$$

where g_1 is microbial growth rate, g_{1max} is the maximum microbial growth rate, S is the concentration of rate-limiting nutrients/substrates, and $K_{n/s}$ is a half saturation constant representing the concentration of nutrients/substrates at which microbial growth rate reaches half of its maximum value.

Environmental engineers discovered that active biomass need energy to maintain their activities including cell functions, osmotic regulation, transport, and heat loss (Rittmann and McCarty, 2001). The flow of energy and electrons to carry out the maintenance activities can induce the endogenous decay. Thus, the net microbial growth rate can be defined as:

$$g = g_{1max} \frac{S}{K_{n/s} + S} - d_1 \tag{1-11}$$

where g is the net microbial growth rate, and d_1 is the microbial decay rate.

1.2.3 Microbial transport in porous media

The fate and movement of microbes in porous media is controlled by several mechanisms which can act simultaneously. Modelling these processes will first require appropriate conceptual models of the biotic phase. Commonly, microbes in water-saturated porous media can be classified into two groups: one group in the aqueous phase and the other group on pore surface (Ginn et al., 2002; Tufenkji, 2007; Masum and Thomas, 2018). The microbes in aqueous phase are commonly referred to those freely living cells suspended in the water phase. Microbes in this group are typical mathematically represented as dilute reactive solute. The dilute assumption ignores the cell interactions in the aqueous phase although it could be invalid in some cases like

those encountered in cell clumping and quorum sensing (Ward et al., 2001). Unlike microbes in aqueous phase, those inhabit on the pore surface are usually treated as biofilms. Biofilms refer to the assembly of microbes which attach to each other and to a surface by a structure of self-produced extracellular polymeric substances (Masum and Thomas, 2018), as shown in Fig. 1-4. Biofilms can be classified into structured biofilm and unstructured biofilm. For structured biofilm, it can be further classified into two categories: (1) continuous biofilm on the pore surface (Taylor and Jaffé, 1990; Taylor et al., 1990), and (2) discontinuous patchy film (Vandevivere and Baveye, 1992; Rittmann, 1993). For unstructured biofilm, microbes are treated as suspended but kinetically sorbing/desorbing species (Zysset et al., 1994).

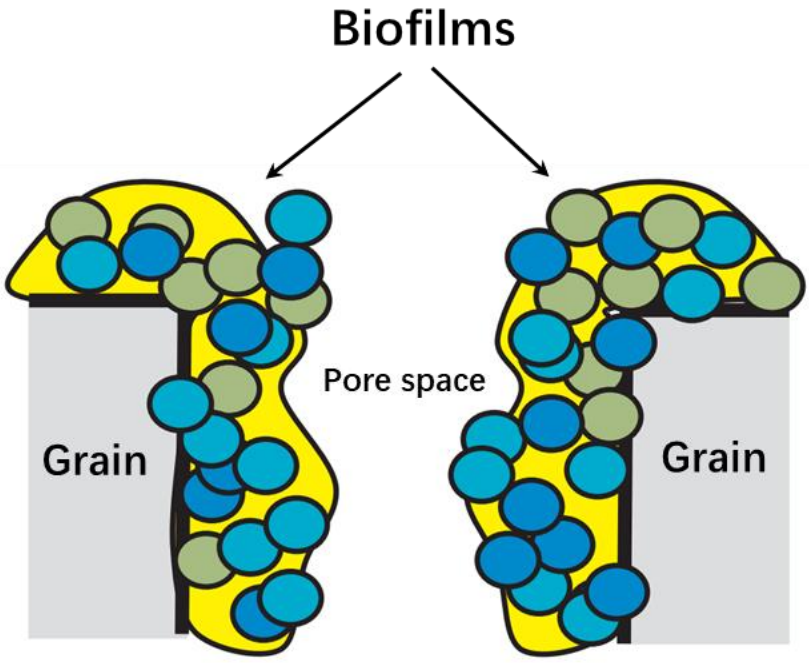

Fig. 1-4 Schematic diagram of biofilm on the grain surface (modified from Chong et al., 2019).

A host of complex and interacting processes dominate microbial transport in subsurface porous media. Overall, these processes can be classified into three groups: (1) microbial transport; (2) microbial adsorption and desorption; and (3) microbial growth and decay.

In aqueous phase, microbes undergo convective transport as a dissolved species in the water whose velocity can be influenced by several factors including the magnitude of water pressure gradient and porosity/permeability of the porous media (Ginn et al., 2002). However, the convection of microbes is a little bit different from the convection of other dissolved chemical species in the water phase as microbial convection can also be influenced by other factors such as filtration, straining, size exclusion and chemotaxis (Ginn et al., 2002). Filtration represents the removal of microbes from water phase via collision with and adsorption on pore surface and this process can be reversible. Straining represents the trapping of microbes in pore throats that are too small for microbes to pass through. Size exclusion represents the phenomenon that microbes transport faster than other dissolved chemical species. Chemotaxis represents the active movement of microbes towards nutrients/substrates and/or away from toxic substances. In porous media, convective transport is usually associated with hydrodynamic dispersion which represents the mixing process arising from the tortuosity of the convective paths (Ginn et al., 2002). The transport of microbes can also be influenced by microbial adsorption/desorption and growth/decay processes (Kim, 2006; Li et al., 2011). Microbial adsorption represents the deposition of microbes from pore fluids and then attachment to the pore/fracture surfaces. Microbial desorption represents the detachment of microbes from pore/fracture surfaces and then return to the pore fluids as the flowing species. The microbial adsorption process can be modelled as either reversible or irreversible. In addition, microbial growth/decay occurs at both the aqueous phase and the pore surfaces. Thus, not only the microbial concentration in the pore fluids but also the microbial population on pore surfaces can be influenced by this mechanism.

At the Darcy scale, the spatial and temporal evolution of microbial concentration in

homogeneous and water saturated porous media can be described by the advection-dispersion equation (Rockhold et al., 2004; Kim, 2006; Li et al., 2011). In this equation, the movement of microbes is controlled by the advection and hydrodynamic dispersion. Meanwhile, source terms should be defined to describe the impacts of microbial adsorption/desorption and growth/decay on the spatial and temporal evolution of microbial concentration in porous media.

1.3 Lab, field and theoretical studies of microbial impacts on gas energy extraction/storage

1.3.1 Studies of microbial impacts on biogenic methane extraction

Great efforts have been made in the laboratory to stimulate biogenic methane generation from coal samples. Those batch experiments conducted under the ambient pressure and temperature conditions, using crushed coal samples with prepared microbial community and nutrients solution have demonstrated the great potential of generating biogenic methane from coal. Experiments have identified various parameters that may influence biogenic methane yield such as microbial source (Gupta and Gupta, 2014; Ponnudurai et al., 2022b), nutrients recipe (Zhang et al., 2016b; Moestedt et al., 2016; Davis et al., 2019), coal rank (Harris et al., 2008; Malik et al., 2020; Robbins et al., 2016; Fallgren et al., 2013), temperature (Zhang et al., 2016a, 2016b; Green et al., 2008; Gupta and Gupta, 2014; Fuertez et al., 2017), PH (Green et al., 2008; Gupta and Gupta, 2014; Fuertez et al., 2017), salinity (Fuertez et al., 2017), particle size (Zhang et al., 2016a; Green et al., 2008; Gupta and Gupta, 2014; Papendick et al., 2011), coal loading (Gupta and Gupta, 2014; Zhang et al., 2016a, 2016b), mixing rate (Zhang et al., 2016b) and etc. Although it is difficult to make direct comparisons of these experiments, one common conclusion that can be drawn based on these experiments is that microbial

activities are controlled by the nutrients available and addition of nutrients can indeed enhance biogenic methane yield (Park and Liang, 2016). Some other experiments focusing on enhancing solubility and bioavailability of coal during microbial stimulation were also performed by use of the chemical treatments (Tamamura et al., 2016; Green et al., 2008; Huang et al., 2013; Guo et al., 2021).

All the above-mentioned experimental studies are conducted in anaerobic bottles under the static conditions, as opposed to dynamic flow conditions in subsurface coal seams. To this end, Davis et al. (Davis et al., 2019) designed a continuous-flow column reactor to study coal-to-methane bioconversion. Using this system, tests can be run at varying flow rates while maintaining the oxygen-free environment. Stephen et al. (Stephen et al., 2014) established a core flooding test system for better understanding coal bioconversion process. Experiments can be conducted under a wide range of pore pressure conditions. Margaux et al. (Margaux et al., 2016) also fabricated a high-pressure reactor system that can simulate flowing conditions of underground coal seams. Experimental results indicate that much more biogenic methane can be generated under the static conditions than the flowing conditions. An important question still not addressed is that whether gas generation behavior measured on crushed coal samples can represent that of intact coal samples. To answer this question, Pandey and Harpalani (Pandey and Harpalani, 2019) performed a group of bioconversion experiments using intact coal samples under the constant confining pressure conditions, with vertical/horizontal stresses remaining at 1000/700 psi throughout. Biogenic methane yield and variations of coal permeability and cleat compressibility due to bioconversion were measured. Lupton et al. (Lupton et al., 2020) completed a series of anaerobic core flooding experiments on intact coal samples under the constant effective stress conditions, with effective stress kept at 1 MPa throughout. Long-term coal permeability

evolution behavior, biogenic methane generation behavior, and nutrients uptake behavior were recorded. Meanwhile, different nutrients delivery strategies were modelled in their experiments.

Although lab experiments are the cost-effective ways to simulate biogenic methane generation, the observed results are based on small scale coal samples which may not reflect in-situ coal properties. Also, the lab-used stress-controlled conditions are different from the in-situ uniaxial strain conditions. Therefore, field scale tests can offer more practical insights into coal-to-methane bioconversion behavior. In 2006, Luca Technologies (Ritter et al., 2015) started the large scale field tests on 260 wells in Powder River Basin with designed well spacing being 40 or 80 acres. In their operation, amendment mixtures were injected into the wells for 1-2 months, followed by well shut-in for another several months to allow new biogas formation in coal seams. In 2012, Ciris Energy (Ritter et al., 2015) carried out a field scale test in Powder River Basin as well. In their test, a continuous-flow injection and extraction strategy is adopted. The project involves 4 injection wells surrounded by 13 production wells with the designed well spacing being 10 acres. Some other companies like Next Fuel (Ritter et al., 2015) also conducted relevant field tests. Since there is no rigorous approach for evaluating these field operations, injection procedures cannot be optimized and production efficiency may be compromised. Thus, development of suitable modeling tools is required to help make decisions on selecting nutrients delivery strategies, optimizing well completions, forecasting biogenic methane generation and extraction, and etc.

Based on the experimental results, several theoretical models have been formulated to quantify biogenic methane generation and extraction processes. These models can be classified into two major categories according to their scope of applications. The models in the first category can be used to simulate biogenic methane generation under

the ex-situ conditions. The models in the second category can be used to simulate biogenic methane generation and extraction under the in-situ conditions.

The ex-situ condition refers to bioconversion of coal overground. Under this condition, no fluid flow is involved and all generated biogenic methane can be collected. Senthamaraikkannan et al. (Senthamaraikkannan et al., 2016a) proposed a kinetic model for describing the complicated bioconversion process under the ex-situ condition. Four bioconversion steps are considered in their work. The model can be used to study the variation of intermediates' concentrations and the impact of each bioconversion step on biogenic methane generation. Following the same method, Sharma et al. (Sharma et al., 2018) proposed a coal-to-methane kinetic model that incorporates more chemical intermediates. Using the concept of logistic population growth, Saurabh and Harpalani (Saurabh and Harpalani, 2018) proposed an easy-to-implement model to simulate biogenic methane generation. Only three parameters, i.e., carrying capacity of the environment, microbial growth rate and initial microbial population, need to be input in their model.

The in-situ condition refers to bioconversion of coal underground. Under this condition, fluid flow plays important role and not all the generated biogenic methane can be extracted. Meanwhile, for coal bioconversion under in-situ conditions, the processes like water-gas two-phase flow, nutrients, microbes and intermediates transport, microbial growth/decay and adsorption/desorption, and dynamic change of coal porosity and permeability are also involved. So far, some works in this area have been published but very few systematically consider these processes. Cokar et al. (Cokar et al., 2013) proposed a reservoir scale numerical model for simulating biogenic methane generation and extraction under the in-situ flowing conditions. The generation rate of biogenic methane was assumed to be proportional to the substrate concentration. In

their model, microbial activities were not considered and coal-to-methane bioconversion process was ignored. Senthamaraikkannan et al. (Senthamaraikkannan et al., 2016b, 2016c) proposed a dual porosity numerical model to simulate biogenic methane generation and extraction. The generation of biogenic methane experiences four sequential bioconversion steps. Based on this model, field scale strategies for commercial biogenic methane extraction can be evaluated. However, microbial activities are not explicitly modeled. Zhi et al. (Zhi et al., 2018) proposed a field scale numerical model based on the equivalent multi-continuum method to study how to improve nutrients delivery in naturally fractured coal seams through hydraulic fracturing. The complex natural fracture network was represented to capture the natural heterogeneity and anisotropy of fracture permeability. The cumulative biogenic methane yield was assumed to be proportional to the area of activated fracture networks. Although nutrients transport was modeled in their work, the microbial activities were not included as well.

1.3.2 Studies of microbial impacts on underground hydrogen storage

In some underground gas storage (UGS) field tests, the phenomenon of microbial consumption of hydrogen has been observed. For example, an UGS project in Lobodice, Czech Republic (Amigáň et al., 1990) reported that nearly half of the stored hydrogen in sandstone reservoir was microbially converted into hydrogen sulfide and methane. Isotropic analysis has proofed the microbial origin of the formed gas. Meanwhile, a decrease in reservoir pressure and an increase in microbe cell numbers during UGS operations were reported. In another example of UGS project in Lehen, Austria (Pichler, 2019), 10% hydrogen was mixed with natural gas and then stored in sandstone reservoir for four months. In this period, 16% of the stored hydrogen cannot be recovered. The DNA analysis and RNA data suggest that different microbial metabolisms like

methanogenesis, acetogenesis and sulphate-reduction could be triggered in this process. In addition, the Argentinian HyChico project (Pérez, 2016) stored hydrogen in a depleted sandstone reservoir. During the storage cycle, microbe-induced hydrogen loss was also observed.

In addition to field tests, laboratory experiments have also been conducted to investigate the impacts of microbial activities on UHS. Strobel et al. (2023) and Khajooie et al. (2024) performed a series of biochemical experiments by use of methanogens and hydrogen/carbon dioxide gas mixture. The experiments were performed in pressurized batch reactors and the experimental results showed that microbial metabolism and growth leads to the decrease of hydrogen concentration and increase of methane concentration. Liu et al. (2023) conducted the pore-scale biochemical experiments by use of halophilic sulfate-reducing bacteria and hydrogen. In their experiments, a silicon-wafer micromodel with a pore pattern from natural sandstone was used for direct observation of microbe-induced sulfate reduction under the conditions of 35 bar and 37 °C. A significant loss of hydrogen from microbial consumption and a change in surface wettability due to microbial growth were observed from the experiments.

Although laboratory experiments are the most direct way to study microbial impacts on UHS, it is sometimes expensive, time-consuming and massive manpower required. Even in some cases, the experiments can only be performed under the very simple conditions. Therefore, theoretical approaches are vital for us to study this problem. Strobel et al. (2023) proposed a mathematical model for microbial growth, substrates conversion and phase mass transfer in batch reactors. This model can only be used to quantify the microbial impacts under the static conditions while for UHS in porous reservoirs where fluid flow involves the model cannot be applied. Ebigbo et al. (2013) proposed a numerical model to investigate microbial impacts on UHS which couples

biofilm growth process with fluid flow and solute transport processes, but the model application is limited to the pore scale. To this end, Hagemann et al. (2016) developed a two-phase bio-reactive transport model to study microbial impacts on UHS in porous reservoir. In their model, microbial growth/decay was considered. Applying this model, the variation of gas composition and concentration during UHS can be captured but an important mechanism, i.e., microbial clogging of pore space, was missed in their study. Eddaoui et al. (2021) built a multi-component two-phase flow model to study the impact of microbial clogging on UHS in porous reservoir. In their model, both microbial growth/decay and adsorption/desorption were considered. However, the model only studied microbial impacts on porosity/permeability variation during UHS while many other important parameters like gas composition, hydrogen injection and withdrawal rates, and hydrogen recovery factor were not investigated. Wang et al. (2024) developed a two-dimension, water-gas two-phase flow model to study bioreaction impacts on UHS. Although hydrogen consumption and gas mixing phenomenon were considered in their model, microbial activities like transport, adsorption/desorption and growth/decay were not considered at all.

1.4 Research objective and approach

As can be known from the above literature review, microbial activities can have significant impacts on gas energy extraction/storage in porous media. Although some efforts have been made to study the impacts, these works either do not account for microbial activities at all or they do it in an incomplete way, i.e., by not actually accounting for microbial activities like transport, adsorption/desorption and growth/decay or by not accounting for the potential effects of microbial activities on physical properties of porous media. Thus, the impacts of microbial activities on gas energy extraction/storage are still not well understood and explained. The objective of

this research is to fill this knowledge gap and systematically quantify how gas energy extraction/storage processes can be influenced by microbial activities using the mathematical tool. This research objective can be achieved through an integrated approach of conceptual analysis, theoretical modeling and numerical simulations:

(1) Conceptual understanding of the issues

Conceptual models explaining the impacts of microbial activities on gas energy extraction/storage are built.

First, a conceptual model for biogenic coalbed methane generation and extraction is proposed. In this conceptual model, how microbial activities are stimulated, how biogenic coalbed methane are generated and extracted, and how the generated gas flow in coal seams along with how coal permeability dynamically changes in this process are introduced.

Secondly, a conceptual model for underground hydrogen storage is proposed. In this conceptual model, how microbial activities are stimulated and how bio-chemical reactions occur during hydrogen storage along with how hydrogen injection and extraction performance are influenced by the bio-chemical reactions are introduced.

(2) Theoretical models development and verification

Based on the conceptual models, the mathematical models describing the multiple processes involved in gas energy extraction/storage are developed and verified.

First, based on the understanding of coal bioconversion processes, porosity and permeability models that consider the impacts of effective stress, coal solubilization and microbial clogging are proposed. Then, the coupled processes during coal-to-methane bioconversion including coal deformation, water-gas two phase flow,

multispecies reactive transport, and microbial adsorption/desorption and growth/decay are formulated into a multiphysics model. In this multiphysics model, all processes are linked together by the coal porosity/permeability models. The multiphysics model is verified against the laboratory data.

Secondly, based on the understanding of hydrogen storage processes, porosity and permeability models that consider the impacts of effective stress, mineral dissolution/precipitation and microbial clogging are proposed. Then, the HMCB coupled processes during hydrogen storage in aquifers are formulated into a multiphyscis model as well. In this multiphysics model, all processes are linked together by porosity/permeability models. The multiphysics model is verified against the laboratory data.

(3) Numerical simulations

When theoretical models are developed, a numerical simulator needs to be selected to solve these governing equations. In this work, we use the commercial software COMSOL MULTIPHYSICS to do the calculation. This software is a general-purpose simulation software based on advanced numerical methods which enables us to combine multiple physics together in any order for simulations of complex problems. In our work, the modules of solid mechanics, Darcy's law and transport of diluted species in porous media are coupled to solve the developed models. In this coupled system, geomechanical variables, fluid flow variables and bio-chemical variables can be simultaneously calculated by solving the input partial differential equations. Based on the simulation results, we can have an in-depth understanding of the impacts of microbial activities on gas energy extraction/storage.

1.5 Thesis outline

The thesis consists of five chapters. The contents of each chapter are introduced as below:

(1) Chapter 1 first introduces two types of low-carbon gas energies: biogenic coalbed methane and hydrogen. Then, a common issue that involved in the extraction of biogenic coalbed methane and storage of hydrogen is identified, i.e., both the two processes can be influenced by microbial activities. After that, literature review on microbiology in subsurface formations and bio-reactive modelling is conducted. In the end, the research motivation, objectives and approaches are given.

(2) In Chapter 2, a generic coupled hydraulic-mechanical-chemical-biological multiphysics framework is developed. This multiphysics framework incorporates rock deformation, water-gas two-phase flow, multispecies reactive transport and microbial adsorption/desorption and growth/decay. All these processes are linked together through the porosity/permeability models. Using this multiphysics framework, various issues in gas energy extraction/storage can be solved.

(3) In Chapter 3, literature review on biogenic coalbed methane generation and extraction is first conducted. Then, the conceptual model for biogenic coalbed methane generation and extraction from coal seams is presented. According to the conceptual model, a coupled hydraulic-mechanical-chemical-biological model is established on the basis of the generic multiphysics framework in Chapter 2. After that, model verification against laboratory data is conducted. In the end, the verified model is used analysis biogenic coalbed methane generation and extraction behavior under the impacts of microbial activities.

(4) In Chapter 4, literature review on underground hydrogen storage is first conducted. Then, the conceptual model for how microbial activities could impact hydrogen storage operations is presented. According to the conceptual model, a coupled

hydraulic-mechanical-chemical-biological model is established on the basis of the generic multiphysics framework in Chapter 2. After that, model verification against laboratory data is conducted. In the end, the verified model is used to analyze hydrogen storage performance in aquifers under the impacts of microbial activities.

(5) In Chapter 5, the main results of this research are summarized and the recommendations for future research are proposed.

Chapter 2 A generic hydraulic-mechanical-chemical-biological multiphysics framework for gas energy extraction/storage

When gas energy is extracted from or stored into the subsurface formations, complex interactions among the hosting rock, pore fluids, the dissolved chemical species and microbes will occur. These interactions can have strong influences on rock deformation, fluids flow, solutes transport, microbial growth, and rock porosity and permeability change. In our research, we define this chain of reactions as coupled processes which implies that one physical process can affect the initiation and progress of another one. Therefore, the inclusion of cross coupling relations is the key to formulate the mathematical models to describe the gas energy extraction/storage processes. In this section, we develop a generic hydraulic-mechanical-chemical-biological multiphysics model which can be applied to simulate different gas energy extraction/storage scenarios. In this model, a set of partial differential equations are defined to describe (1) rock deformation, (2) fluid flow, (3) reactive transport, (4) mineral dissolution/precipitation, and (5) microbial activities. All these processes are linked together through the porosity and permeability models. When applying this generic multiphysics model to a specific gas energy extraction or storage scenario, the defined partial differential equations can be further modified to include the corresponding characteristics of the specific problem. Meanwhile, the porosity and permeability models can also be modified to include more influencing factors.

2.1 Introduction

The starting point to characterize the role of microbial activities during gas energy extraction/storage is to know the fundamental physical processes involved (Li et al.,

2011). Commonly, subsurface gas energy extraction/storage involves coupled thermal-hydraulic-mechanical-chemical-biological processes (Senthamaraikkannan et al., 2016a; Heinemann et al., 2021). Each individual process, on their own, forms the basis of corresponding disciplines such as heat transfer, hydraulics, mechanics, chemistry and biology (Liu et al., 2011). In this research, it is assumed that all processes evolve under the isothermal conditions which means that the impact of temperature change within the subsurface formation is not ignored.

During gas energy extraction/storage, fluids are either extracted or injected into the subsurface formations. In these processes, formation pore pressure changes and leads to effective stress variation. As a result, hosting rock deforms. The deformation of hosting rock can be influenced by rock types. For non-sorptive rock like sandstone, the rock deformation is controlled by stress variation magnitude. For sorptive rock like coal, the rock deformation can be further influenced by gas adsorption/desorption induced swelling/shrinkage (Zhang et al., 2008; Peng et al., 2014). Once rock deformation occurs, the hydraulic properties, i.e., porosity and permeability, are changed and thus the fluid flow and solutes transport processes are influenced.

Typically, water-gas two-phase flow presents in subsurface formations during gas energy extraction/storage. In this case, both water and gas phases flow are influenced by phase saturations and relative permeabilities (Cao et al., 2017; Cui et al., 2020). During gas energy extraction, gas saturation and relative permeability decrease in subsurface formations and thus gas flow capacity decreases. On the contrary, gas flow capacity increases during gas energy storage. The fluid flow behavior in subsurface formations can also be influenced by the magnitude of pore size. When pore size falls within the nanometer scale range, Klinkenberg effect may play an important role on fluid flow (Javadpour et al., 2009; Cao et al., 2016; Gao et al., 2021). The smaller the

pore size is, the more pronounced the effect will be. Once fluid flow initiates during gas energy extraction/storage, pore pressure and effective stress will be changed and thus rock deformation will be induced. Meanwhile, fluid flow also influences solutes transport and microbial distribution in pore space.

Multiple species could dissolve and transport within the aqueous phase during gas energy extraction/storage. Chemical reactions may occur among these dissolved species or between the dissolved species and the minerals in the hosting rock. This process is typically called reactive transport (MacQuarrie and Mayer, 2005; Steefel et al., 2005). The transport of dissolved species is commonly controlled by advection and dispersion. The dispersion of dissolved species consists of two processes: molecular diffusion and mechanical dispersion (Li et al., 2011; Zhi et al., 2018). When chemical reactions between dissolved species and minerals occur, the hydraulic properties and mechanical properties of rock can be altered which subsequently influences fluid flow and rock deformation behaviors. Moreover, the reactive transport can also influence microbial distribution in porous media.

In porous media, microbes can be conceptually represented as either being dissolved in the aqueous phase or adsorbed on the grains surface (Ginn et al., 2002; Rockhold et al., 2004; Masum and Thomas, 2018). For those dissolved in the aqueous phase, they are commonly treated as suspended cells and will be transported with the flowing water. For those adsorbed on the grains surface, they are commonly treated as uniform biofilms (Li et al., 2011; Masum and Thomas, 2018). There will be microbial transfer between the dissolved phase and the adsorbed phase. The transfer is achieved through microbial attachment and detachment (Rockhold et al., 2004). Meanwhile, in both the dissolved phase and the adsorbed phase, microbes can grow and decay depending on the substrates supply. When microbes grow, a fraction of pore space can be occupied,

thus influencing hydraulic properties of rock and multispecies reactive transport process.

The above introduced mechanical, hydraulic, chemical and biological processes can be linked together through rock porosity and permeability models. During gas energy extraction/storage, rock porosity and permeability may significantly vary due to stress variation, chemical reaction and microbial growth.

As a basis to understand the coupled hydraulic-mechanical-chemical-biological processes during gas energy extraction/storage, the governing equations for rock deformation, fluid flow, reactive transport, mineral dissolution/precipitation, microbial activities, and porosity/permeability evolution are first presented in sections 2.2.1 to 2.2.6. Then, the required initial and boundary conditions are provided in section 2.2.7.

2.2 Governing equations for the coupled processes

2.2.1 Rock deformation

All equations in this subsection are derived after the traditional conventions: A comma followed by subscripts represents the differentiation with respect to spatial coordinates, and repeated indices in the same equation imply summation over the range of the indices (Zhang et al., 2008).

The stress equilibrium equation neglecting the inertial term is expressed in the form of:

$$\sigma_{ij,j} + f_i = 0 \tag{2-1}$$

where σ_{ij} is the component of stress tensor, and f_i is the component of body force.

The strain-displacement relationship is defined as:

$$\varepsilon_{ij} = \frac{1}{2}\left(u_{i,j} + u_{j,i}\right) \tag{2-2}$$

where ε_{ij} is the component of strain tensor, and u_i is the component of displacement.

For dual porosity sorbing porous media like coal, the whole system consists of two components, i.e., matrix and fracture. For matrix, the percentage of matrix volume over the total rock volume is defined as γ_m. The bulk modulus of matrix is defined as K_m. The bulk modulus of solid skeleton of matrix is defined as K_{ms}. For fracture, the percentage of fracture volume over the total rock volume is defined as γ_f. The bulk modulus of fracture is defined as K_f and the bulk modulus of solid skeleton of fracture is defined as K_{fs}. Here, we can have the relation $\gamma_m + \gamma_f = 1$. Then, according to the previous studies (Mehrabian and Abousleiman, 2015; Cao et al., 2016; Li et al., 2022), the Biot's coefficient for each component can be derived:

$$\bar{\alpha}_f = 1 - \frac{K_f}{K_{fs}} \tag{2-3}$$

$$\bar{\alpha}_m = 1 - \frac{K_m}{K_{ms}} \tag{2-4}$$

where $\bar{\alpha}_f$ and $\bar{\alpha}_m$ are Biot's coefficients of fracture and matrix, respectively.

According to the work by Berryman (2002) and Mehrabian and Abousleiman (2015), the drained bulk modulus of the rock can be defined as:

$$\frac{1}{K} = \frac{\gamma_f}{K_f} + \frac{\gamma_m}{K_m} \tag{2-5}$$

Then, the effective Biot's coefficients of fracture and matrix can be obtained:

$$\alpha_f = \frac{\gamma_f K \bar{\alpha}_f}{K_f} = \gamma_f \left(\frac{K}{K_f} - \frac{K}{K_{fs}} \right) \tag{2-6}$$

$$\alpha_m = \frac{\gamma_m K \bar{\alpha}_m}{K_m} = \gamma_m \left(\frac{K}{K_m} - \frac{K}{K_{ms}} \right) \tag{2-7}$$

For homogeneous, isotropic and elastic media, it can be assumed that gas sorption only results in volumetric strain and does not produce any shear strain which means that its effects on all three normal strains are the same. Through making the analogy between

thermal expansion and matrix swelling, the constitutive equation for deformable dual porosity sorbing rock can be given by (Chen et al., 2013):

$$\varepsilon_{ij} = \frac{1}{2G}\sigma_{ij} - \left(\frac{1}{6G} - \frac{1}{9K}\right)\sigma_{kk}\delta_{ij} + \frac{\alpha_f p_f}{3K}\delta_{ij} + \frac{\alpha_m p_m}{3K}\delta_{ij} + \frac{\varepsilon_s}{3}\delta_{ij} \qquad (2\text{-}8)$$

where $G = E/2(1+v)$, $K = E/3(1-2v)$, $\sigma_{kk} = \sigma_{11} + \sigma_{22} + \sigma_{33}$. G is shear modulus, K is bulk modulus, E is elastic modulus, v is Poisson's ratio, δ_{ij} is Kronecker delta, p_f is fracture pressure, p_m is matrix pressure, and ε_s is gas sorption induced strain.

According to the classification by de Boer (1958), the isotherms related to physical adsorption can be grouped into six types. For unconventional reservoir rocks like coal and shale, the most commonly used sorption model is the type I isotherm depicted by Langmuir isotherm owing to its simplicity and practical applications (Yang and Liu, 2020):

$$\varepsilon_s = \frac{\varepsilon_L p_b}{P_L + p_b} \qquad (2\text{-}9)$$

where ε_L is the Langmuir strain constant which represents the sorption strain at infinite pore pressure, P_L is the Langmuir pressure constant representing the pore pressure at which the measured sorption strain equals to half of its maximum value, p_b is the pore pressure of the entire rock which can be defined as $(1-\emptyset_f)p_m + \emptyset_f p_f$, and $\emptyset_f$ is fracture porosity.

Integrating Eqs. (2-1), (2-2) and (2-8), the Navier-type equation for dual porosity sorbing rock deformation can be derived:

$$Gu_{i,kk} + \frac{G}{1-2v}u_{k,ki} - \alpha_f p_{f,i} - \alpha_m p_{m,i} - K\varepsilon_L \frac{p_L}{(p_b + p_L)^2} p_{b,i} + f_i = 0 \qquad (2\text{-}10)$$

In Eq. (2-10), the two parameters p_f and p_m are linked to fluid flow equations as will be derived in the following subsection. It should be noted that this equation is derived

for dual porosity sorbing porous media. For single porosity sorbing porous media, only one pore pressure term exists in the Navier-type equation. Moreover, for non-sorbing porous media, the sorption term should be deleted.

2.2.2 Fluid flow

For gas energy extraction/storage in subsurface formations, water and gas commonly jointly presents in the pore space. Namely, it is a typical two-phase fluid flow process. For dual porosity porous media like coal, it is usually assumed that water-gas two-phase flow only presents in the fracture system while for matrix system water is considered not accessible due to the small pore dimensions (King et al., 1986; Senthamaraikkannan et al., 2016a; Le et al., 2020; Zhu et al., 2020). Then, applying the mass conservation law, we can obtain the flow equations for water and gas in fracture system:

$$\frac{\partial(\emptyset_f S_w \rho_w)}{\partial t} = \nabla \cdot \left(\rho_w \cdot \frac{k_f k_{rw}}{\mu_w} \nabla p_{fw}\right) + Q_w \tag{2-11}$$

$$\frac{\partial(\emptyset_f S_g \rho_{gf})}{\partial t} = \nabla \cdot \left(\rho_{gf} \cdot \frac{k_f k_{rg}}{\mu_g} \nabla p_{fg}\right) + Q_g - Q_{fm} \tag{2-12}$$

where S_w is water saturation, ρ_w is water density, k_f is fracture permeability, k_{rw} is relative permeability of water, μ_w is water viscosity, p_{fw} is water pressure in fracture, Q_w is the source term of water phase, S_g is gas saturation, ρ_{gf} is gas density in fracture, k_{rg} is relative permeability of gas, μ_g is gas viscosity, p_{fg} is gas pressure in fracture, Q_g is the source term of gas phase, and Q_{fm} is the source term representing gas mass transfer from fracture to matrix.

The total saturation for water and gas phases in the same fracture system should be equal to one:

$$S_w + S_g = 1 \tag{2-13}$$

When water and gas present in the fracture system, water is preferentially attracted by

the surface of the solid grains and in this case water is called the wetting phase (Allen, 2021). As water and gas are immiscible fluids, there exists a well-defined interface between the two phases. Since the cohesion between water molecules is different from that between gas molecules, the interface is characterized by some interfacial tension (Cao et al., 2017). It is this interfacial tension that leads to a pressure difference between the water and gas phases. This pressure difference between water and gas is commonly called capillary pressure. The magnitude of capillary pressure is equivalent to the pressure difference between the non-wetting phase and the wetting phase and is always non-zero. When water is the wetting phase, it can be defined as:

$$p_c = p_{fg} - p_{fw} \tag{2-14}$$

where p_c represents capillary pressure.

Many previous works have revealed that the magnitude of capillary pressure has a close relationship with the wetting phase saturation. In this research, we apply the widely used Brooks and Corey (1966) formulation to calculate it:

$$p_c = p_e {S_w^*}^{-1/\lambda} \tag{2-15}$$

where p_e is the entry capillary pressure, S_w^* is the effective saturation of water phase, and λ is the coefficient related to pore size distribution.

The effective saturations of water and gas phases are defined as:

$$S_w^* = \frac{S_w - S_{wi}}{1 - S_{gr} - S_{wi}} \tag{2-16}$$

$$S_g^* = \frac{S_g - S_{gr}}{1 - S_{gr} - S_{wi}} \tag{2-17}$$

where S_{wi} is the irreducible water saturation, S_{gr} is the residual gas saturation, and S_g^* is the effective saturation of gas phase.

When water and gas flow co-exist in fracture, the concept of absolute permeability should be modified and relative permeability should be used. Mathematically, relative permeability is defined as the ratio of effective permeability of one phase at a specific saturation to the absolute permeability. In this research, the relative permeabilities of water and gas phases are expressed in the forms of (Brooks and Corey, 1966):

$$k_{rw} = S_w^{*(3+2/\lambda)} \tag{2-18}$$

$$k_{rg} = S_g^{*2}\left[1-\left(1-S_g^{*}\right)^{(1+2/\lambda)}\right] \tag{2-19}$$

Fig. 2-1 and Fig. 2-2 show the typical capillary pressure curve and relative permeability curves for water-gas two-phase flow in porous media.

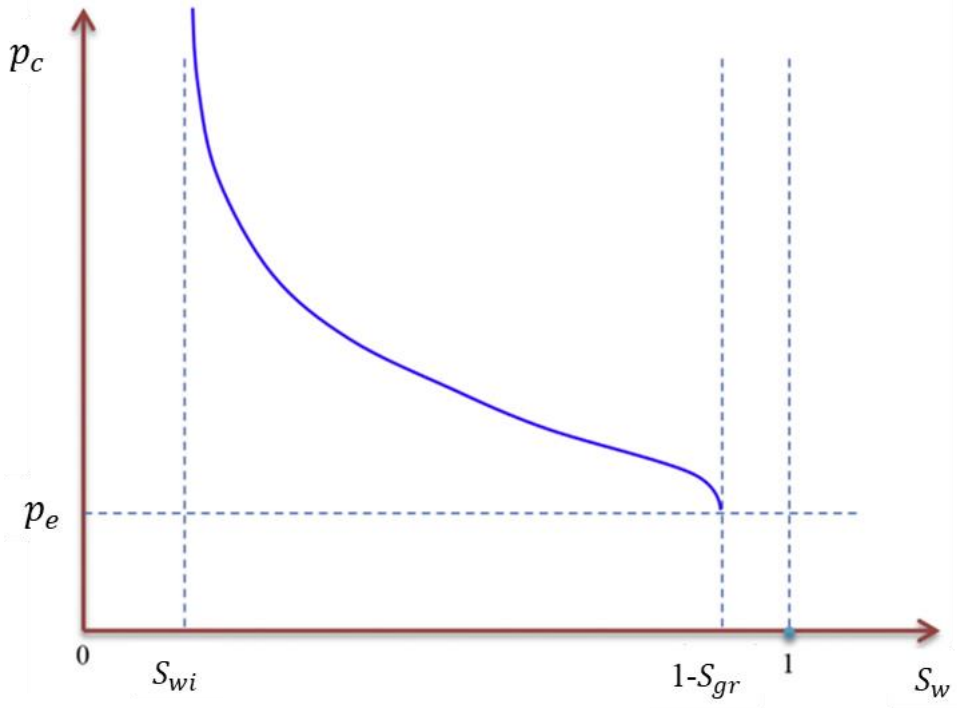

Fig. 2-1 Capillary pressure curve for water-gas two-phase flow in porous media (Cao et al., 2017).

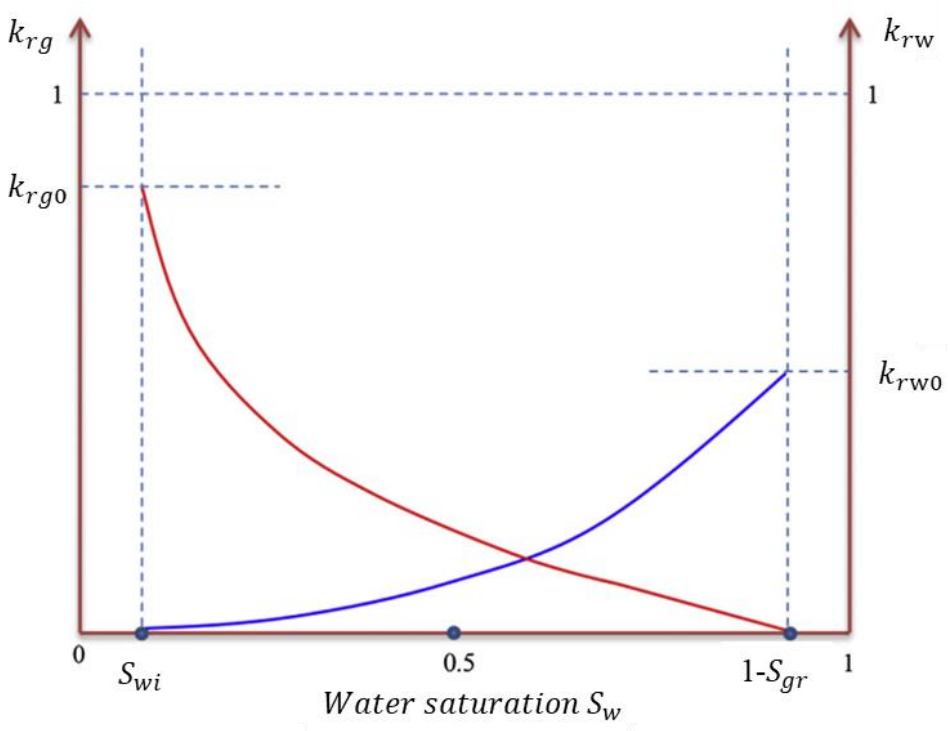

Fig. 2-2 Relative permeability curves for water-gas two-phase flow in porous media (Cao et al., 2017).

For matrix system, we consider gas mass transfer and adsorption processes (Le et al., 2020; Zhu et al., 2020). Then, we can get the flow equation for matrix by use of the mass conservation law:

$$\frac{\partial(m_{mg})}{\partial t} + \nabla \cdot \left(\rho_{gm} \cdot \frac{-k_m}{\mu_g} \nabla p_m \right) = Q_{fm} \tag{2-20}$$

where $m_{mg} = \emptyset_m \rho_{gm} + \rho_{ga} \rho_c \frac{V_L p_m}{p_m + P_L}$ represents gas mass content in coal matrix including both the free phase gas and adsorbed gas, $\emptyset_m$ is matrix porosity, ρ_{gm} is gas density in matrix, ρ_{ga} is gas density at the standard condition, ρ_c is coal density, V_L is Langmuir volume constant which represents gas sorption volume at the infinite pore pressure, and k_m is matrix permeability.

When gas pressures are different in fracture and matrix systems, gas mass transfer occurs between fracture and matrix under the pressure difference. The term for gas mass transfer from fracture to matrix can be defined as (Lim and Aziz, 1995):

$$Q_{fm} = a\rho_{gm}\frac{k_m}{\mu_g}(p_{fg} - p_m) \tag{2-21}$$

where a is the fracture-matrix transfer shape factor which depends on the type of the models selected for the dual porosity media. By using different models, the values of the shape factor will also be different. The difference is mainly caused by different assumptions in flow geometries or boundary conditions in the derivation of these models. Currently, the models proposed by Warren and Root (1963), Kazemi (1969) and Lim and Aziz (1995) are the most frequently used. In this research, we adopt the model proposed by Lim and Aziz (1995) to describe gas mass transfer process between fracture and matrix:

$$a = \pi^2\left(\frac{1}{L_x^2} + \frac{1}{L_y^2} + \frac{1}{L_z^2}\right) \tag{2-22}$$

where L_x, L_y, L_z represent fracture spacing in three orthogonal directions.

As can be summarized here, Eqs. (2-11), (2-12) and (2-20) jointly define the fluid flow behavior in dual porosity sorbing porous media. For single porosity porous media, water-gas two-phase flow can be described by Eqs. (2-11) and (2-12). Note that the gas mass transfer term in Eq. (2-12) should be deleted in this case.

2.2.3 Reactive transport

In porous media, the movement of dissolved species in the water phase is controlled by advective-dispersive transport. Applying the mass conservation law, the transport equations for dissolved species can be written as (Rockhold et al., 2004; Li et al., 2011):

$$\frac{\partial(\emptyset_f S_w C_i)}{\partial t} = \nabla\cdot(\emptyset_f S_w D_i \nabla C_i) - \nabla\cdot(v_w C_i) + R_i \tag{2-23}$$

where C_i represents the concentration of a given dissolved species in aqueous phase which can be nutrients, microbes, bioproducts or any other substances, D_i is the hydrodynamic dispersion coefficient of a given dissolved species in aqueous phase, v_w

is the water flow velocity, and R_i is the reaction source term of a given dissolved species in aqueous phase.

The term on the left hand side of Eq. (2-23) corresponds to the accumulation of dissolved species within the water phase. On the right hand side of Eq. (2-23), the first term and second term correspond to the advection and dispersion of dissolved species in the water phase, respectively.

It should be noted that the hydrodynamic dispersion of dissolved species consists of two processes: molecular diffusion and mechanical dispersion (Zhi et al., 2018). Molecular diffusion represents the process by which dissolved species move from the areas of higher chemical potentials to the areas of lower chemical potentials. Mechanical dispersion is a more complex process which is caused by mixing within the porous media. When water molecules flow through the porous media, they can move at different velocities. Some are faster than the average velocity while some are slower. The friction on pore surface, the variation of pore size and the difference in path length are the three main causes for this phenomenon (Fetter, 2018). As water molecules are not moving at the same velocity, mixing occurs along the flow path. This mixing process is termed mechanical dispersion. Further, the mixing that occurs parallel to the direction of water flow is termed as longitudinal dispersion while the mixing that occurs normal to the direction of water flow is termed as transverse dispersion. Normally, the longitudinal dispersivity exceeds the transverse dispersivity from up to an order of magnitude. As molecular diffusion is driven by concentration gradient alone, the rate of molecular diffusion is lower than mechanical dispersion, except that the water flow velocity is very low.

As hydrodynamic dispersion consists of molecular diffusion and mechanical dispersion,

the hydrodynamic dispersion coefficient can then be defined as below:

$$D_i = D_i^{dif} + D_i^{dis} \tag{2-24}$$

where D_i^{dif} represents the molecular diffusion coefficient, and D_i^{dis} represents the mechanical dispersion coefficient.

In porous media, molecular diffusion cannot proceed as fast as it can in the water as molecules can bounce around the rock grain surfaces when pass by. In order to account for this effect, the molecular diffusion coefficient is defined as:

$$D_i^{dif} = \tau D^0 \tag{2-25}$$

where τ is the porous media tortuosity factor, and D^0 is the molecular diffusion coefficient of dissolved species in free water.

As the longitudinal dispersivity typically exceeds the transverse dispersivity from up to an order of magnitude, we only consider the effect of longitudinal dispersivity in this research. Therefore, we can get mechanical dispersion coefficient in the form of:

$$D_i^{dis} = \alpha_L v \tag{2-26}$$

where α_L is the longitudinal dispersivity, and v is the average linear velocity of the aqueous phase.

2.2.4 Mineral dissolution/precipitation

When dissolved species transport in the porous media, some chemical reactions may occur between the dissolved species and the minerals in the rock. These reactions can lead to mineral dissolution or precipitation. In this process, the concentration of minerals change with time (Wang and Jaffe, 2004):

$$\frac{\partial\left[\left(1-\emptyset_f\right)C_j^s\right]}{\partial t} = R_j \tag{2-27}$$

where C_j^S represents the concentration of a given mineral phase in the rock, and R_j is the reaction source term of a given mineral phase.

2.2.5 Microbial activities

Traditionally, it is assumed that microbes in porous media live in two different forms: suspended in the water phase and/or adsorbed on the pore surface (Ginn et al., 2002).

For these microbes suspended in the water phase, they will be transported through porous media with water flow and this process is called convection. Meanwhile, hydrodynamic dispersion plays a significant role as well. In this research, we consider the convection and hydrodynamic dispersion of microbes in the water phase as well as the impacts of adsorption/desorption and growth/decay on microbial transport. The convection and hydrodynamic dispersion of microbes in the water phase can be described using Eq. (2-23) while the impacts of adsorption/desorption and growth/decay on microbial transport in the water phase can be described through adding a source term on the right hand side of Eq. (2-23).

For these microbes adsorbed on the pore surface, biofilm models are usually used to represent it. In this research, we assume that microbes living on the pore surface exist in the form of continuous uniform biofilm covering the surface of rock grains. Meanwhile, it is assumed that the change of hydraulic properties of porous media is attributed to the volume fraction occupied by these microbes adsorbed on the pore surface and to the subsequent growth of biofilm on the pore surface (Li et al., 2011). This research does not consider the change of hydraulic properties due to suspended microbes in the water phase that may also represent sizable fraction of the pore space. On the basis of these assumptions and applying the mass conservation law, the governing equations for microbes adsorbed reversibly and irreversibly on the pore

surface can be obtained as below:

$$\frac{\partial(\rho_m \emptyset_1)}{\partial t} = k_1 \emptyset_f S_w C_m - k_2 \rho_m \emptyset_1 + (g_1 - d_1)\rho_m \emptyset_1 \quad (2\text{-}28)$$

$$\frac{\partial(\rho_m \emptyset_2)}{\partial t} = k_3 \emptyset_f S_w C_m + (g_1 - d_1)\rho_m \emptyset_2 \quad (2\text{-}29)$$

where ρ_m is the microbial density, C_m is the microbial concentration in the water phase, $\emptyset_1$ is the porosity occupied by these microbes adsorbed reversibly on the pore surface, $\emptyset_2$ is the porosity occupied by these microbes adsorbed irreversibly on the pore surface, k_1 is the reversible microbial adsorption rate on the pore surface, k_2 is the microbial desorption rate on the pore surface, k_3 is the irreversible microbial adsorption rate on the pore surface, g_1 is the microbial growth rate, and d_1 is the microbial decay rate. The microbial adsorption and desorption processes in porous media are depicted in Fig. 2-3.

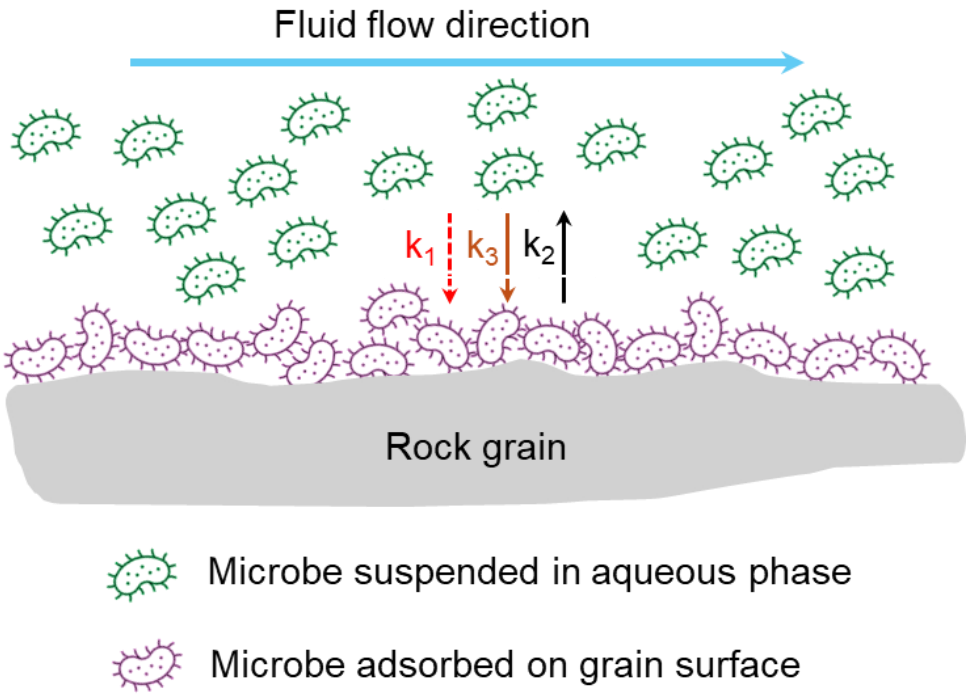

Fig. 2-3 Schematic diagram of microbial adsorption and desorption processes in porous media.

From the above two equations, it can be known that microbial activities on the pore

surface involve microbial adsorption/desorption and growth/decay. Microbial adsorption can be further classified into reversible adsorption and irreversible adsorption. Under the combined effects of these activities, microbial clogging of pore space occurs and the hydraulic properties of rock are changed. The reduction of rock porosity as a result of microbial clogging is defined as:

$$\emptyset_{bc} = \emptyset_1 + \emptyset_2 \tag{2-30}$$

where $\emptyset_{bc}$ represents the fraction of porosity occupied by these microbes adsorbed on the pore surface.

In Eqs. (2-28) and (2-29), the parameters including reversible microbial adsorption rate k_1, microbial desorption rate k_2, irreversible microbial adsorption rate k_3 and microbial decay rate d_1 are usually treated as constants (Li et al., 2011; Sivasankar and Kumar, 2014; Sivasankar and Kumar, 2019; Chakraborty et al., 2020) while the microbial growth rate g_1 is defined as a function of nutrients/substrates concentration. The mathematical model that is most frequently used to describe microbial growth is the Monod equation:

$$g_1 = g_{1max} \frac{C_n}{K_{n/s} + C_n} \tag{2-31}$$

where g_{1max} is the maximum microbial growth rate, C_n is the concentration of rate-limiting nutrients/substrates, and $K_{n/s}$ represents the nutrients concentration at which the microbial growth rate reaches half of its maximum value. It should be noted that Eq. (2-31) relates the microbial growth rate to a limiting substrate. When microbial growth is controlled by multiple substrates, double Monod equation or even triple Monod equation can be used.

2.2.6 Rock porosity and permeability

During gas energy extraction/storage, reservoir porosity and permeability can be influenced by many factors. In this subsection, reservoir porosity and permeability models that consider the impacts of these factors are developed. It should be noted that for dual porosity porous media the porosity and permeability models are developed for the fracture system as the micro-porous matrix system has negligible contribution to the permeability (Cui and Bustin, 2005).

Considering a dual porosity sorbing porous media containing solid volume V_s and fracture volume V_f, we can have the bulk volume $V = V_s + V_f$ and the rock porosity $\emptyset_f$ can be defined:

$$\emptyset_f = \frac{V_f}{V} \tag{2-32}$$

Then, the change of rock porosity can be expressed as:

$$d\emptyset_f = d\left(\frac{V_f}{V}\right) = \frac{V_f}{V}\left(\frac{dV_f}{V_f} - \frac{dV}{V}\right) \tag{2-33}$$

Substituting Eq. (2-32) into Eq. (2-33) and rearranging yields:

$$\frac{d\emptyset_f}{\emptyset_f} = \frac{dV_f}{V_f} - \frac{dV}{V} \tag{2-34}$$

According to Cui and Bustin (2005), the bulk volumetric strain and fracture volumetric strain can be obtained:

$$\frac{dV}{V} = -\frac{1}{K}\left[d\bar{\sigma} - \left(1 - \frac{K}{K_m}\right)dp\right] + d\varepsilon_s \tag{2-35}$$

$$\frac{dV_f}{V_f} = -\frac{1}{K_f}d\bar{\sigma} - \left(\frac{1}{K_f} - \frac{1}{K_m}\right)dp + d\varepsilon_s \tag{2-36}$$

Inserting Eqs. (2-35) and (2-36) into Eq. (2-34), it gives:

$$\frac{d\emptyset_f}{\emptyset_f} = \left(\frac{1}{K} - \frac{1}{K_f}\right)(d\bar{\sigma} - dp) \tag{2-37}$$

Assuming the constant K and K_f, integrating Eq. (2-37) with time yields:

$$\emptyset_f = \emptyset_{f0} exp\left\{\left(\frac{1}{K} - \frac{1}{K_f}\right)[(\bar{\sigma} - \bar{\sigma}_0) - (p - p_0)]\right\} \quad (2\text{-}38)$$

where $\bar{\sigma}$ represents the mean compressive stress, and the subscript "0" represents the initial value of the corresponding parameter.

Because the bulk modulus K is commonly several orders of magnitude larger than the fracture modulus K_f, we can obtain $\frac{1}{K} - \frac{1}{K_f} \approx -\frac{1}{K_f}$ and $c_f = \frac{1}{K_f}$ is defined as the fracture compressibility. Then, Eq. (2-38) can be simplified into:

$$\emptyset_f = \emptyset_{f0} exp\{-c_f[(\bar{\sigma} - \bar{\sigma}_0) - (p - p_0)]\} \quad (2\text{-}39)$$

Apart from effective stress and gas sorption, rock permeability can also be influenced by microbial clogging, mineral dissolution and precipitation and other factors. The impacts of these factors can be included into the rock porosity model as well:

$$\emptyset_f = \emptyset_{f0} exp\{-c_f[(\bar{\sigma} - \bar{\sigma}_0) - (p - p_0)]\} - \emptyset_{bc} + \emptyset_d - \emptyset_p \quad (2\text{-}40)$$

where $\emptyset_d$ represents the porosity change induced by mineral dissolution, and $\emptyset_p$ represents the porosity change induced by mineral precipitation. For single porosity porous media like sandstone, rock permeability can then be obtained by applying the Kozeny law on the basis of Eq. (2-40).

Dividing both sides of Eq. (2-40) by $\emptyset_{f0}$, rock porosity ratio can be obtained:

$$\frac{\emptyset_f}{\emptyset_{f0}} = exp\{-c_f[(\bar{\sigma} - \bar{\sigma}_0) - (p - p_0)]\} - \frac{\emptyset_{bc}}{\emptyset_{f0}} + \frac{\emptyset_d - \emptyset_p}{\emptyset_{f0}} \quad (2\text{-}41)$$

For dual porosity porous media like coal, cubic relation is typically used to relate permeability ratio with porosity ratio:

$$\frac{k_f}{k_{f0}} = \left\{exp\{-c_f[(\bar{\sigma} - \bar{\sigma}_0) - (p - p_0)]\} - \frac{\emptyset_{bc}}{\emptyset_{f0}} + \frac{\emptyset_d - \emptyset_p}{\emptyset_{f0}}\right\}^3 \quad (2\text{-}42)$$

2.2.7 Initial and boundary conditions

In order to solve the above governing equations, appropriate initial and boundary

conditions are still required.

For initial conditions, the initial rock displacement, the initial water and gas saturations and pressures, the initial concentrations of dissolved species, the initial concentrations of minerals, and the initial population of microbes adsorbed on the pore surface need to be known.

For boundary conditions, the mechanical boundary conditions, the fluid flow boundary conditions, and the concentration boundary conditions need to be applied.

For mechanical boundary conditions, the displacement and confining pressure/stress on each boundary need to be known.

For fluid flow boundary conditions, the water/gas pressure, saturation and/or flux on each boundary need to be known.

For concentration boundary conditions, the concentration and/or flux of each dissolved species on each boundary need to be known.

When all the required governing equations and initial and boundary conditions are prepared, the research question can be numerically solved. In our research, the whole set of governing equations are solved on the Comsol Multiphysics platform. This software automatically defines a solution sequence for the simulation based on the selected physics and the study type.

2.3 Conclusions

In this chapter, a generic coupled hydraulic-mechanical-chemical-biological multiphysics model is developed. In this model, different processes including rock deformation, fluid flow, reactive transport, mineral dissolution/precipitation, and microbial activities can be captured. For rock deformation, the impacts of effective

stress and gas sorption are considered. For fluid flow, water-gas two-phase flow in fracture and gas flow and sorption in matrix are considered. For reactive transport, the impacts of convection and hydrodynamic dispersion on the movement of solutes in the water phase are considered. For mineral dissolution/precipitation, it leads to both the change of mineral concentration and solutes concentration. For microbial activities, the adsorption/desorption and growth/decay of microbes on fracture/pore surface are considered. All these processes are linked together through the rock porosity and permeability models. Through applying different initial and boundary conditions, this multiphysics model can be used to simulate different gas energy extraction/storage scenarios.

Chapter 3 Impacts of microbial activities on biogenic methane extraction from coal seams

Biogenic methane can be generated in situ through introducing nutrients solution, either with or without microbes, into coal seams. Under the nutrient-rich condition, metabolic activities of the introduced or naturally occurring microbes are stimulated and then organic components in coal can be microbially decomposed into biogenic methane. In this process, some microbes may adsorb and grow on the fracture surface. The adsorption and growth of microbes on fracture surface can lead to microbial clogging of the fracture system. Once fracture clogging occurs, subsequent nutrients solution injection and biogenic methane extraction will be hindered. In this chapter, the generic geo-multiphysics model is tailored to the case of biogenic methane generation and extraction in coal seams under the influence of microbial clogging. A set of partial differential equations are defined to describe the processes involved: (1) coal deformation; (2) water-gas two-phase flow; (3) multispecies reactive transport; and (4) microbial adsorption/desorption and growth/decay. This multiphysics model is verified against laboratory data available in the literatures. The verified model is then used to model various important processes involved during biogenic methane generation and extraction. The simulation results indicate that (1) nutrients injection can lead to microbial clogging of fracture while water injection can play the declogging role. Thus, repeated cycles of nutrients alternating water injection can ensure sustainable biogenic CBM generation and extraction; (2) coal-to-methane bioconversion not only can generate additional biogenic methane but also has the great potential to enhance gas flow capacity in coal seams; (3) In each cycle of nutrients alternating water injection, biogenic CBM generation rate exhibits inverted-V shape variation trend while

extraction rate exhibits inverted-W shape variation trend; and (4) biogenic methane extraction efficiency, defined as the ratio of extraction rate to generation rate, gradually increases with the progress of coal-to-methane bioconversion.

3.1 Introduction

Coalbed methane (CBM) can be generated through either thermogenic or biogenic processes in coal seams. Thermogenic methane is generated through thermal cracking of organic matter under the elevated temperature and pressure conditions while biogenic methane is generated as a result of microbial degradation of organic matter (Park and Liang, 2016; Strapoc et al., 2011). Studies have suggested that approximately 20% of global natural gas resources could be microbial in origin (Rice and Claypool, 1981) with over 33 CBM basins around the world having identified the existence of biogenic gas (Strapoc et al., 2011). This discovery has aroused great interests in developing microbial stimulation techniques in aim to enhance CBM recovery. Taking cue from the successful application of microbial-enhanced oil recovery (MEOR) technique in the oil industry, Scott (Scott, 1999) proposed the concept of microbially enhanced coalbed methane (MECBM) recovery. The MECBM concept aims to convert organic matter in coal into biogenic methane through introducing nutrients, either with or without microbes, into coal seams. Since then, this concept has been investigated from both experimental and theoretical perspectives.

However, it can be known from the literature review in section 1.3.1 that the impact of microbial activities on biogenic methane generation and extraction under the in-situ fluid flowing conditions are rarely theoretically investigated. In this work, the impact of microbial adsorption (an interesting phenomenon that has been observed in the laboratory as shown in Fig. 3-1) and growth induced fracture clogging on biogenic

methane generation and extraction under the in-situ fluid flowing conditions is investigated through the development of a coupled hydrological-mechanical-chemical-biological multiphysics model. In the following, the conceptual model for coal-to-methane bioconversion is first introduced. Then, governing equations for the coupled processes are defined. After that, model verifications against laboratory data available in the literatures are conducted. Finally, the impact of microbial clogging on biogenic methane generation and extraction is analyzed.

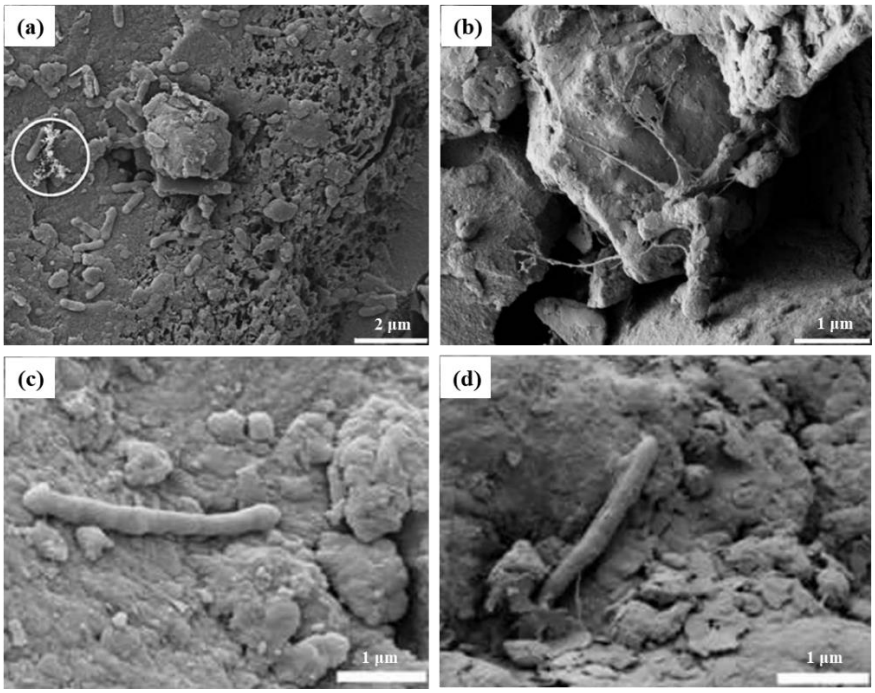

Fig. 3-1 Laboratory observation of microbes adsorbed on coal particle surface during coal-to-methane bioconversion (Stephen et al., 2014).

3.2 The conceptual model

During microbial stimulation of coal seams, the nutrients solution, either with or without microbes, is injected into the target zones using the produced formation water from other parts of the field in a recirculation process in order to have little to no net water removal from underground coal seams (Ritter et al., 2015). When pumped into the formation, the water-based nutrients solution transport in the fracture system as coal

matrix nanopores are considered inaccessible to water due to their small dimensions (King et al., 1986). Meanwhile, microbes also inhabit in the fracture system as coal matrix nanopores (typically less than 50 nm in diameter) are usually too small for microbes (typically 1000 to 3000 nm in size) to live (Scott, 1999). Under the nutrient-rich condition, the growth and metabolic activities of microbes are stimulated and then the organic components in coal can be microbially decomposed. In this process, biogenic methane along with various other metabolic products are generated. Therefore, water-gas two-phase flow presents in the fracture system during coal-to-methane bioconversion, with nutrients, microbes and metabolic products dissolved in the aqueous phase, see Fig. 3-2. As nutrients injection pressure is typically greater than the initial formation pressure, a portion of the generated biogenic methane will diffuse into coal matrix, adsorb on coal grains, and become adsorbed gas under the pressure difference between fracture and matrix systems.

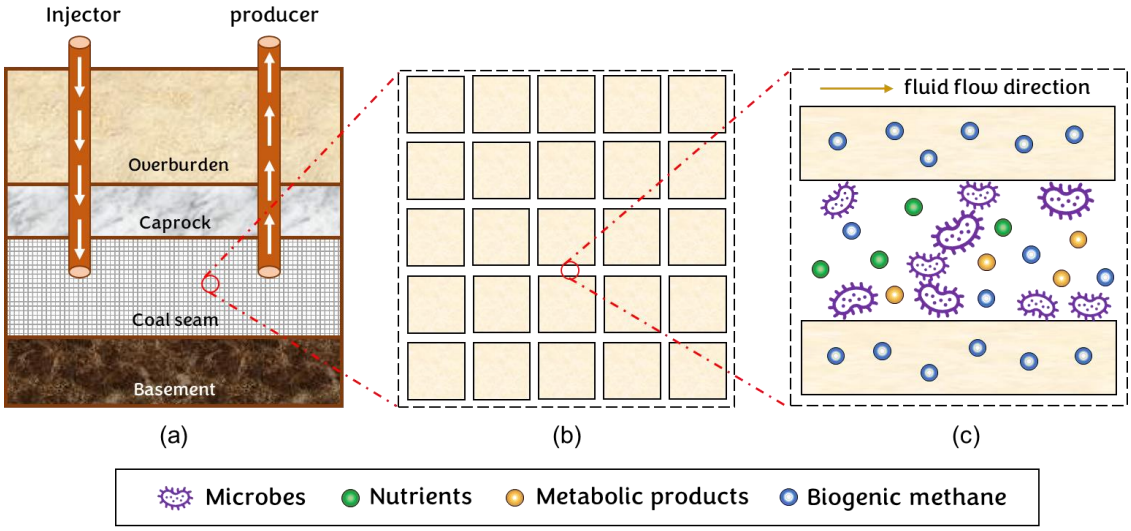

Fig. 3-2 Processes involved during coal-to-methane bioconversion: (a) nutrients solution injection and biogenic methane extraction; (b) fracture-matrix network in coal seam; and (c) multispecies reactive transport in the fracture.

During coal-to-methane bioconversion, the permeability of coal dynamically changes. The evolution of coal permeability is assumed to be influenced by three main factors

including effective stress, microbial clogging and coal solubilization. Specifically, when nutrients solution is injected into coal seams, the decline of effective stress will lead to coal permeability increase. Meanwhile, microbial activities will be stimulated by the injected nutrients. Some microbes will adsorb and then grow on the fracture surface, occupy a fraction of fracture porosity, and lead to fracture clogging and associated coal permeability decline. But on the other hand, these microbes adsorbed on the fracture surface will induce coal solubilization (i.e., convert coal into biogenic methane), widen the fracture aperture, and lead to coal permeability increase. Whether the ultimate coal permeability will be greater or less than the initial value depends on the net influences of these factors. Here, it should be noted that in this work we assume that only the microbes adsorbed on the fracture surface contribute to coal porosity/permeability change while these microbes suspended in the aqueous phase do not make any modification of coal porosity/permeability.

When fracture system is fully bioclogged, nutrients solution cannot be further injected into coal seams and biogenic methane cannot be extracted from coal seams as well. Under this condition, declogging operation should be undertaken to recover coal porosity/permeability and biogenic methane extraction. To this end, nutrients solution injection should be suspended and replaced by water injection. The reason why water injection can aid the declogging of fracture system is given in section 3.5.2.2 and will not be discussed here. When bioclogged fracture space is released, water injection ends and nutrients solution injection restarts. In this work, we name this injection scheme as “nutrients alternating water injection”. This injection scheme can ensure long-term generation and extraction of biogenic methane.

3.3 Governing equations for the coupled processes

In this section, we translate the conceptual model as described above into the mathematical model. The mathematical model couples the involved hydrological, mechanical, chemical and biological processes together. The coupled processes imply that one physical process affects the initiation and progress of another. The individual process, in absence of cross-couplings, forms the basis of different disciplines such as hydrology, mechanics, chemistry, and biology. Therefore, the inclusion of cross-coupling relations among these multiple processes is the key to mathematically describe biogenic methane generation and extraction processes in coal seams.

3.3.1 Coal deformation

In this subsection, all equations are derived after the traditional conventions: A comma followed by subscripts represents the differentiation with respect to spatial coordinates, and the repeated indices in the same expression imply the summation over the range of the indices (commonly 1-3, unless otherwise specified).

Following the above conventions, the stress equilibrium equation ignoring the inertial term can be expressed as:

$$\sigma_{ij,j} + f_i = 0 \tag{3-1}$$

where σ_{ij} represents the stress tensor component, and f_i represents the body force component.

The displacement-strain relationship can be expressed as:

$$\varepsilon_{ij} = \frac{1}{2}\left(u_{i,j} + u_{j,i}\right) \tag{3-2}$$

where ε_{ij} represents the strain tensor component, and u_i represents the displacement component.

For solid coal, gas adsorption is supposed to only induce volumetric strain which means

that its effects on all three normal strains are the same. Through making the analogy between thermal expansion and gas adsorption, the stress-strain relationship for deformable coal can be expressed as:

$$\varepsilon_{ij} = \frac{1}{2G}\sigma_{ij} - \left(\frac{1}{6G} - \frac{1}{9K}\right)\sigma_{kk}\delta_{ij} + \frac{\alpha p_f}{3K}\delta_{ij} + \frac{\beta p_m}{3K}\delta_{ij} + \frac{\varepsilon_s}{3}\delta_{ij} \qquad (3\text{-}3)$$

where $G = E/2(1+v)$, $K = E/3(1-2v)$, $\sigma_{kk} = \sigma_{11} + \sigma_{22} + \sigma_{33}$, $\alpha = 1 - K/K_m$, and $\beta = 1 - K_m/K_s$. G is shear modulus, K is bulk modulus, E is elastic modulus, v is Poisson's ratio, δ_{ij} is Kronecker delta, p is pore pressure with the subscript "f" representing fracture and the subscript "m" representing matrix, ε_s is gas adsorption induced strain which is commonly defined as a function of gas pressure $\frac{\varepsilon_L p_b}{p_b + P_L}$, ε_L is the Langmuir strain of coal, P_L is the Langmuir pressure of coal, p_b is the gas pressure in coal bulk which is defined as $(1-\emptyset_f)p_m + \emptyset_f p_f$, and $\emptyset_f$ is fracture porosity.

Integrating Eqs. (3-1) to (3-3), the Navier-type equation for coal deformation can be derived:

$$Gu_{i,kk} + \frac{G}{1-2v}u_{k,ki} - \alpha p_{f,i} - \beta p_{m,i} - K\varepsilon_L \frac{p_L}{(p_b + p_L)^2}p_{b,i} + f_i = 0 \qquad (3\text{-}4)$$

In this Navier-type equation, the parameters p_f and p_m are linked to the fluid flow equations. As gas-water two-phase flow presents in the fracture system during coal bioconversion, the fracture pressure p_f should be defined as the average pressure of water and gas phases, i.e., $p_f = S_w p_{fw} + S_g p_{fg}$. In this expression, S_w and S_g represent water and gas saturations in fracture, respectively. p_{fw} and p_{fg} represent water and gas pressures in fracture, respectively.

3.3.2 Fluid flow in coal

3.3.2.1 Water-gas two-phase flow in fracture

We consider a water-wet fractured coal with fracture system fully occupied by water and gas two phases. These two phases are assumed to be immiscible with each phase having the constant viscosity and density. The mass balance equations for water and gas are defined as below:

$$\frac{\partial(\emptyset_f S_w \rho_w)}{\partial t} = \nabla \cdot \left(\rho_w \cdot \frac{k_f k_{rw}}{\mu_w} \nabla p_{fw}\right) + Q_w \quad (3\text{-}5)$$

$$\frac{\partial(\emptyset_f S_g \rho_{gf} + V_{bg} \cdot (1 - \emptyset_{ns} - \emptyset_s) \cdot \rho_c \cdot \rho_{ga})}{\partial t} = \nabla \cdot \left(\rho_{gf} \cdot \frac{k_f k_{rg}}{\mu_g} \nabla p_{fg}\right) - Q_{fm} + Q_g \quad (3\text{-}6)$$

where $\emptyset_f$ and k_f are fracture porosity and permeability, respectively; S_w and S_g are water and gas saturations, respectively; ρ_w and ρ_{gf} are water and gas densities in fracture, respectively; μ_w and μ_g are water and gas viscosities, respectively; k_{rw} and k_{rg} are water and gas relative permeabilities, respectively; p_{fw} and p_{fg} are water and gas pressures in fracture, respectively; Q_w and Q_g are water and gas source/sink terms, respectively; and Q_{fm} is the gas mass transfer term representing gas mass transfer from fracture to matrix.

It should be further explained that the term $V_{bg} \cdot (1 - \emptyset_{ns} - \emptyset_s) \cdot \rho_c \cdot \rho_{ga}$ in Eq. (3-6) defines the total mass of biogenic methane that can be generated per unit volume of coal during microbial stimulation. In this term, V_{bg} represents the volume of biogenic methane that can be generated per unit mass of coal; $\emptyset_s$ represents the degradable fraction of coal that can be converted into biogenic methane; $\emptyset_{ns}$ represents the fraction of coal that cannot be converted; ρ_c is coal density; and ρ_{ga} is gas density at the standard condition.

In order to solve these four variables S_w, S_g, p_{fw}, and p_{fg} in Eqs. (3-5) and (3-6), supplementary relations for phase saturation and capillary pressure are required. In the fully saturated coal fracture system, the total saturation of water and gas should be equal to one:

$$S_w + S_g = 1 \tag{3-7}$$

As water and gas are assumed to be immiscible, these two phases should be separated by a well-defined interface. The interface is characterized by some surface tension which leads to the pressure difference between water and gas phases. The pressure difference between water and gas phases is called capillary pressure:

$$p_c = p_{fg} - p_{fw} \tag{3-8}$$

where p_c is capillary pressure which is defined as the difference between non-wetting phase pressure and wetting phase pressure.

Previous studies have found that capillary pressure is also closely related to the wetting phase saturation. In this work, Brooks and Corey formulation (Brooks and Corey, 1966) is used to represent this relation:

$$p_c = p_e {S_w^*}^{-1/\lambda} \tag{3-9}$$

where p_e is the non-wetting phase entry pressure, S_w^* is effective water saturation, and λ is the parameter related to pore size distribution.

The effective water and gas saturations are defined as below:

$$S_w^* = \frac{S_w - S_{wi}}{1 - S_{gr} - S_{wi}} \tag{3-10}$$

$$S_g^* = \frac{S_g - S_{gr}}{1 - S_{gr} - S_{wi}} \tag{3-11}$$

where S_{wi} is irreducible water saturation, and S_{gr} is residual gas saturation.

Then, both water and gas relative permeabilities can be defined as a function of the effective saturations (Brooks and Corey, 1966):

$$k_{rw} = {S_w^*}^{(3+2/\lambda)} \tag{3-12}$$

$$k_{rg} = S_g^{*2}\left[1 - \left(1 - S_g^*\right)^{(1+2/\lambda)}\right] \quad (3\text{-}13)$$

In addition, gas mass transfer from fracture to matrix is controlled by gas pressure difference between the two systems:

$$Q_{fm} = a\rho_{gm}\frac{k_m}{\mu_g}\left(p_{fg} - p_m\right) \quad (3\text{-}14)$$

where $a = 4\left(\frac{1}{L_{mx}^2} + \frac{1}{L_{my}^2}\right)$ is shape factor which reflects the effect of matrix size on gas mass transfer rate; L_{mx} and L_{my} are fracture spacing in two orthogonal directions; ρ_{gm} is gas density in matrix; k_m is matrix permeability; and p_m is gas pressure in matrix.

3.3.2.2 Gas storage in matrix

Studies (Liu and Rutqvist, 2010; Gao et al., 2022) have indicated that adjacent coal matrix blocks are connected with each other through rock bridges. As rock bridge size is very small, gas mass transfer between adjacent coal matrix blocks can be neglected. Thus, it is reasonable to make the assumption that naturally fractured coal is a dual porosity single permeability porous medium. Based on this assumption, coal matrix only stores biogenic methane that is transferred from the fracture system:

$$\frac{\partial\left(\emptyset_m\rho_{gm} + \frac{V_L p_m}{p_m + P_L}(1 - \emptyset_m)\rho_c\rho_{ga}\right)}{\partial t} = Q_{f2m} \quad (3\text{-}15)$$

where $\emptyset_m$ is matrix porosity; ρ_{gm} is gas density in matrix; V_L is Langmuir volume constant; and P_L is Langmuir pressure constant.

3.3.3 Multispecies reactive transport

Coal-to-methane bioconversion involves multiple nutrient ingredients, microbes, and metabolic products. For simplification, it is assumed that the dominant reaction kinetics during coal-to-methane bioconversion can be represented by a single-lumped nutrient variable, a single-lumped microbe variable, and a single-lumped metabolic product

variable. Therefore, a three-variable multispecies reactive transport model is introduced in this work.

In naturally fractured coal, the transport of nutrients, microbes and metabolic products in aqueous phase can be defined by the advection-dispersion equations:

$$\frac{\partial(\emptyset_f S_w C_n)}{\partial t} = \nabla \cdot (\emptyset_f S_w D_n \nabla C_n) - \nabla \cdot (u_w C_n) + R_n \quad (3\text{-}16)$$

$$\frac{\partial(\emptyset_f S_w C_m)}{\partial t} = \nabla \cdot (\emptyset_f S_w D_m \nabla C_m) - \nabla \cdot (u_w C_m) + R_m \quad (3\text{-}17)$$

$$\frac{\partial(\emptyset_f S_w C_p)}{\partial t} = \nabla \cdot (\emptyset_f S_w D_p \nabla C_p) - \nabla \cdot (u_w C_p) + R_p \quad (3\text{-}18)$$

where C_n, C_m and C_p are concentrations of nutrients, microbes and metabolic products, respectively; D_n, D_m and D_p are hydrodynamic dispersion coefficients of nutrients, microbes and metabolic products, respectively; u_w is Darcy flow velocity of the aqueous phase; and R_n, R_m, R_p are the source/sink terms for reactions which are defined in the forms of:

$$R_n = -Y_s(\emptyset_f S_w C_m + \rho_m \emptyset_1 + \rho_m \emptyset_2) \quad (3\text{-}19)$$

$$R_m = -(k_1 + k_3)\emptyset_f S_w C_m + k_2 \rho_m \emptyset_1 + (g_1 - d_1)\emptyset_f S_w C_m \quad (3\text{-}20)$$

$$R_p = \mu_p(\emptyset_f S_w C_m + \rho_m \emptyset_1 + \rho_m \emptyset_2) \quad (3\text{-}21)$$

where Y_s is microbial growth yield coefficient which represents the consumption of nutrients; k_1 and k_3 are the rates for reversible and irreversible microbial adsorption to the fracture surface, respectively; k_2 is the rate for microbial desorption from the fracture surface; g_1 and d_1 are microbial growth and decay rates, respectively; μ_p is metabolic products generation rate; ρ_m is microbial density; and $\emptyset_1$ and $\emptyset_2$ are the fractions of porosity occupied by the microbes reversibly and irreversibly adsorbed on the fracture surface, respectively.

The microbial growth rate is controlled by nutrients concentration and can be defined by the widely used Monod equation (Jeong et al., 2019):

$$g_1 = g_{1max}\frac{C_n}{K_{n/s} + C_n} \tag{3-22}$$

where g_{1max} is the maximum microbial growth rate; and the half saturation constant $K_{n/s}$ represents the nutrients concentration at which the microbial growth rate reaches half of its maximum value. Clearly, the Monod equation defines a first-order relation at the low concentration condition and a zero-order relation at the high concentration condition.

3.3.4 Microbial adsorption/desorption and growth/decay

Microbial adsorption and growth on fracture surface induces microbial clogging of fracture, thereby reducing coal porosity and permeability. Traditionally, microbial adsorption in porous media is assumed to be in the form of uniform biofilm covering the pore surface (Li et al., 2011). Accordingly, in this work, coal porosity reduction magnitude is assumed to be equal to the fraction of porosity occupied by the microbes adsorbed on the fracture surface. The adsorption of microbes can be further categorized into reversible adsorption and irreversible adsorption. The mass balance equations for reversibly and irreversibly adsorbed microbes can be expressed as below (Kim, 2006):

$$\frac{\partial(\rho_m \emptyset_1)}{\partial t} = k_1 \emptyset_f S_w C_m - k_2 \rho_m \emptyset_1 + (g_1 - d_1)\rho_m \emptyset_1 \tag{3-23}$$

$$\frac{\partial(\rho_m \emptyset_2)}{\partial t} = k_3 \emptyset_f S_w C_m + (g_1 - d_1)\rho_m \emptyset_2 \tag{3-24}$$

From Eqs. (3-23) and (3-24), it can be known that the fraction of porosity occupied by the microbes adsorbed on the fracture surface dynamically changes under the combined effects of microbial adsorption, desorption, growth and decay.

Then, the reduction of coal porosity as a result of microbial clogging can be obtained:

$$\emptyset_{bc} = \emptyset_1 + \emptyset_2 \tag{3-25}$$

3.3.5 Coal porosity and permeability

During coal-to-methane bioconversion, it is assumed that fracture porosity and permeability are mainly influenced by three factors including effective stress, microbial clogging and coal solubilization. In this section, fracture porosity and permeability models that consider the joint impacts of these factors are developed.

In this work, we apply the widely used C&B model (Cui and Bustin, 2005) to describe the impact of effective stress on fracture porosity change:

$$\emptyset_f = \emptyset_{f0} exp\{-c_f[(\bar{\sigma} - p_f) - (\bar{\sigma}_0 - p_f)]\} \tag{3-26}$$

where the subscript "0" represents the initial state, c_f represents the fracture compressibility, and $\bar{\sigma}$ represents the mean compressive stress.

As microbial clogging reduces fracture porosity while coal solubilization increases fracture porosity, the final form of fracture porosity model can be derived:

$$\emptyset_f = \emptyset_{f0} exp\{-c_f[(\bar{\sigma} - p_f) - (\bar{\sigma}_0 - p_f)]\} - \emptyset_{bc} + \emptyset_s \tag{3-27}$$

where $\emptyset_{bc} = \emptyset_1 + \emptyset_2$ represents the fraction of porosity occupied by the microbes adsorbed on the fracture surface, and $\emptyset_s$ represents the fraction of porosity created through coal solubilization. In this work, it is assumed that coal solubilization rate is directly proportional to the amounts of microbes adsorbed on the fracture surface and the specific surface area of coal matrix blocks (Gao et al., 2023):

$$\frac{d\emptyset_s}{dt} = k_+ \cdot \frac{\emptyset_{bc}}{\emptyset_{bc} + K_{bc/s}} \cdot (1 - \emptyset_{f0} - \emptyset_s)^{-\frac{1}{3}} \tag{3-28}$$

where k_+ is coal solubilization rate constant, and the half saturation constant $K_{bc/s}$ represents the bioclogged fraction of porosity at which coal solubilization rate reaches

half of its maximum value. The third term on the right-hand side of this equation represents the effect of matrix size on coal solubilization.

Considering the cubic relation between fracture porosity and permeability, fracture permeability model can be obtained:

$$\frac{k_f}{k_{f0}} = \left\{ exp\{-c_f[(\bar{\sigma} - p_f) - (\bar{\sigma}_0 - p_f)]\} - \frac{\emptyset_{bc}}{\emptyset_{f0}} + \frac{\emptyset_s}{\emptyset_{f0}} \right\}^3 \quad (3\text{-}29)$$

From section 3.3.2.2, it can be known that we only consider gas sorption in coal matrix and thus only matrix porosity model needs to be given. In this work, we still use the relation proposed by Cui and Bustin (2005) to define matrix porosity change:

$$\emptyset_m = \emptyset_{m0} exp\{-c_m[(\bar{\sigma} - p_m) - (\bar{\sigma}_0 - p_m)]\} \quad (3\text{-}30)$$

where c_m represents matrix compressibility.

3.3.6 Cross coupling relations

The Eq. (3-4) for coal geomechanical deformation, the Eqs. (3-5), (3-6) and (3-15) for fluid flow, the Eqs. (3-16), (3-17) and (3-18) for multispecies reactive transport, and the Eqs. (3-23) and (3-24) for microbial activities together define the interactions among the coupled processes during coal-to-methane bioconversion. Fig. 3-3 presents the specific coupling relations among different fields. As can be seen, coal deformation impacts fluid flow through compaction of fracture/pore space. Fluid flow impacts coal deformation and reactive transport through changing effective stress and multispecies concentration distribution, respectively. Reactive transport impacts fluid flow and microbial activities through generating biogenic methane and changing microbial concentration, respectively. Microbial activities impact fluid flow and reactive transport through microbial clogging of fracture space and changing multispecies' concentrations, respectively. At this point, it can be known that the multiphysics model we build is not

fully coupled as some coupling relations are still not clear at the current stage. These interactions as shown in Fig. 3-3 are solved on the platform of Comsol Multiphysics, a commercial software that enables the solution of coupled partial differential equations.

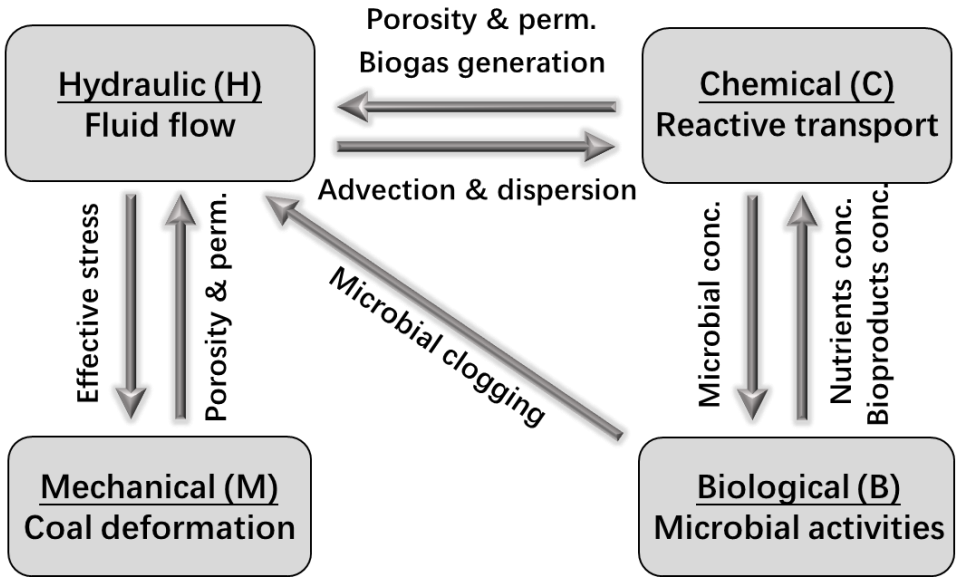

Fig. 3-3 Coupling relations among multiple processes during coal-to-methane bioconversion.

3.4 Model verification

In this section, the developed multiphysics model is verified through comparing the modeling results with the laboratory data available in the literatures. The verification consists of two parts. The first part is to verify the multiphysics model against laboratory microbial transport data reported by Hendry et al. (1997). The second part is to verify the multiphysics model against laboratory biogenic methane generation data reported by Stephen et al. (2014).

3.4.1 Verification against lab data of microbial transport

The microbial transport model that considers reversible and irreversible adsorption of microbes on pore surface along with advective and dispersive transport of microbes in aqueous phase is verified through comparing the modeling result with the experimental

data reported by Hendry et al. (1997). In their experiment, constant water flux of 6.6 cm^3/h was maintained through a 40 cm long column. This water flux is equivalent to a linear fluid velocity of 0.84 cm/h. The whole experiment consisted of two steps. In the first step, microbial suspensions of $2.4*10^7$ CFU/ml (equivalent to 4.32 mg/L) were injected through the column for the initial 38.4 hours. After introducing the microbial suspensions, ground water was then injected through the column for the following 470 hours. Effluent samples from the column outlet were collected throughout the experiment and the microbial concentration in the effluent was constantly recorded.

For verifying the microbial transport model, we also numerically simulate the variation of microbial concentration at the column outlet as a function of time. As the reported experiment data has a wide range of distribution, three different microbial growth rates as listed in Table 3-1 were used in our simulation. Fig. 3-4 shows the comparison between modeling results and experimental data. As can be seen, the simulation results can cover the experiment data distribution area which implies that our model has the capability to simulate microbial transport and adsorption process in porous medium.

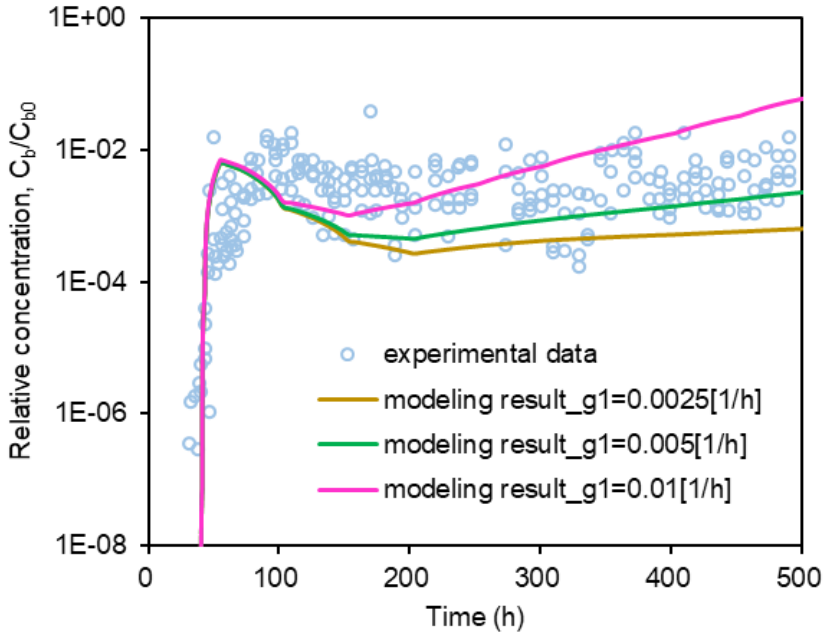

Fig. 3-4 Comparison between the numerical result and the experimental data (Hendry

et al., 1997).

Table 3-1 Input parameters for verifying the microbial transport model.

Parameters (unit)	Values
Reversible microbial adsorption rate (1/h)	0.065
Microbial desorption rate (1/h)	0.0012
Irreversible microbial adsorption rate (1/h)	0.01
The microbial growth rate (1/h)	2.5e-3/5e-3/1e-2
Microbial decay rate (1/h)	0
Microbial density (kg/m^3)	1085

3.4.2 Verification against lab data of biogenic methane generation

Laboratory biogenic methane generation data recorded by Stephen et al. (2014) are used for verifying our multiphysics model. In their core flooding experiment, crushed coal particles with the average size of 200 μm were used. These crushed coal particles were compacted in the core holder as a core. The whole experiment consisted of three steps. In the first step, three pore volumes of mineral salts medium with nutrients concentration of 5g/L were injected into the coal pack to fully saturate it, followed by the injection of 1.25 pore volumes of microbial culture. In the second step, the entire system was isolated and incubated for 14 days under the room temperature condition. This long-term incubation allows the establishment of microbial culture in the coal pack. After the incubation step, the compacted coal particles were continuously flooded with the nutrients solution once again at the rate of 0.006 ml/min to feed the microbes. In this process, effluent samples from the outlet of the core holder were collected. Each effluent sample was limited to the volume of 100 mL. Totally eight effluent samples were collected during the 90-day-long flooding cycle. Each effluent sample was then analyzed for biogenic methane generation.

Applying the multiphysic model, we also numerically simulate the biogenic methane generation behavior. In our simulation, coal porosity, permeability and injected

nutrients concentration reported by Stephen et al. (2014) are used. Other fitted and sourced parameters are summarized in Table 3-2. Fig. 3-5 shows the comparison between laboratory recorded and numerically simulated biogenic methane generation data. As can be seen, the modeling result matches the laboratory data well. This good agreement demonstrates the capability of our model on modeling biogenic methane generation.

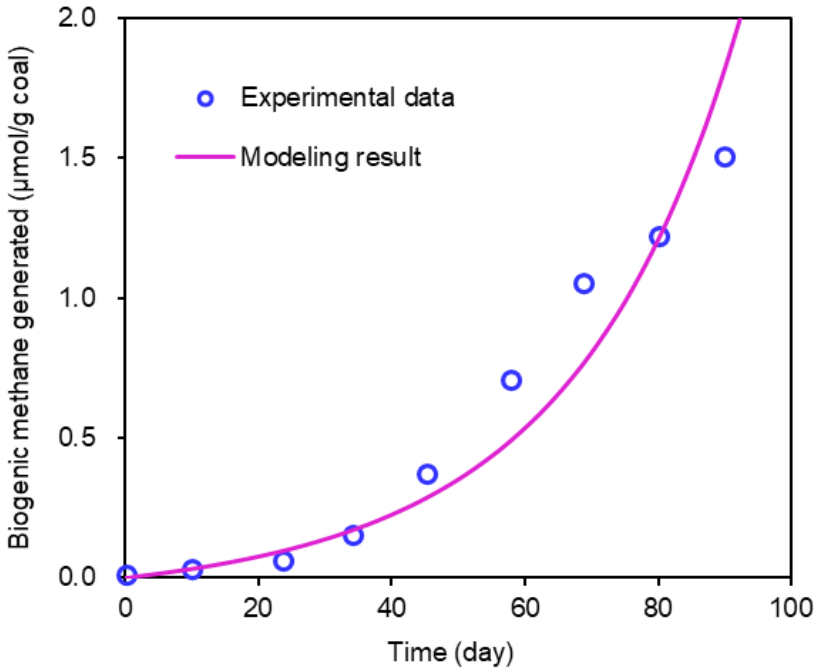

Fig. 3-5 Comparison between the numerical result and the experimental data (Stephen et al., 2014).

Table 3-2 Input parameters for verifying the multiphysics model.

Parameters (unit)	Values	References
Initial porosity	0.39	Stephen et al. (2014)
Initial permeability (m^2)	13e-15	Stephen et al. (2014)
Methane density at standard condition (kg/m^3)	0.717	Zhang et al. (2008)
Biogas volume generated per unit mass of coal (m^3/kg)	0.05	
Degradable fraction of coal	0.15	
Non-degradable fraction of coal	0.46	
Coal solubilization rate constant (m/s)	2.5e-12	
Reversible microbial adsorption rate (1/h)	0.065	Kim (2006); Li et al. (2011)

Microbial desorption rate (1/h)	0.0012	Kim (2006); Li et al. (2011)
Irreversible microbial adsorption rate (1/h)	0.01	Kim (2006); Li et al. (2011)
The maximum microbial growth rate (1/h)	0.021	Kim (2006); Li et al. (2011)
Microbial decay rate (1/h)	0.005	Kim (2006); Li et al. (2011)
Microbial density (kg/m^3)	1600	Kim (2006); Li et al. (2011)
Nutrients consumption rate (1/h)	1.2e-4	Li et al. (2011)
Metabolic products generation rate (1/h)	2.5e-4	Li et al. (2011)
Half-saturation constant for coal solubilization (mg/mL)	0.001	
Half-saturation constant for microbial growth (mg/mL)	20	Chakraborty et al. (2020)
Hydrodynamic dispersion coefficients (m^2/s)	1e-8	Kim (2006); Li et al. (2011)
Initial water saturation	1	Tian et al. (2022)
Irreducible water saturation	0.2	Tian et al. (2022)
Residual gas saturation	0	Tian et al. (2022)
Nonwetting phase entry pressure (MPa)	0.1	Tian et al. (2022)
Pore size distribution coefficient	2	Tian et al. (2022)
Initial nutrients concentration (mg/mL)	0.01	
Initial microbial concentration (mg/mL)	0.01	
Initial by-product concentration (mg/mL)	0	
Injected nutrients concentration (mg/mL)	5	
Injected microbial concentration (mg/mL)	0	

3.5 Model application and results analysis

In this section, the verified model is applied to analyze biogenic methane generation and extraction behavior. First, the geometry and the initial and boundary conditions of the numerical model is introduced. Then, the simulation results of the base case are presented and analyzed. After that, parametric studies are carried out to investigate the impacts of bioclogging-related parameters on coal-to-methane bioconversion.

3.5.1 Numerical model description

Fig. 3-6 shows the geometry and meshing of the numerical model for coal bioconversion modeling. The length and width of the model are 1 m and 0.3 m, respectively. In the center of the model, an observation point A at the location of (0.5m, 0.15m) is set to monitor the dynamic variation of coal permeability during bioconversion treatment. In order to solve the above governing equations, appropriate initial and boundary conditions are still required to be set.

For initial conditions, the initial rock displacement, the initial water pressure and saturation, the initial concentrations of nutrients, microbes and metabolic products in the aqueous phase, and the initial fraction of porosity occupied by microbes adsorbed on the fracture surface need to be set.

For boundary conditions, the mechanical boundary conditions, fluid flow boundary conditions and multispecies transport boundary conditions need to be set. For mechanical boundary conditions, the normal displacements of the left and lower sides are constrained to zero and the confining pressure is applied to the right and upper sides. For fluid flow boundary conditions, the injection pressure is set on the left side and the production pressure is set on the right side. On both the upper and lower sides, no flow is allowed. For multispecies transport boundary conditions, the concentrations of injected nutrients and microbes are specified on the left side and meanwhile the flux of metabolic products is taken as zero on this side. On the right side, the concentration gradients of nutrients, microbes and metabolic products are set as zero. On both the upper and lower sides, the fluxes of nutrients, microbes and metabolic products are specified as zero.

Combining the governing equations with the initial and boundary conditions, coal-to-methane bioconversion can be simulated. Table 3-3 provides the input parameters for the base case modeling.

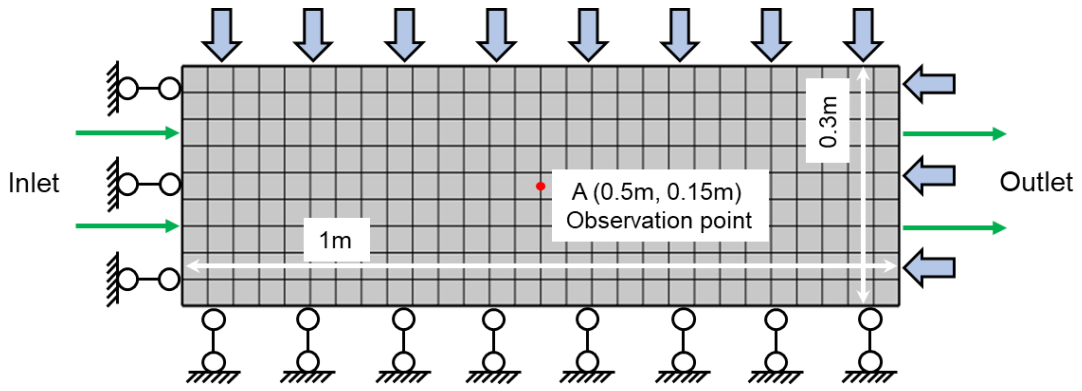

Fig. 3-6 Geometry of the numerical model for coal bioconversion modeling.

Table 3-3 Input parameters for base case analysis.

Parameter (unit)	Symbols	Value	References
Fracture compressibility (MPa^{-1})	c_f	0.09	-
Elastic modulus (GPa)	E	2.5	-
Poisson's ratio	v	0.3	-
Initial porosity of matrix	$\emptyset_{m0}$	0.08	-
Initial permeability of matrix (m^2)	k_{m0}	5e-19	-
Initial porosity of fracture	$\emptyset_{f0}$	0.03	-
Initial permeability of fracture (m^2)	k_{f0}	2e-16	-
Fracture-matrix transfer shape factor ($1/m^2$)	a	400	-
Density of coal (kg/m^3)	ρ_c	1500	Chen et al. (2013)
Methane density at standard condition (kg/m^3)	ρ_{ga}	0.717	Zhang et al. (2008)
Biogas volume generated per unit mass of coal (m^3/kg)	V_{bg}	0.05	-
Degradable fraction of coal	$\emptyset_s$	0.15	-
Non-degradable fraction of coal	$\emptyset_{ns}$	0.82	-
Coal solubilization rate constant (m/s)	k_+	1.5e-12	-
Reversible microbial adsorption rate (1/h)	k_1	0.065	Kim (2006); Li et al. (2011)
Microbial desorption rate (1/h)	k_2	0.0012	Kim (2006); Li et al. (2011)
Irreversible microbial adsorption rate (1/h)	k_3	0.01	Kim (2006); Li et al. (2011)
The maximum microbial growth rate (1/h)	g_{1max}	0.024	Kim (2006); Li et al. (2011)
Microbial decay rate (1/h)	d_1	0.005	Kim (2006); Li et al. (2011)
Microbial density (kg/m^3)	ρ_m	1600	Kim (2006); Li et al. (2011)
Nutrients consumption rate (1/h)	Y_s	1.5e-4	Li et al. (2011)
Metabolic products generation rate (1/h)	μ_p	3e-4	Li et al. (2011)
Half-saturation constant for coal solubilization (mg/mL)	$K_{mc/s}$	0.001	-
Half-saturation constant for microbial growth (mg/mL)	$K_{m/s}$	20	Chakraborty et al. (2020)
Langmuir strain of coal	ε_L	0.02	Jiang et al. (2020)
Langmuir pressure of coal (MPa)	p_L	4	Jiang et al. (2020)
Hydrodynamic dispersion coefficients (m^2/s)	D_n, D_m, D_p	1e-8	Kim (2006); Li et al. (2011)
Initial water saturation	$S_{w,0}$	1	Tian et al. (2022)
Irreducible water saturation	S_{wi}	0.2	Tian et al. (2022)
Residual gas saturation	S_{gr}	0	Tian et al. (2022)
Nonwetting phase entry pressure (MPa)	p_e	0.1	Tian et al. (2022)
Pore size distribution coefficient	λ	2	Tian et al. (2022)
Initial nutrients concentration (mg/mL)	-	0.005	-
Initial microbial concentration (mg/mL)	-	0.001	-
Initial by-product concentration (mg/mL)	-	0	-
Initial fraction of porosity occupied by microbes	-	0	-
Injected nutrients concentration (mg/mL)	-	5	-
Injected microbial concentration (mg/mL)	-	0.006	-

Confining pressure (MPa)	-	7	-
Inlet pressure (MPa)	-	4	-
Outlet pressure (MPa)	-	1	-
Initial pressure (MPa)	-	1	-

3.5.2 Base case results

In this work, we define the nutrients injection phase as the clogging phase and the subsequent water injection phase as the declogging phase. This is mainly because microbial clogging occurs due to microbial adsorption and growth on the fracture surface during the nutrients solution injection phase and then the bioclogged fracture space can be released as a result of microbial decay during the water injection phase. In the following, we will present and analyze the simulation results for both the clogging phase and the declogging phase.

3.5.2.1 Simulation results during nutrients injection

We assume that a very low concentration of nutrients (0.005 mg/mL) has been in coal before nutrients solution injection. During nutrients solution injection, a constant nutrients concentration of 5 mg/mL is applied at the inlet. The modelled spatial distribution of nutrients concentration in the aqueous phase is shown in Fig. 3-7(a). As can be seen, nutrients concentration front moves from the inlet to the outlet as the injection continues. After injection for 7 hours, nutrients concentration across the coal stabilizes at 5 mg/mL.

We assume that a very low concentration of microbes (0.001 mg/mL) has been in coal before nutrients solution injection. During nutrients solution injection, a constant microbial concentration of 0.006 mg/mL is applied at the inlet. The modelled spatial distribution of microbial concentration in the aqueous phase is shown in Fig. 3-7(b). As can be seen, microbial concentration front moves from the inlet to the outlet as the injection continues. After injection for 4 hours, microbial concentration front reaches

the outlet. After that, microbial concentration at the outlet constantly increases with time, as both the injected and newly grown microbes flow out of coal through this boundary.

We assume no biogenic methane in coal before nutrients solution injection. During nutrients solution injection, gas saturation is set as zero at the inlet. The modelled spatial distribution of gas saturation in coal is shown in Fig. 3-7(c). As can be seen, gas saturation constantly increases with time. As biogenic methane flows out of coal through the outlet, gas saturation at the outlet is always larger than that at the inlet.

During nutrients solution injection, coal permeability evolution is controlled by three factors including effective stress, coal solubilization and microbial clogging. Fig. 3-7(d) shows the response of coal permeability to these factors. As can be seen, effective stress decline and coal solubilization leads to permeability increase while microbial clogging leads to permeability decline. Under the joint impacts of these factors, coal permeability first increases and then declines. If nutrients injection continues, fracture space will be fully occupied by microbes and coal permeability will decline to zero.

Fig. 3-7(e) shows the variation of biogenic methane generation and extraction rates during nutrients injection. As can be seen, biogenic methane generation rate is not influenced by microbial clogging because the gas generation rate is controlled by the amounts of microbes adsorbed on the fracture surface as defined in Eq. (3-28). By contrast, biogenic methane extraction rate is strongly influenced by microbial clogging. Specifically, the extraction rate initially increases when coal permeability increases and then starts to decline when coal permeability declines. If nutrients injection continues, the extraction rate will continue to decline as a result of coal permeability decline.

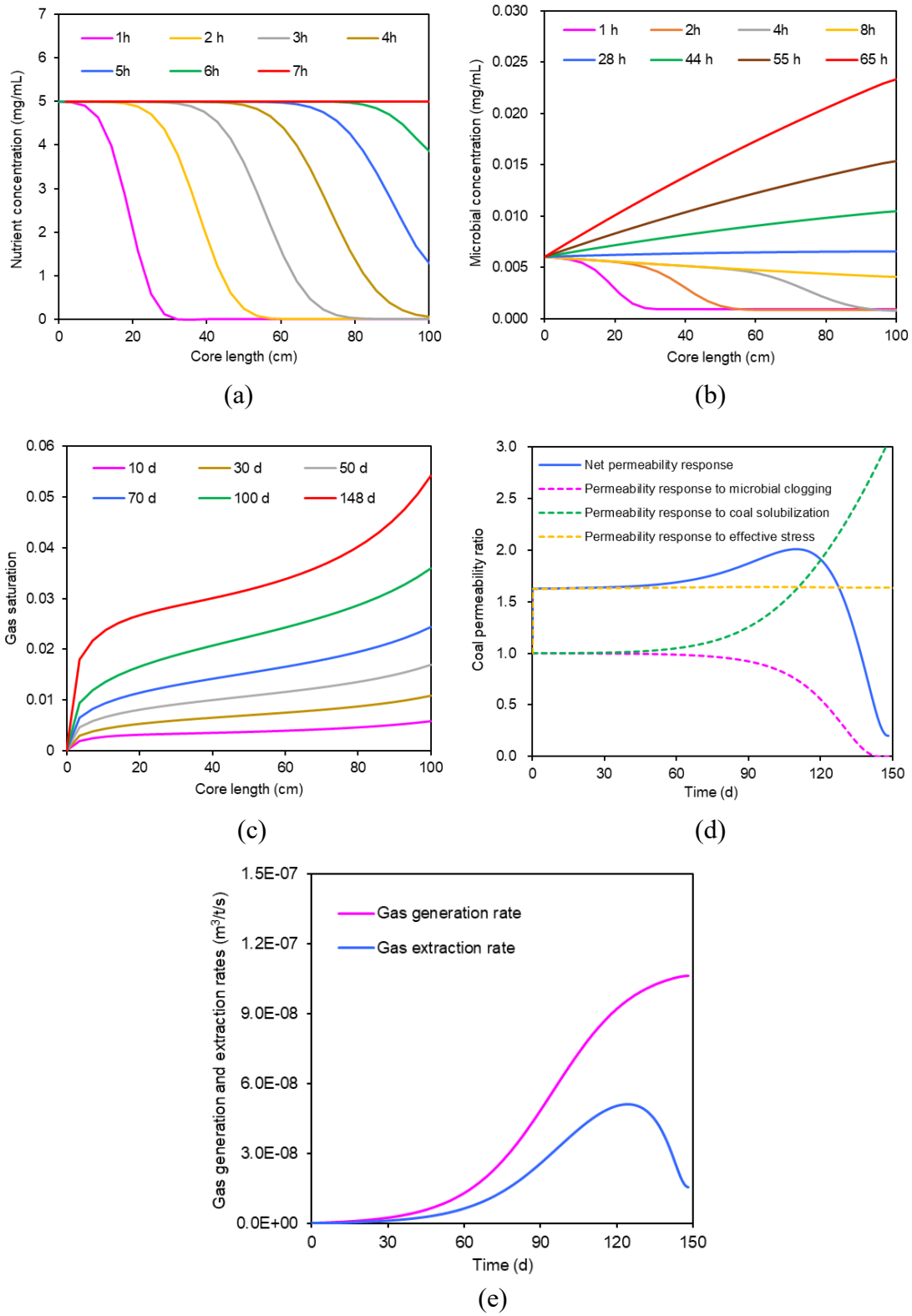

Fig. 3-7 Dynamic variation of different parameters during nutrients injection: (a) nutrients concentration across coal sample; (b) microbial concentration across coal sample; (c) gas saturation across coal sample; (d) coal permeability at the observation point; and (e) biogenic methane generation and extraction rates.

3.5.2.2 Simulation results during water injection

From the above analysis, it can be known that microbial adsorption and growth on fracture surface can induce microbial clogging of the fracture system in the later stage of nutrients injection. The occurrence of microbial clogging results in the loss of coal permeability and decline of biogenic methane extraction rate. When fracture is fully bioclogged, nutrients solution cannot be further injected into coal seams and biogenic methane cannot be extracted from coal seams as well. Under this condition, declogging operation should be undertaken to recover biogenic methane extraction. To this end, nutrients solution injection should be stopped and replaced by water injection. Here, further explanation on why water can be used to declog the fracture is provided. According to Eq. (3-22), microbial growth rate will decline to a very low value when water injection starts. In this case, the microbial growth rate will be lower than microbial decay rate. Thus, microbes can be gradually removed from fracture surface during water injection and this is the primary reason why we call the water injection phase as the declogging phase.

During water injection, a constant nutrients concentration of 0.005 mg/mL is applied at the inlet. This is because water produced from other wells in the field is used as the injection water and we assume that this water contains a low concentration of nutrients. The modelled spatial distribution of nutrients concentration in the aqueous phase is shown in Fig. 3-8(a). As can be seen, nutrients concentration in aqueous phase decreases with time and finally stabilizes at 0.005 mg/mL.

We assume that the injection water contains a very low concentration of microbes (0.001 mg/mL). During water injection, a constant microbial concentration of 0.001 mg/mL is applied at the inlet. The modelled spatial distribution of microbial

concentration in aqueous phase is shown in Fig. 3-8(b). As can be seen, microbial concentration decreases with time during water injection as a portion of microbes decay due to the lack of nutrients supply and the remaining flows out of coal with the injected water.

During water injection, zero gas saturation is set at the inlet. The modelled spatial distribution of gas saturation in coal is shown in Fig. 3-8(c). As can be seen, gas saturation decreases with time in this phase as biogenic methane generation rate constantly decreases and finally becomes zero in this phase.

During water injection, coal permeability is also influenced by three factors, i.e., effective stress, coal solubilization and microbial decay. Fig. 3-8(d) shows the response of coal permeability to these factors. As can be seen, both coal solubilization and microbial decay lead to permeability rebound. It should be noted that coal solubilization still occurs during water injection but the rate of coal solubilization decreases with time as microbes gradually decay in this process. When water injection ends, all microbes in fracture including those in the aqueous phase and on the fracture wall are removed. Thus, coal permeability recovers and coal permeability ratio reaches 6.8 at the end of the declogging phase.

Fig. 3-8(e) shows the variation of biogenic methane generation and extraction rates during water injection. As can be seen, biogenic methane generation rate decreases with time. This is because the population of microbes adsorbed on the fracture surface gradually declines in this phase as a result of microbial decay and desorption. By contrast, the variation of biogenic methane extraction rate is a little bit different. The extraction rate first increases due to coal permeability rebound and then decreases as a result of gas generation rate decline.

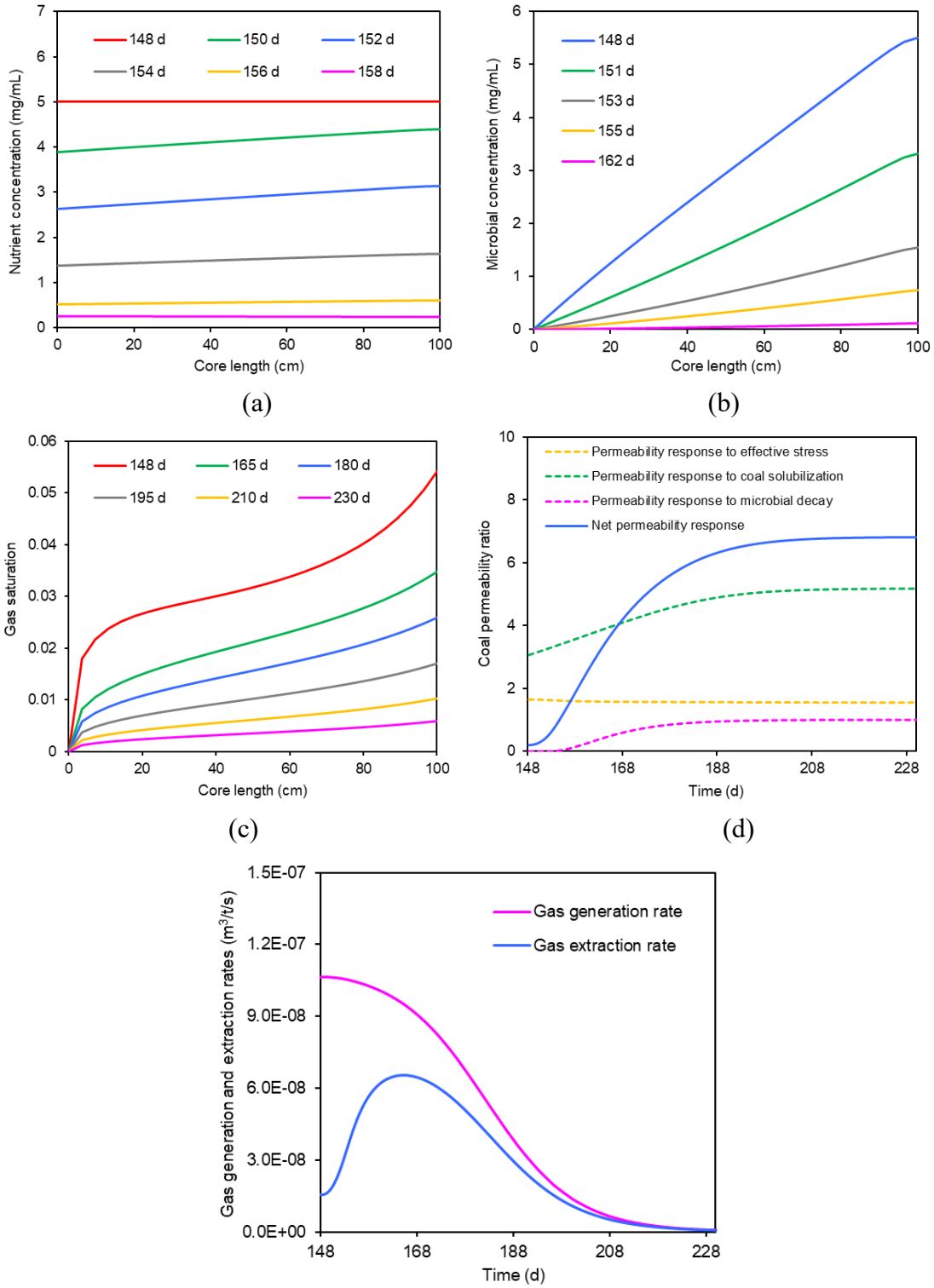

Fig. 3-8 Dynamic variation of different parameters during water injection: (a) nutrients concentration across coal sample; (b) microbial concentration across coal sample; (c) gas saturation across coal sample; (d) coal permeability at the observation point; and (e) biogenic methane generation and extraction rates.

3.5.2.3 Simulation results for one cycle of nutrients alternating water injection

Fig. 3-9(a) shows the variation of coal permeability in one cycle of nutrients alternating water injection. As can be seen, coal permeability gains net increase at the end of the cycle.

Fig. 3-9(b) shows the variation of biogenic methane generation and extraction rates in one cycle of nutrients alternating water injection. As can be seen, gas generation rate increases during nutrients solution injection but decreases during water injection. By contrast, in both of the nutrients and water injection phases, gas extraction rate first increases and then declines. In nutrients injection phase, gas extraction rate decline implies the occurrence of microbial clogging. The more the extraction rate declines, the more the fracture space is occupied by microbes. In water injection phase, gas extraction rate decline implies the removal of microbes from the fracture system. The more the extraction rate declines, the better the performance of the declogging operation.

Fig. 3-9(c) shows the cumulative biogenic methane generated and extracted in one cycle of nutrients alternating water injection. As can be seen, not all the generated biogenic methane can be extracted from coal as a portion of biogenic methane diffuses into coal matrix, adsorbs on coal grains and becomes adsorbed gas.

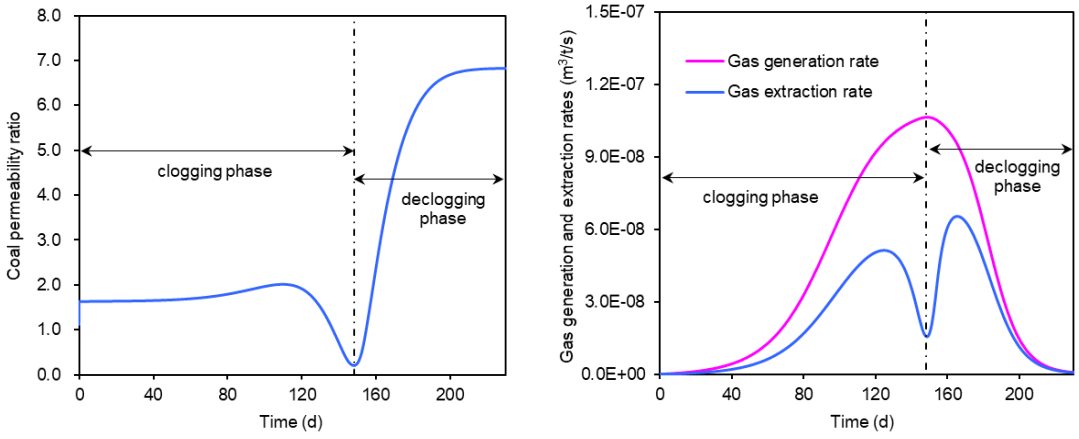

(a) (b)

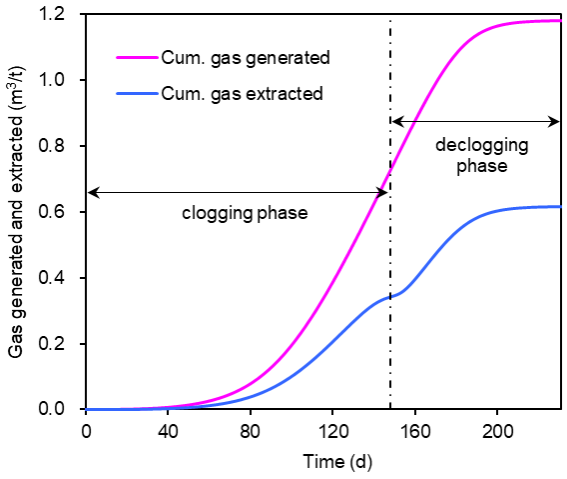

(c)

Fig. 3-9 Dynamic variation of different parameters in one cycle of nutrients alternating water injection: (a) coal permeability at the observation point; (b) biogenic methane generation and extraction rates; and (c) cumulative biogenic methane generated and extracted.

3.5.2.4 Simulation results for repeated cycles of nutrients alternating water injection

After completing one cycle of nutrients alternating water injection, the concentrations of nutrients and microbes in coal becomes very low (see Figs. 3-8(a) and 3-8(b)) and cannot sustain the subsequent biogenic methane generation and extraction. Thus, nutrients solution should be reinjected into coal which represents the beginning of the second cycle operations. In this subsection, simulation results for repeated cycles of nutrients alternating water injection are presented and analyzed.

Fig. 3-10(a) shows the variation of coal permeability during repeated cycles of nutrients alternating water injection. As can be seen, coal permeability gains net increase at the end of each cycle. When the degradable fraction of coal is completely converted, coal permeability ratio reaches a huge magnitude of 240. This indicates that applying the nutrients alternating water injection scheme coal bioconversion not only can generate

additional biogenic methane but also has the potential to greatly enhance gas flowing capacity in coal.

Fig. 3-10(b) shows the variation of biogenic methane generation and extraction rates during repeated cycles of nutrients alternating water injection. When biogenic methane is generated, a portion of gas diffuses into coal matrix under the pressure difference between fracture and matrix systems and thus coal matrix pressure increases. As injection pressure remains unchanged throughout, the pressure difference between fracture and matrix systems gradually decreases. Thus, less generated biogenic methane diffuses into coal matrix with the continuation of coal bioconversion. This explains why the difference between generation and extraction rates gradually diminishes during coal-to-methane bioconversion. This finding also indicates that the recovery efficiency of biogenic methane gradually increases during coal bioconversion.

Fig. 3-10(c) shows the cumulative biogenic methane generated and extracted during repeated cycles of nutrients alternating water injection. As can be seen, the difference between generated gas volume and extracted gas volume first increases and then gradually stabilizes.

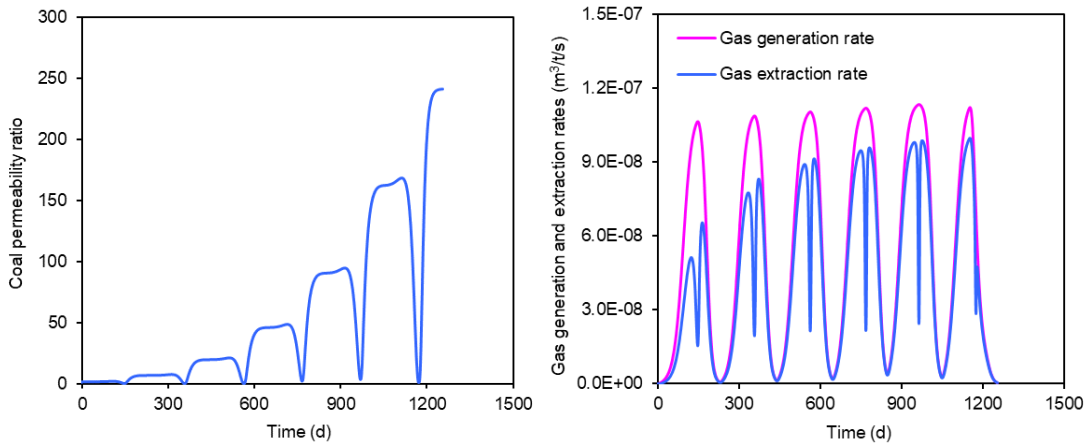

(a) (b)

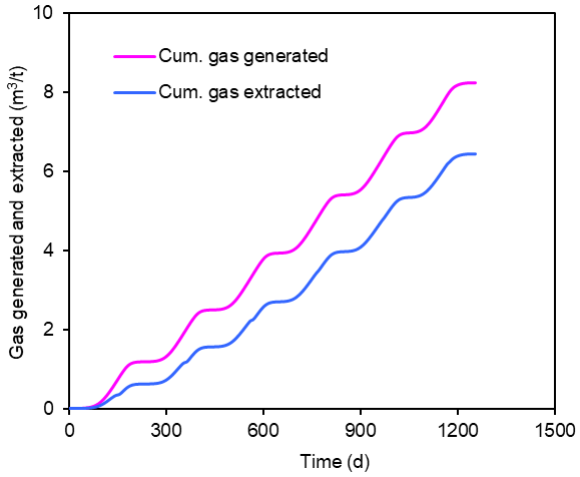

(c)

Fig. 3-10 Dynamic variation of different parameters during the whole coal bioconversion process: (a) coal permeability at the observation point; (b) biogenic methane generation and extraction rates; and (c) cumulative biogenic methane generated and extracted.

3.5.3 Parametric studies

For parametric studies, the impacts of a series of bioclogging-related parameters on coal-to-methane bioconversion are analyzed. In each group of parametric study, only one input parameter is changed with all the other input parameters kept identical to that of the base case. The investigated parameters include microbial adsorption rate, microbial growth rate, injected nutrients concentration, and injected microbial concentration.

3.5.3.1 The impact of microbial adsorption rate

In this subsection, the impact of microbial adsorption rate on coal-to-methane bioconversion is studied. From Fig. 3-11, it can be known that coal permeability reaches the maximum value in a shorter time and biogenic methane is generated and extracted at a faster rate when microbial adsorption rate increases from 0.065 1/h to 0.585 1/h. This is because the larger microbial adsorption rate leads to more microbes adsorbed

on the fracture surface and thereby coal solubilizes faster. For further observation, it can be found that the maximum coal permeability value and the cumulative biogenic methane generated and extracted remain the same for all three cases. This is due to the same degradable fraction of coal and Langmuir parameters in all these cases.

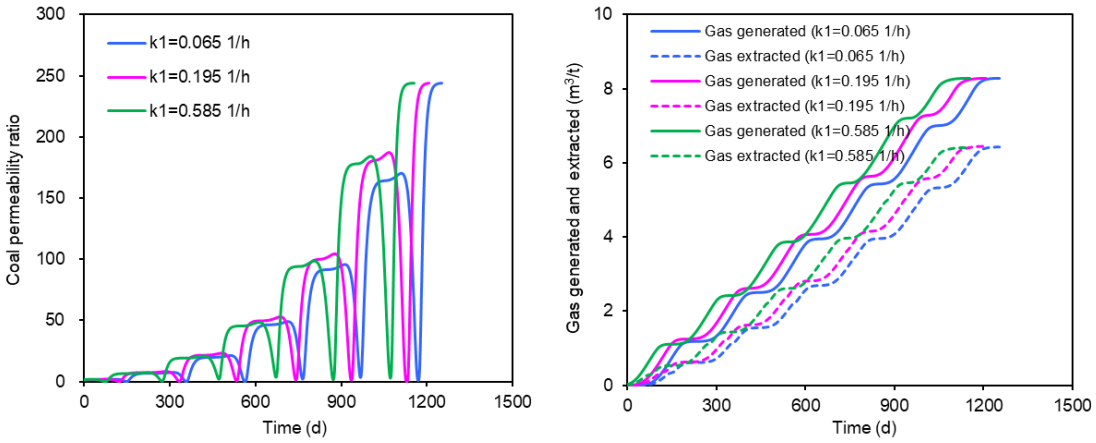

(a) (b)

Fig. 3-11 The impact of microbial adsorption rate on: (a) coal permeability evolution at the observation point; and (b) cumulative biogenic methane generated and extracted.

3.5.3.2 The impact of microbial growth rate

In this subsection, the impact of microbial growth rate on coal-to-methane bioconversion is studied. From Fig. 3-12, it can be known that coal permeability reaches the maximum value in a shorter time and biogenic methane is generated and extracted at a faster rate when microbial growth rate increases from 0.024 1/h to 0.036 1/h. This is mainly because the larger microbial growth rate leads to more microbes adsorbed on the fracture surface and thereby coal solubilizes faster. It can also be found that the maximum coal permeability value and the cumulative biogenic methane generated and extracted from coal remain the same for all these cases.

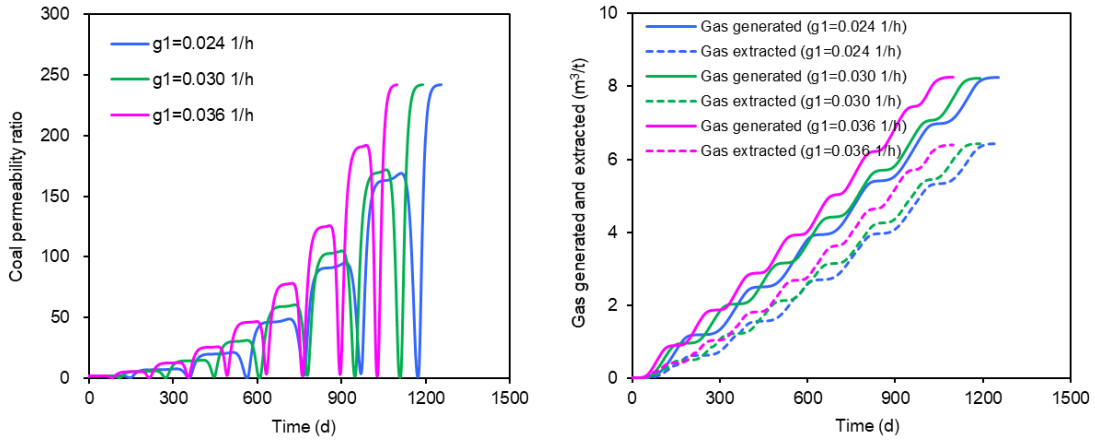

(a) (b)

Fig. 3-12 The impact of microbial growth rate on: (a) coal permeability evolution at the observation point; and (b) cumulative biogenic methane generated and extracted.

3.5.3.3 The impact of injected nutrients concentration

In this subsection, the impact of injected nutrients concentration on coal-to-methane bioconversion is studied. From Fig. 3-13, it can be known that coal permeability reaches the maximum value in a shorter time and biogenic methane is generated and extracted at a faster rate when injected nutrients concentration increases from 5 mg/mL to 20 mg/mL. This is because the larger nutrients concentration leads to the greater microbial growth rate and thereby more microbes adsorb on the fracture surface and consequently coal solubilizes faster. For further observation, it can be found that the maximum coal permeability value and the cumulative biogenic methane generated and extracted remain the same for all three cases.

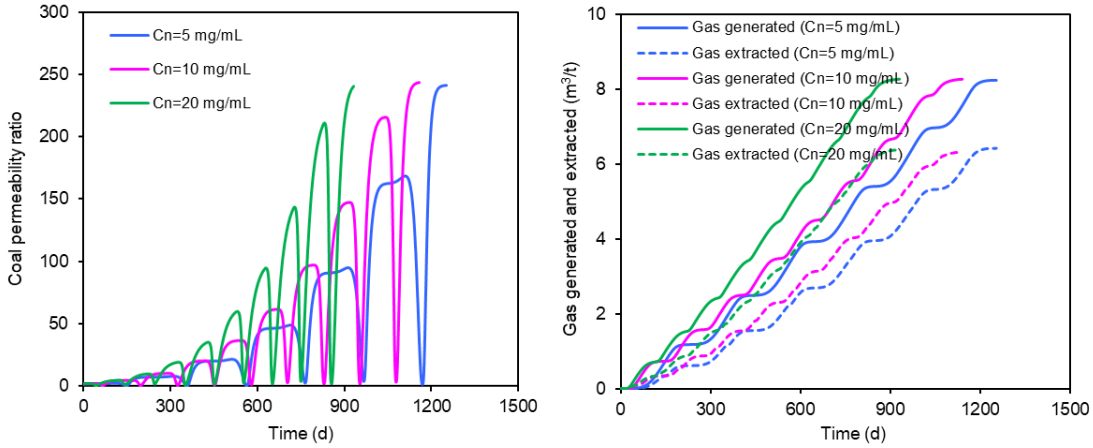

(a) (b)

Fig. 3-13 The impact of injected nutrients concentration on: (a) coal permeability evolution at the observation point; and (b) cumulative biogenic methane generated and extracted.

3.5.3.4 The impact of injected microbial concentration

In this subsection, the impact of injected microbial concentration on coal-to-methane bioconversion is studied. From Fig. 3-14, it can be known that coal permeability reaches the maximum value in a shorter time and biogenic methane is generated and extracted at a faster rate when injected microbial concentration increases from 0.006 mg/mL to 0.6 mg/ml. This is because the larger microbial concentration leads to more microbes adsorbed on the fracture surface and thus coal solubilizes faster. For further observation, it can be found that the maximum coal permeability value and the cumulative biogenic methane generated and extracted from coal remain the same for all cases.

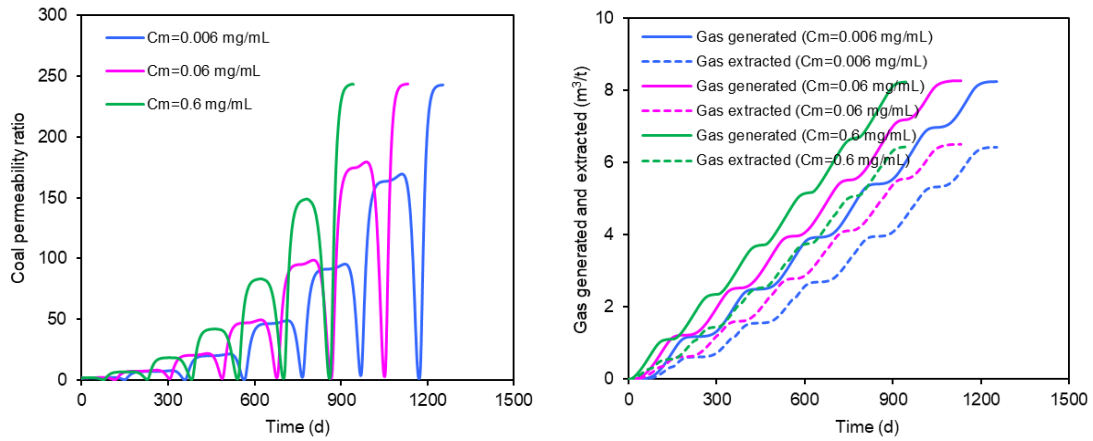

(a) (b)

Fig. 3-14 The impact of injected microbial concentration on: (a) coal permeability evolution at the observation point; and (b) cumulative biogenic methane generated and extracted.

3.6 Conclusions

In this work, a coupled hydrological-mechanical-chemical-biological multiphysics model is developed to investigate biogenic methane generation and extraction behavior in coal seams under the influence of microbial clogging. The model can be used to quantify various important processes involved during coal-to-methane bioconversion. Based on the simulation results, the following conclusions can be drawn:

(1) Repeated cycles of nutrients alternating water injection can ensure long-term biogenic methane generation and extraction. During nutrients injection, metabolic activities of microbes are stimulated which convert coal to biogenic methane but meanwhile microbial adsorption and growth on fracture surface leads to microbial clogging of the fracture system. In order to declog the fracture system, nutrients delivery should be temporally suspended and replaced by water injection. When the bioclogged fracture space is released, nutrients injection can restart.

(2) Coal-to-methane bioconversion has the great potential to enhance gas flow capacity in coal seams. During coal bioconversion, effective stress decline and coal solubilization increases coal permeability while microbial clogging leads to coal permeability decline. As adsorbed microbes on fracture surface are removed in the declogging phase, coal permeability can get net increase after each cycle of nutrients alternating water injection. Therefore, gas flow capacity in coal seams can be gradually enhanced in the progress of coal-to-methane bioconversion.

(3) Biogenic methane generation rate exhibits inverted-V shape variation trend while

extraction rate exhibits inverted-W shape variation trend in each cycle of nutrients alternating water injection. During nutrients injection, biogenic methane generation rate continuously increases due to microbial growth while extraction rate first increases due to the increase of gas generate rate and then decreases due to microbial clogging. During water injection, biogenic methane generation rate continuously decreases due to microbial decay while extraction rate first increases due to microbial decay and then decreases due to the decrease of gas generation rate.

(4) Biogenic methane extraction efficiency gradually increases during coal-to-methane bioconversion. When biogenic methane is generated, a fraction of it diffuses into coal matrix, adsorbs on coal grains and becomes adsorbed gas under the pressure difference between fracture and matrix systems. With the progress of coal-to-methane bioconversion, more gas will be extracted instead of becoming adsorbed gas as fracture-matrix pressure difference gradually diminishes. Thus, the extraction efficiency of biogenic methane can be enhanced through multiple cycles of nutrients alternating water injection.

Chapter 4 Impact of microbial activities on underground hydrogen storage in aquifers

Underground hydrogen storage (UHS) has been considered as an integral part of energy transition from fossil fuels to renewable sources. Porous aquifers can serve as typical sites for this purpose due to their worldwide distribution and huge storage capacity. However, the diverse microbial species that inhabit the aquifers are known to be able to catalyze in-situ biochemical reactions within the hosting rock. These reactions can normally lead to microbial consumption of hydrogen, microbial clogging of pore space and thus affect hydrogen injection and withdrawal rates as reported in the literature. So far, these phenomena have been widely reported but rarely quantified. In this chapter, the generic geo-multiphysics model is tailored to the case of UHS in aquifers with consideration of the impacts of microbial activities. A complete set of partial differential equations are defined to describe the processes involved: (1) rock deformation; (2) water-hydrogen two-phase flow; (3) microbes and dissolved hydrogen transport; (4) mineral dissolution/precipitation; and (5) microbial activities involving adsorption/desorption and growth/decay. All these processes are linked together through the porosity/permeability models which consider the joint impacts of microbial clogging, mineral dissolution/precipitation and effective stress. This multiphysics model is verified against laboratory biochemical reaction data and microbial transport data. Then, the verified model is used to investigate the impacts of iron-reduction bacteria (IRB) activities on UHS in aquifers. Based on the simulation results, it can be concluded that (1) hydrogen saturation at the top surface of the aquifer is the greatest while microbial activities surrounding the injection well is stimulated the most; (2) microbial activities influence the initial few cycles of hydrogen injection and

withdrawal but the impacts gradually diminish with the dissolution of Fe_2O_3; (3) hydrogen recovery efficiency is degraded due to the combined effects of hydrogen consumption, water production and microbial clogging with the microbial clogging impact being the most significant; and (4) effective stress impacts aquifer permeability throughout UHS operations while microbial clogging influences it in the initial few cycles. For mineral dissolution/precipitation, the impact can be neglected.

4.1 Introduction

In the context of decarbonization and achieving the net-zero emission target, renewable energies like solar energy, wind energy and tidal energy are now attracting more and more attention around the world (Herbert et al., 2007; Kannan and Vakeesan, 2016; Chowdhury et al., 2021). However, production of these renewable energies is greatly dependent on seasonal atmospheric conditions (i.e., sunlight level and wind scale) and geographic locations (Heinemann et al., 2021). Considering the annual varying but steady energy demand, the fluctuating production of these renewable energies inevitably leads to the mismatches between energy demand and supply (Gabrielli et al., 2020). Therefore, renewable energy production with excess energy storage should be adopted to bridge this energy gap (Heidaryan and Aryana, 2024).

The excess renewable energy can be converted to hydrogen, a type of low-carbon energy carrier, and then stored to be used during high energy demand periods. As surface hydrogen storage facilities have limited storage and discharge capacity, UHS in geo-structures like salt caverns, aquifers and depleted oil and gas reservoirs is required (Caglayan et al., 2020; Raad et al., 2022; Okoroafor et al., 2022; Hematpur et al., 2023). Compared to surface storage options, UHS requires lower investment and smaller surface space, offers higher safety standards, induces less environmental impacts, and

more importantly provides a large-scale and long-term storage option (Wallace et al., 2021; Mahdi et al., 2021; Amirthan and Perera, 2023; Zeng et al., 2023). However, most of these subsurface environments are not life-free and harbor a variety of microbial communities (Pedrós-Alió and Manrubia, 2016; Varjani and Gnansounou, 2017). The activities of these microbes can be stimulated by the stored hydrogen and then have significant impacts on UHS operations.

As can be summarized from the literature review in section 1.3.2, both field tests and laboratory experiments have confirmed the undesired side effects induced by microbial activities during UHS. To quantify these microbial impacts, several theoretical studies have been undertaken. However, works on modeling the impacts of microbial activities on UHS in porous reservoirs are still very limited at the current stage which limits our understanding of this problem. To this end, a coupled hydrological-mechanical-chemical-biological multiphysics model is developed in this work to quantify all important processes involved. In the following, the conceptual model for UHS in aquifers in first introduced. In this conceptual model, the impacts of microbial activities on UHS are illustrated in detail. Then, a complete set of partial differential equations are defined to describe the involved processes with all these processes linked by the porosity and permeability models. After that, the proposed model is verified against laboratory iron reduction data and microbial transport data. In the end, the multiphysics model is applied to analyze microbial impacts on UHS in aquifers.

4.2 The conceptual model

The starting point to model the impacts of microbial activities on UHS in aquifers is to understand the fundamental processes involved. During UHS, hydrogen is cyclically injected into and withdrawn from the subsurface aquifers, see Fig. 4-1. Depending on

the underground pressure, temperature and salinity conditions, a certain amount of hydrogen would dissolve into the formation water. The dissolved hydrogen serves as one of the most important electron donors for many subsurface microbial processes. According to the available literatures, it is expected that at least seven hydrogenotrophic microbial processes could be important for UHS (Dopffel et al., 2021; Thaysen et al., 2021; Kumari and Ranjith, 2023). Simultaneous survival and competition among these microbes are possible. Studies have also shown that these microbes have different minimum threshold concentrations for hydrogen consumption. Among these microbes, IRB have the lowest threshold concentration and consequently have the best potential to out-compete other species (Hagemann et al., 2016). Therefore, in this work, we take IRB as an example to investigate the impacts of microbial activities on UHS in aquifers.

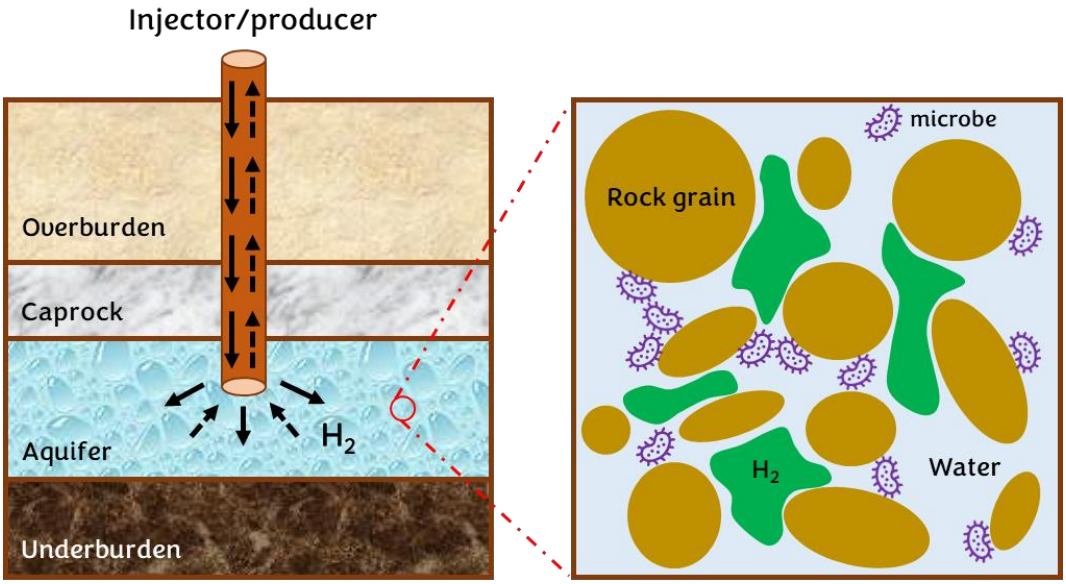

Fig. 4-1 Schematic diagram of hydrogen injection and withdrawal in aquifers where microbes live.

Following hydrogen injection, the elevation of hydrogen concentration in formation water stimulates the growth of IRB in subsurface pore space. The microbial growth occupies a fraction of pore space and reduces the porosity and permeability of aquifers.

Thus, bioclogging occurs during UHS and this will impact hydrogen injection and withdrawal rates. Meanwhile, during IRB growth, specific enzymes are produced which can catalyze the chemical reaction between hydrogen and the mineral Fe_2O_3 (Dopffel et al., 2021) in porous rock:

$$3Fe_2O_3 + H_2 \rightarrow 2Fe_3O_4 + H_2O \quad (4\text{-}1)$$

The above reaction couples hydrogen oxidation with Fe(III) reduction. From the chemical reaction equation, it can be known that during iron reduction process a certain amount of hydrogen is consumed and additionally a certain amount of water is produced. This process lowers hydrogen saturation and relative permeability in aquifers and thus impacts hydrogen injection and withdrawal rates as well. From the chemical reaction equation, it can also be known that mineral dissolution and precipitation simultaneously take place during UHS. The dissolution of Fe_2O_3 leads to porosity and permeability increase while the precipitation of Fe_3O_4 leads to porosity and permeability decline. Thus, hydrogen injection and withdrawal rates may also be changed under the impacts of these two competing processes.

Overall, UHS in aquifers involves the interactions of multiple processes. These processes mainly include rock deformation, water-gas two-phase flow, multispecies reactive transport, and microbial growth/decay and adsorption/desorption. All these processes can be linked together through the porosity and permeability models. During UHS in aquifers, rock porosity and permeability are mainly influenced by the following three factors including effective stress, microbial clogging, and mineral dissolution and precipitation.

4.3 Governing equations for the coupled processes

From the above introduced conceptual model, it can be known that complex interactions

occur among rock, formation water, hydrogen and microbes during UHS in aquifers. These interactions exert strong influences on rock deformation, water-gas two-phase flow, multispecies reactive transport, microbial activities, and porosity and permeability change. Therefore, in this work, we define UHS operations as the coupled hydrological-mechanical-chemical-biological processes, which implies that one physical process affects the initiation and progress of another. The inclusion of cross-coupling relations among these physical processes is the key to formulate the mathematical model to describe UHS operations. In the following, the derivation of the governing equations for the coupled processes involved is presented.

4.3.1 Rock deformation

In the following equations, all derivations are made after the traditional conventions: A comma followed by subscripts represents the differentiation with respect to spatial coordinates, and repeated indices in the same equation imply the summation over the range of indices. Following the conventions, the stress equilibrium equation ignoring the inertial term is expressed as:

$$\sigma_{ij,j} + f_i = 0 \tag{4-2}$$

where σ_{ij} is the component of stress tensor, and f_i is the component of body force.

The relation between strain and displacement is expressed as:

$$\varepsilon_{ij} = \frac{1}{2}\left(u_{i,j} + u_{j,i}\right) \tag{4-3}$$

where ε_{ij} is the component of strain tensor, and u_i is the component of displacement.

The relation between strain and stress can be defined in the form of:

$$\varepsilon_{ij} = \frac{1}{2G}\sigma_{ij} - \left(\frac{1}{6G} - \frac{1}{9K}\right)\sigma_{kk}\delta_{ij} + \frac{\alpha}{3K}p\delta_{ij} \tag{4-4}$$

where G is shear modulus, K is bulk modulus, α is Biot's coefficient, $\sigma_{kk} = \sigma_{11} + \sigma_{22} + \sigma_{33}$, δ_{ij} is Kronecker delta, and p is pore pressure.

Integrating Eqs. (4-2) to (4-4), the Navier-type equation for rock deformation can be derived:

$$Gu_{i,kk} + \frac{G}{1-2v}u_{k,ki} - \alpha p_{,i} + f_i = 0 \tag{4-5}$$

It should be mentioned that water-gas two-phase flow presents in aquifers during UHS. Thus, the pore pressure term in Eq. (4-5) should be treated as the average pressure of water and gas phases (Tian et al., 2022; Gao et al., 2023):

$$p = S_w p_w + S_g p_g \tag{4-6}$$

where S_w and S_g represent the water saturation and hydrogen saturation, respectively. p_w and p_g represent the water pressure and hydrogen pressure, respectively.

4.3.2 Water-gas two-phase flow

During UHS in aquifers, water-gas two-phase flow presents in the pore system. The mass conservation equation for each phase can be expressed as:

$$\frac{\partial(\emptyset S_w \rho_w)}{\partial t} = \nabla \cdot \left[\rho_w \frac{k k_{rw}}{\mu_w}(\nabla p_w - \rho_w g h)\right] + Q_w \tag{4-7}$$

$$\frac{\partial(\emptyset S_g \rho_g)}{\partial t} = \nabla \cdot \left[\rho_g \frac{k k_{rg}}{\mu_g}(\nabla p_g - \rho_g g h)\right] + Q_g \tag{4-8}$$

where $\emptyset$ is porosity; ρ_w and ρ_g are densities of water and hydrogen, respectively; k is absolute permeability; k_{rw} and k_{rg} are relative permeabilities of water and hydrogen, respectively; μ_w and μ_g are viscosities of water and hydrogen, respectively; g is gravitational acceleration; Q_w and Q_g are source terms for water and hydrogen, respectively, which are defined in the following forms:

$$Q_w = \frac{1}{Y_w} \cdot \frac{C_m}{K_{m/s} + C_m} \cdot M_{H_2O} \tag{4-9}$$

$$Q_g = -\xi\left(p_g - H_c C_{H_2}\right) \tag{4-10}$$

where $\frac{1}{Y_w}$ is the reaction yield coefficient representing the water production rate; C_m is microbial concentration in water phase; $K_{m/s}$ is the half saturation constant representing the microbial concentration at which the iron reduction reaction rate reaches half of its maximum value; M_{H_2O} is the molar mass of water; ξ is the hydrogen mass transfer rate from gaseous phase to water phase; H_c is the corrected Henry's constant; and C_{H_2} is hydrogen concentration in water phase.

Eqs. (4-7) to (4-10) define the fluids flow process during UHS in aquifers. In these equations, hydrogen density, viscosity and solubility are not constant and will change under different temperature, pressure and salinity conditions. The equations describing the variation of these hydrogen properties are provided in the appendixes at the end of the thesis.

In addition, the total saturation of water and hydrogen should equal to one in the pore system:

$$S_w + S_g = 1 \tag{4-11}$$

In the pore system, water and hydrogen are separated by a well-defined interface and there exists a pressure difference between the two phases across the interface (Szymkiewicz, 2012). This pressure difference is called capillary pressure. The magnitude of capillary pressure is equivalent to the difference between the non-wetting phase pressure and wetting phase pressure. In this work, hydrogen is considered as the non-wetting phase and water is considered as the wetting phase. Thus, capillary pressure can be expressed as:

$$p_c = p_g - p_w \tag{4-12}$$

where p_c denotes the capillary pressure which can also be defined as a function of wetting phase saturation (Brooks and Corey, 1966):

$$p_c = p_e S_w^{*\,-1/\lambda} \tag{4-13}$$

where p_e is the entry pressure, S_w^* is the effective saturation of water, and λ is the pore size distribution coefficient.

The effective water saturation S_w^* and effective hydrogen saturation S_g^* are expressed in the forms of:

$$S_w^* = \frac{S_w - S_{wi}}{1 - S_{gr} - S_{wi}} \tag{4-14}$$

$$S_g^* = \frac{S_g - S_{gr}}{1 - S_{gr} - S_{wi}} \tag{4-15}$$

where S_{wi} is the irreducible water saturation, and S_{gr} is the residual hydrogen saturation.

Then, relative permeabilities of water and hydrogen can be defined as (Brooks and Corey, 1966):

$$k_{rw} = S_w^{*\,(3+2/\lambda)} \tag{4-16}$$

$$k_{rg} = S_g^{*2}\left[1 - \left(1 - S_g^*\right)^{(1+2/\lambda)}\right] \tag{4-17}$$

4.3.3 Multispecies reactive transport

During UHS in aquifers, the movement of dissolved hydrogen and microbes in aqueous phase is mainly controlled by advective-dispersive transport (Li et al., 2011; Zhi et al., 2018). The transport equations for dissolved hydrogen and microbes can be expressed as follows:

$$\frac{\partial\left(\emptyset S_w C_{H_2}\right)}{\partial t} = \nabla \cdot \left(\emptyset S_w D_{H_2} \nabla C_{H_2}\right) - \nabla \cdot \left(v_w C_{H_2}\right) + R_{H_2} \tag{4-18}$$

$$\frac{\partial(\emptyset S_w C_m)}{\partial t} = \nabla \cdot (\emptyset S_w D_m \nabla C_m) - \nabla \cdot (v_w C_m) + R_m \quad (4\text{-}19)$$

where C_{H_2} and C_m represent hydrogen concentration and microbial concentration in the aqueous phase, respectively; D_{H_2} and D_m represent the hydrodynamic dispersion coefficients of dissolved hydrogen and microbes, respectively; v_w is the Darcy flow velocity for the aqueous phase; and R_{H_2} and R_m represent the source/sink terms for reactions of dissolved hydrogen and microbes, respectively, which can be defined in the following forms:

$$R_{H_2} = \xi\left(p_g - H_c C_{H_2}\right)/M_{H_2} - \frac{1}{Y_w} \cdot \frac{C_m}{K_{m/s} + C_m} \quad (4\text{-}20)$$

$$R_m = -(k_1 + k_3)\emptyset_f S_w C_m + k_2 \rho_m \emptyset_1 + (g_1 - d_1)\emptyset_f S_w C_m \quad (4\text{-}21)$$

where M_{H_2} is the molar mass of hydrogen, k_1 is the reversible microbial adsorption rate, k_3 is the irreversible microbial adsorption rate, k_2 is the microbial desorption rate, ρ_m is the microbial density, $\emptyset_1$ is the volumetric fraction of microbes adsorbed reversibly on pore surface, g_1 is the microbial growth rate, and d_1 is the microbial decay rate. Here, more explanation is given for these two reaction source terms. The two terms on the right-hand side of Eq. (4-20) represent hydrogen transfer from gaseous phase to aqueous phase and the consumption of hydrogen induced by chemical reaction, respectively. The three terms on the right-hand side of Eq. (4-21) represent microbial adsorption on pore surface, microbial desorption from pore surface, and microbial growth and decay, respectively.

The microbial growth rate can be defined by the double Monod model with hydrogen and Fe_2O_3 serving as the limited substrates (Hagemann et al., 2016; Shojaee et al., 2024):

$$g_1 = g_{1max} \cdot \frac{C_{H_2}}{K_{H_2/s} + C_{H_2}} \cdot \frac{C_{Fe_2O_3}}{K_{Fe_2O_3/s} + C_{Fe_2O_3}} \quad (4\text{-}22)$$

where g_{1max} is the maximum microbial growth rate, $C_{Fe_2O_3}$ is the Fe_2O_3

concentration in porous rock, $K_{H_2/s}$ is the half saturation constant representing the hydrogen concentration at which microbial growth rate reaches half of its maximum value, and $K_{Fe_2O_3/s}$ is the half saturation constant representing the Fe_2O_3 concentration at which microbial growth rate reaches half of its maximum value as well. From the double Monod model, it can be known that the microbial growth rate is controlled by both the concentration of dissolved hydrogen in the aqueous phase and the concentration of Fe_2O_3 in porous rock.

4.3.4 Minerals dissolution and precipitation

As the iron reduction process leads to the dissolution of Fe_2O_3 and precipitation of Fe_3O_4, the mineral concentration in porous rock changes as well. The mass conservation equations for Fe_2O_3 and Fe_3O_4 can then be defined as:

$$\frac{\partial\left[(1-\emptyset)C_{Fe_2O_3}\right]}{\partial t} = R_{Fe_2O_3} \tag{4-23}$$

$$\frac{\partial\left[(1-\emptyset)C_{Fe_3O_4}\right]}{\partial t} = R_{Fe_3O_4} \tag{4-24}$$

where $C_{Fe_3O_4}$ is the Fe_3O_4 concentration in porous rock, and $R_{Fe_2O_3}$ and $R_{Fe_3O_4}$ are the reaction source terms for Fe_2O_3 and Fe_3O_4, respectively, which can be expressed in the following forms:

$$R_{Fe_2O_3} = -3 \cdot \frac{1}{Y_w} \cdot \frac{C_m}{K_{m/s} + C_m} \tag{4-25}$$

$$R_{Fe_3O_4} = 2 \cdot \frac{1}{Y_w} \cdot \frac{C_m}{K_{m/s} + C_m} \tag{4-26}$$

4.3.5 Microbial activities

During UHS, microbial growth is stimulated by the elevation of hydrogen concentration in the aqueous phase. Many studies have suggested that the microbial growth can lead to bioclogging of the pore system with subsequent changes in porosity and permeability of the porous media. From the traditional point of view, the distribution of microbes in

porous media is assumed to be in the form of biofilm covering the surface of the grain particles. Based on this assumption, bioclogging induced porosity change can be attributed to the volumetric fraction of microbes adsorbed on the pore surface and to the subsequent growth of this biofilm (Li et al., 2011; Sivasankar and Kumar, 2019; Chakraborty et al., 2020). In this work, we also make the assumption that those microbes suspended in the aqueous phase doesn't make contribution to the change of rock porosity. According to the above two assumptions, the mass conservation equations for microbes adsorbed reversibly and irreversibly on pore surface can be defined as:

$$\frac{\partial(\rho_m \emptyset_1)}{\partial t} = k_1 \emptyset_f S_w C_m - k_2 \rho_m \emptyset_1 + g_1 \rho_m \emptyset_1 - d_1 \rho_m \emptyset_1 \quad (4\text{-}27)$$

$$\frac{\partial(\rho_m \emptyset_2)}{\partial t} = k_3 \emptyset_f S_w C_m + g_1 \rho_m \emptyset_2 - d_1 \rho_m \emptyset_2 \quad (4\text{-}28)$$

From the above two equations, it can be known that microbial activities in pore system involve microbial adsorption/desorption and microbial growth/decay. Further, microbial adsorption includes reversible microbial adsorption and irreversible microbial adsorption.

4.3.6 Rock porosity and permeability

In this section, rock porosity and permeability models are developed. Considering a porous medium containing the pore volume V_p and the bulk volume V, we can have the porosity $\emptyset$ as follows:

$$\emptyset = \frac{V_p}{V} \quad (4\text{-}29)$$

Then, the porosity change can be expressed as:

$$d\emptyset = d\left(\frac{V_p}{V}\right) = \frac{V_p}{V}\left(\frac{dV_p}{V_p} - \frac{dV}{V}\right) \quad (4\text{-}30)$$

Substituting Eq. (4-29) into Eq. (4-30) and rearranging, we can obtain:

$$\frac{d\emptyset}{\emptyset} = \frac{dV_p}{V_p} - \frac{dV}{V} \tag{4-31}$$

The terms on the right-hand side of Eq. (4-31) represent the volumetric strains of pores and the rock, respectively. And these two strains can also be defined using the poroelasticity theory:

$$\frac{dV}{V} = -\frac{1}{K}(d\bar{\sigma} - \alpha dp) \tag{4-32}$$

$$\frac{dV_p}{V_p} = -\frac{1}{K_p}(d\bar{\sigma} - \beta dp) \tag{4-33}$$

where $\alpha = 1 - K/K_s$ and $\beta = 1 - K_p/K_s$ are the Biot coefficients of the rock and the pores, respectively; K, K_p and K_s represent the bulk modulus of the rock, the pores and the grains, respectively; and $\bar{\sigma} = -(\sigma_{11} + \sigma_{22} + \sigma_{33})/3$ is the mean stress.

Substituting Eqs. (4-32) and (4-33) into Eq. (4-31), the following relation can be derived:

$$\frac{d\emptyset}{\emptyset} = \left(\frac{1}{K} - \frac{1}{K_p}\right)(d\bar{\sigma} - dp) \tag{4-34}$$

Assuming the constant K and K_p, integrating the above equation with time yields:

$$\emptyset = \emptyset_0 exp\left\{\left(\frac{1}{K} - \frac{1}{K_p}\right)[(\bar{\sigma} - \bar{\sigma}_0) - (p - p_0)]\right\} \tag{4-35}$$

where the subscript "0" denotes the parameter value at the initial state. As the value of K is commonly several orders of magnitude larger than the value of K_p, we can have the simplification $\frac{1}{K} - \frac{1}{K_p} \approx -\frac{1}{K_p}$. Further, $\frac{1}{K_p}$ can be defined as the compressibility of pores. Then, we can have the relation between porosity and effective stress:

$$\emptyset = \emptyset_0 exp\{-c_p[(\bar{\sigma} - \bar{\sigma}_0) - (p - p_0)]\} \tag{4-36}$$

where $c_p = \frac{1}{K_p}$ represents pore compressibility.

As rock porosity changes under the joint impacts of effective stress, microbial clogging and mineral dissolution/precipitation, the final form of porosity model can be expressed

as below:

$$\emptyset = \emptyset_0 exp\{-c_p[(\bar{\sigma} - \bar{\sigma}_0) - (p - p_0)]\} - \emptyset_{bc} + \emptyset_d - \emptyset_p \quad (4\text{-}37)$$

where $\emptyset_{bc} = \emptyset_1 + \emptyset_2$ is the porosity change induced by microbial clogging; and $\emptyset_d$ and $\emptyset_p$ are the porosity change induced by mineral dissolution and precipitation, respectively, which can be defined as follows:

$$\emptyset_d = \frac{\Delta C_{Fe_2O_3} M_{Fe_2O_3}}{\rho_{rock}} \quad (4\text{-}38)$$

$$\emptyset_p = \frac{\Delta C_{Fe_3O_4} M_{Fe_3O_4}}{\rho_{rock}} \quad (4\text{-}39)$$

where $\Delta C_{Fe_2O_3}$ and $\Delta C_{Fe_3O_4}$ represent the change of Fe_2O_3 and Fe_3O_4 concentrations in rock, respectively; $M_{Fe_2O_3}$ and $M_{Fe_3O_4}$ represent the molar mass of Fe_2O_3 and Fe_3O_4, respectively; and ρ_{rock} is the rock density.

Finally, rock permeability can be derived applying the Kozeny law (Chen et al., 2016):

$$k = \frac{\emptyset^3}{c\tau^2 S_p^2} \quad (4\text{-}40)$$

where $\emptyset$ is rock porosity, c is the Kozeny constant that depends on the geometry of the porous media, τ is the tortuosity factor of porous media, and S_p is the pore surface area per unit volume.

4.3.7 Cross coupling relations

As can be summarized here, rock geomechanical deformation is defined by Eq. (4-5). Water-hydrogen two-phase flow is defined by Eqs. (4-7) and (4-8). Multispecies reactive transport are defined by Eqs. (4-18) and (4-19). Minerals dissolution and precipitation are defined by Eqs. (4-23) and (4-24). Microbial adsorption/desorption and growth/decay are defined by Eqs. (4-27) and (4-28). The interactions and coupling relations of all these processes are depicted in Fig. 4-2.

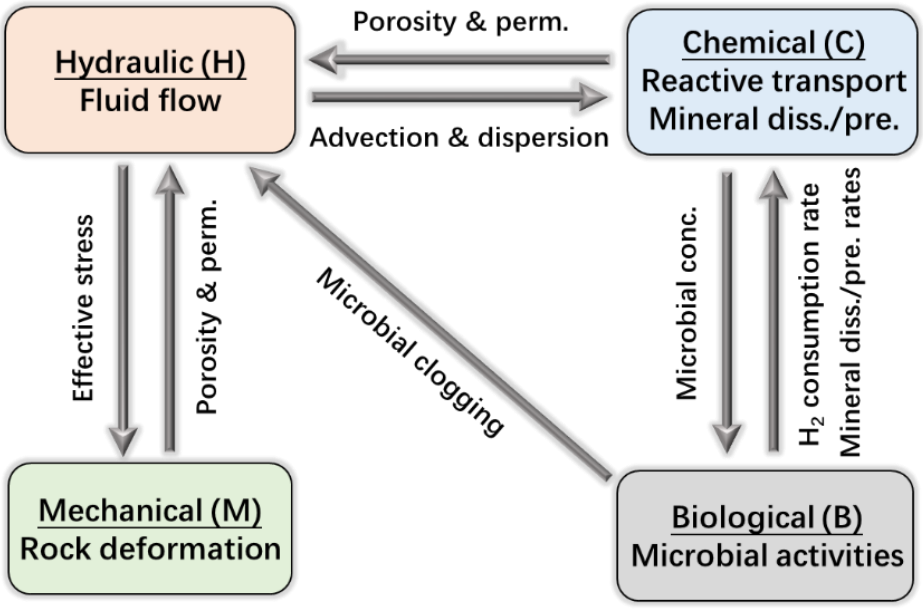

Fig. 4-2 Coupling relations among different physical fields during UHS in aquifers.

As can be seen, rock deformation impacts fluid flow through changing porosity and permeability. Fluid flow impact rock deformation and reactive transport through changing effective stress and solutes advection-dispersion, respectively. Minerals dissolution and precipitation impact fluid flow through changing rock porosity and permeability while reactive transport impacts microbial activities through controlling microbial concentration and distribution. Microbial activities impact fluid flow, reactive transport and mineral dissolution/precipitation through microbial clogging of pore space, changing hydrogen consumption rate and mineral dissolution/precipitation rates, respectively.

4.4 Model verification

4.4.1 Model verification for chemical reaction between hydrogen and Fe(III) in rock

Since there is a lack of core flooding experiment data on chemical reaction between hydrogen and Fe(III) in rock, a zero-dimension problem is modeled here and the modeling results are compared with the batch reactor experiment data reported by

Roden and Zachara (1996). In their experiment, goethite (source of Fe(III)) and hydrogen were collected for the chemical reaction. Goethite serves as the sole electron acceptor and hydrogen serves as the sole electron donor. The goethite-hydrogen medium was first filled into a 100 mL culture bottle with goethite concentration being 500 mmol/L and hydrogen volume being 30 mL. The goethite-hydrogen medium also contained 10mM malate as the carbon source (but not the electron donor) for microbial growth. Then, BrY cells (the microbe) were added into the bottle to catalyze the redox reaction. The experiment was conducted at the static condition with the temperature remaining at 35 °C. The whole experiment lasts for 18 days. During this period, samples for Fe(II) and BrY cells were collected at a 2-4 days interval and the concentrations of the collected samples were measured. It should be noted here that the chemical reaction involved in the experiment by Roden and Zachara (1996) is not exactly the same as the chemical reaction described by Eq. (4-1), but verifying our model against this experiment data is still necessary as both these reactions involve hydrogen oxidation and Fe(III) reduction.

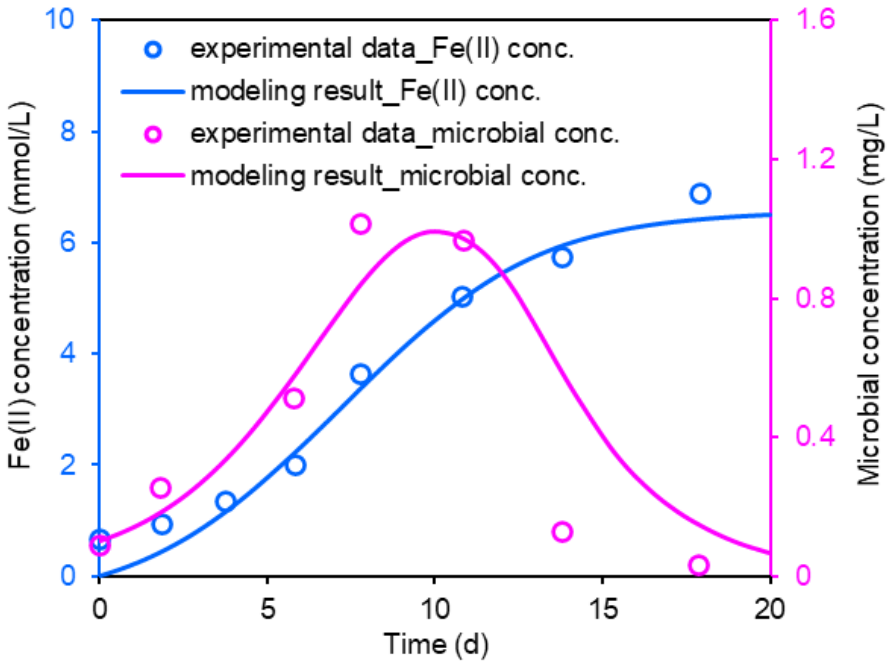

Fig. 4-3 Comparison between the modeling results and the experimental data reported by Roden and Zachara (1996).

To model the variation of Fe(II) concentration and microbial concentration in the batch reactor environment, the partial differential equations of the proposed multiphysics model were reduced to the ordinary differential equations. Applying the ordinary differential equations and the parameters listed in Table 4-1, the variation of Fe(II) concentration and microbial concentration can be calculated, see Fig. 4-3. From this figure, it can be found that our modeling results can match the experimental data in a good manner. For further observation, it can be known that microbial concentration increases in the first week. This is because substrates are rich enough in this stage to support microbial growth. Correspondingly, Fe(II) concentration exponentially increases. One week later, microbial concentration starts to decline. This is because substrates for microbial growth are gradually consumed and thus microbial decay outcompetes microbial growth in this period. Correspondingly, the increase of Fe(II) concentration slows down and remains almost unchanged in the end of the experiment.

Table 4-1 Input parameters for model verification on the chemical reaction process.

Parameters (unit)	Symbols	Values
The maximum microbial growth rate (1/h)	g_{1max}	0.08
Microbial decay rate (1/h)	d_1	0.005
Reaction yield coefficient (mol/m^3/h)	$1/Y$	0.02
Half-saturation constant for iron reduction (mg/mL)	$K_{m/s}$	0.2
Half-saturation constant for microbial growth (mg/mL)	$K_{H_2/s}$	0.5
Half-saturation constant for microbial growth (mg/mL)	$K_{Fe(III)/s}$	200
Initial hydrogen concentration in aqueous phase (mg/mL)	$C_{H_2,0}$	8.5e-10
Initial microbial concentration in aqueous phase (mg/mL)	$C_{m,0}$	1e-4
Initial Fe(III) concentration (mol/m^3)	$C_{Fe(III),0}$	500
Initial Fe(II) concentration (mol/m^3)	$C_{Fe(II),0}$	0

4.4.2 Model verification for microbial transport and adsorption process

In this section, the model describing microbial transport and adsorption in porous media

is verified through comparing the numerical results with the core flooding experiment data reported by Henry et al. (1997). In the experimental study, medium to coarse grained silica sand was used to create the sand column (5 cm in diameter and 40 cm in length). Sieve analysis shows that the sand size was in the range of 250 to 1000 μm in diameter. The porosity of the sand column was measured to be around 0.4. During the experiment, artificial ground water was used as the solution and constant bottom-to-top water flux of 6.6 cm^3/h was maintained through the long sand column. This water flux was equivalent to the linear velocity of 0.84 cm/h. In the first step, artificial ground water was flushed through the 40 cm long sand column for 192 h. Then, the water containing microbes with microbial concentration of 4.32 mg/L was introduced into the sand column for 38.4 h. After introducing the microbes, artificial ground water was flushed through the sand column once again for another 240 h. Effluent samples from the top side of the column were collected throughout the experiment to analyze microbial concentration in the effluent water. To make comparison between the modeling and experimental results, we also calculate the evolution of microbial concentration at the outlet of our numerical model. As the experimental data has a wide range of distribution, three different microbial growth rates as listed in Table 4-2 were used in our simulation. From Fig. 4-4, it can be known that the modelling results can cover the experiment data distribution area which implies that our model has the capability to describe the microbial transport and adsorption process in porous medium.

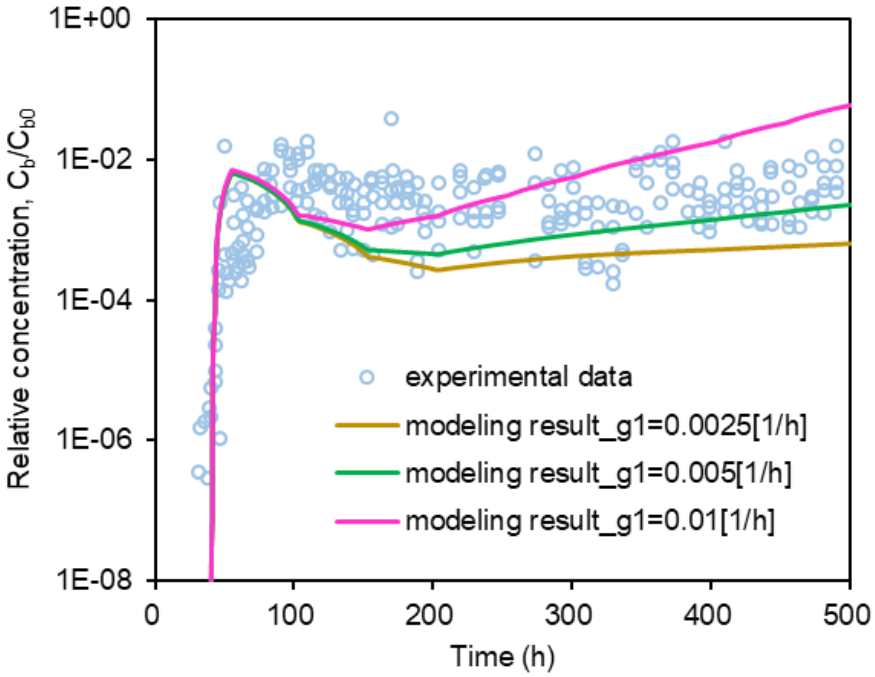

Fig. 4-4 Comparison between the modeling results and the experimental data reported by Henry et al. (1997).

Table 4-2 Input parameters for model verification on the microbial transport process.

Parameters (unit)	Symbols	Values
Reversible microbial adsorption rate (1/h)	k_1	0.065
Microbial desorption rate (1/h)	k_2	0.0012
Irreversible microbial adsorption rate (1/h)	k_3	0.01
Microbial growth rate (1/h)	g_1	2.5e-3/5e-3/1e-2
Microbial decay rate (1/h)	d_1	0
Microbial density (kg/m^3)	ρ_m	1600

4.5 Model applications and results analysis

In this section, the proposed multiphysics model is applied to investigate the impacts of microbial activities on UHS in aquifers. First, the geometry and initial and boundary conditions of the numerical model is introduced. Then, the numerical results of the base case are presented and analyzed. After that, parametric studies are performed to investigate the impacts of a series of parameters on UHS in aquifers. In each group of parametric study, only one input parameter is changed with all the other parameters

kept identical to that of the base case unless otherwise specified. The investigated parameters include microbial growth rate, initial Fe_2O_3 concentration, Fe_2O_3 dissolution rate, injection pressure and withdrawal pressure.

4.5.1 Numerical model description

Fig. 4-5 shows the geometry and meshing of the numerical model that is used for modeling UHS in aquifer. Due to the symmetry, only a half of the aquifer is modeled. The length of the model is 500 m and the height is 250 m. The top surface of the model is located at the depth of 1000 m and the whole domain is assumed at an isothermal condition with the temperature remaining at 320 K. A horizontal wellbore (wellbore radius equals to 5 cm) that is perpendicular to this vertical plane is set on the left boundary of the model with the distance between the wellbore and the top surface of the aquifer being 30 m. The wellbore is used for both hydrogen injection and withdrawal. To evaluate the dynamic responses of reservoir properties during UHS, an observation point is set near the wellbore with the horizontal distance between the observation point and the wellbore being 30 m as well.

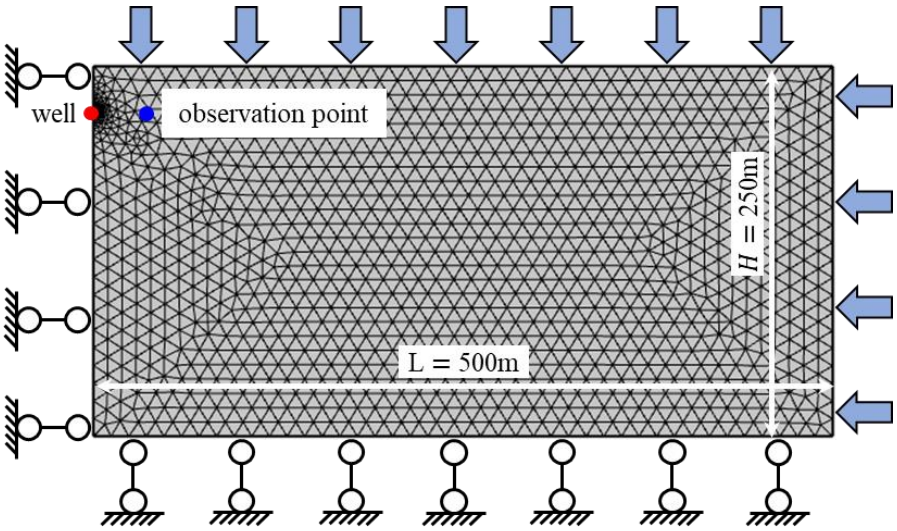

Fig. 4-5 Geometry of the 2D numerical model for UHS modeling.

For initial conditions, the pore space of aquifer is assumed initially 100% filled by the

formation water. Also, the aquifer is assumed initially under the hydrostatic pressure conditions. In addition, the initial hydrogen concentration and microbial concentration in the aqueous phase, the initial Fe_2O_3 and Fe_3O_4 concentration in the rock, and the initial volumetric fraction of microbes adsorbed on the pore surface are set.

For boundary conditions, the normal displacements of the left and bottom boundaries are restricted to zero and the confining pressure is applied to the top and right boundaries. Meanwhile, the top, right and bottom boundaries are considered as impervious which means that no flow/flux is allowed through these boundaries (Sainz-Garcia et al., 2017). During UHS, constant injection pressure and withdrawal pressure are applied on the wellbore wall.

In our simulation, a certain amount of cushion gas (hydrogen in this work) is first injected into the aquifer for 10 months with the purpose of maintaining the operation pressure. Then during the storage operation, hydrogen is first injected into the aquifer for two months and then withdrawn from the aquifer for four months in each cycle. Totally, six storage cycles are simulated. In each cycle, the hydrogen injection pressure is kept as 18 MPa and the withdrawn pressure is kept as 8 MPa. All the input parameters involved in the numerical simulation for the base case are summarized in Table 4-3.

Table 4-3 Input parameters for the base case simulation.

Parameters (unit)	Symbols	Values	References
Pore compressibility (MPa^{-1})	c_p	0.02	-
Elastic modulus (GPa)	E	20	-
Poisson's ratio	v	0.2	-
Confining pressure (MPa)	σ_c	20	-
Initial porosity	$\emptyset_0$	0.1	-
Initial permeability (m^2)	k_0	1e-13	-
Rock density (kg/m^3)	ρ_c	2400	-
Reversible microbial adsorption rate (1/h)	k_1	0.065	Kim (2006); Li et al. (2011)
Microbial desorption rate (1/h)	k_2	0.0012	Kim (2006); Li et al. (2011)

Irreversible microbial adsorption rate (1/h)	k_3	0.01	Kim (2006); Li et al. (2011)
The maximum microbial growth rate (1/h)	g_{1max}	0.024	Kim (2006); Li et al. (2011)
Microbial decay rate (1/h)	d_1	0.005	Kim (2006); Li et al. (2011)
Microbial density (kg/m^3)	ρ_m	1600	Kim (2006); Li et al. (2011)
Reaction yield coefficient (mol/m^3/h)	$1/Y$	0.02	-
Half-saturation constant for iron reduction (mg/mL)	$K_{m/s}$	0.2	-
Half-saturation constant for microbial growth (mg/mL)	$K_{H_2/s}$	0.5	-
Half-saturation constant for microbial growth (mg/mL)	$K_{Fe_2O_3/s}$	200	-
Hydrodynamic dispersion coefficient for hydrogen (m^2/s)	D_{H_2}	1e-6	-
Hydrodynamic dispersion coefficient for microbe (m^2/s)	D_m	1e-9	Kim (2006); Li et al. (2011)
Initial water saturation	$S_{w,0}$	1	Zhao et al., (2024)
Irreducible water saturation	S_{wi}	0.2	Zhao et al. (2024)
Residual gas saturation	S_{gr}	0	Zhao et al. (2024)
Nonwetting phase entry pressure (KPa)	p_e	5	Zhao et al. (2024)
Pore size distribution coefficient	λ	2	-
Initial hydrogen concentration in aqueous phase (mg/mL)	$C_{H_2,0}$	0	-
Initial microbial concentration in aqueous phase (mg/mL)	$C_{m,0}$	0.0001	-
Initial fraction of porosity occupied by reversibly adsorbed microbes	$\emptyset_{1,0}$	1e-6	-
Initial fraction of porosity occupied by irreversibly adsorbed microbes	$\emptyset_{2,0}$	1e-6	-
Initial Fe_2O_3 concentration in porous rock (mol/m^3)	$C_{Fe_2O_3,0}$	450	-
Initial Fe_3O_4 concentration in porous rock (mol/m^3)	$C_{Fe_3O_4,0}$	0	-

4.5.2 Simulation results for the base case

Fig. 4-6 shows the temporal evolution of hydrogen saturation in aquifer during repeated hydrogen injection and withdrawal cycles. As can be seen, hydrogen tends to migrate upwards and then accumulates at the top surface of the aquifer. This is mainly because the density of hydrogen is much smaller than the density of formation water and thus buoyant flow, which is caused by gravitational force, plays a significant role during hydrogen migration. With the increase of injection and withdrawal cycles, the hydrogen saturation at the top surface gradually increases which means that more and more hydrogen accumulates at the top of the storage aquifer with the progress of UHS. This finding implies that the production well should be placed at the upper part of the storage aquifer instead of the lower part in terms of enhancing hydrogen recovery. Fig. 4-7

shows the variation of hydrogen saturation at the observation point. From this figure, it can be known that hydrogen saturation increases in the injection phase while decreases in the withdrawal phase. Overall, hydrogen saturation exhibits an increasing trend with the progress of UHS.

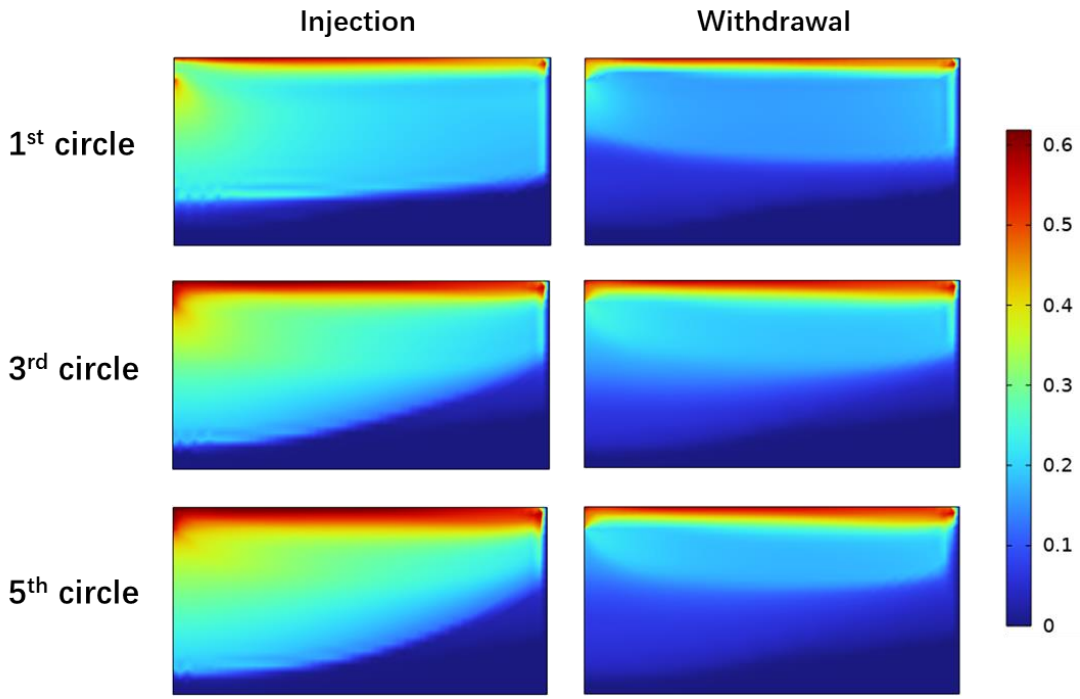

Fig. 4-6 Hydrogen saturation distribution in aquifer at the end of different injection and withdrawal cycles.

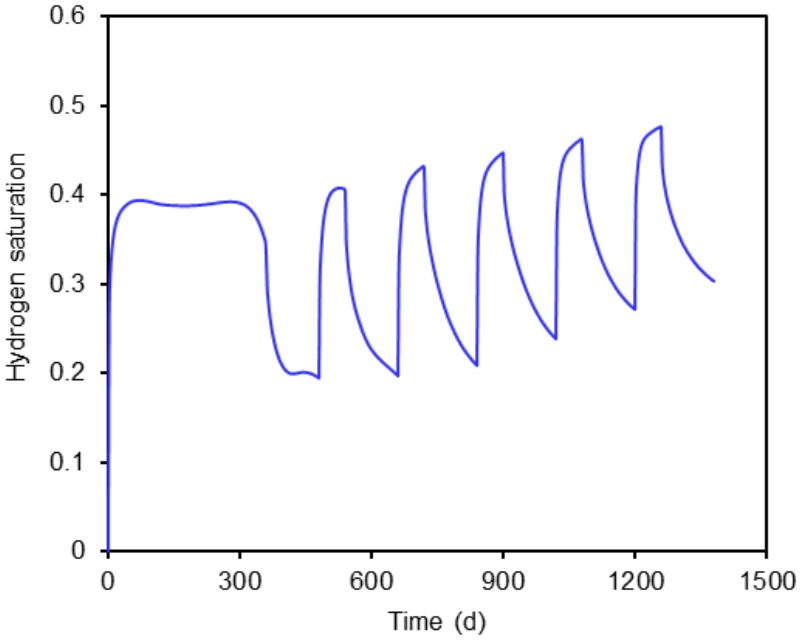

Fig. 4-7 Variation of hydrogen saturation at the observation point during cyclic hydrogen injection and withdrawal.

Fig. 4-8 and Fig. 4-9 show the temporal evolution of adsorbed microbe population in the aquifer and at the observation point during repeated hydrogen injection and withdrawal cycles, respectively. The value of these two figures represents the fraction of porosity occupied by those microbes attached on the pore surface. The larger the value, the greater the microbe population. As can be seen, microbes distribute surrounding the wellbore instead of at the top surface of the aquifer. This is mainly because injection pressure is applied at wellbore and thus the dissolved hydrogen concentration surrounding the wellbore is the greatest which stimulates microbial activities in this region the most. It can also be found that microbe population on pore surface increases during hydrogen injection while declines during hydrogen withdrawal as the hydrogen concentration in formation water (see Fig. 4-10(a)) periodically changes with reservoir pressure during UHS. For further observation, it can be found that the microbes almost die out after three cycles of hydrogen injection and withdrawal. This is mainly attributed to the dissolution of Fe_2O_3 during UHS, see Fig. 4-10(b). The dissolution of Fe_2O_3 leads to the decrease of microbial growth rate (see Eq. (4-22)). Thus, the net microbial growth rate decreases in the increased cycle of hydrogen injection while the net microbial decay rate increases in the increased cycle of hydrogen withdrawal. This is the primary reason why microbes die out after three cycles of UHS.

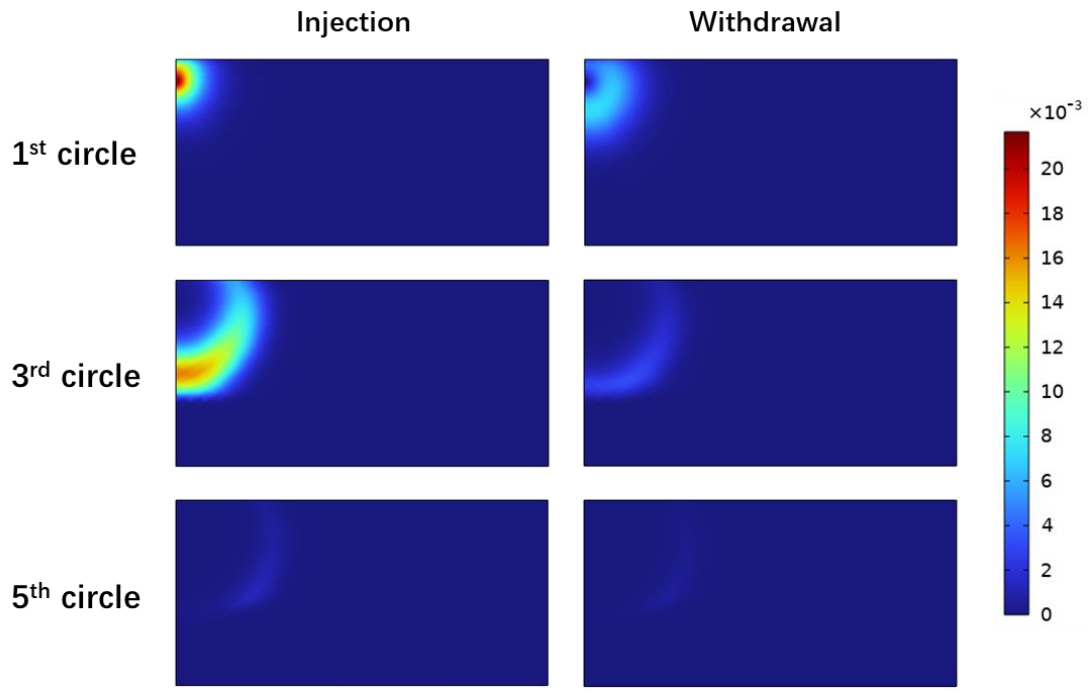

Fig. 4-8 Distribution of adsorbed microbe population ($\emptyset_1 + \emptyset_2$) in aquifer at the end of different injection and withdrawal cycles.

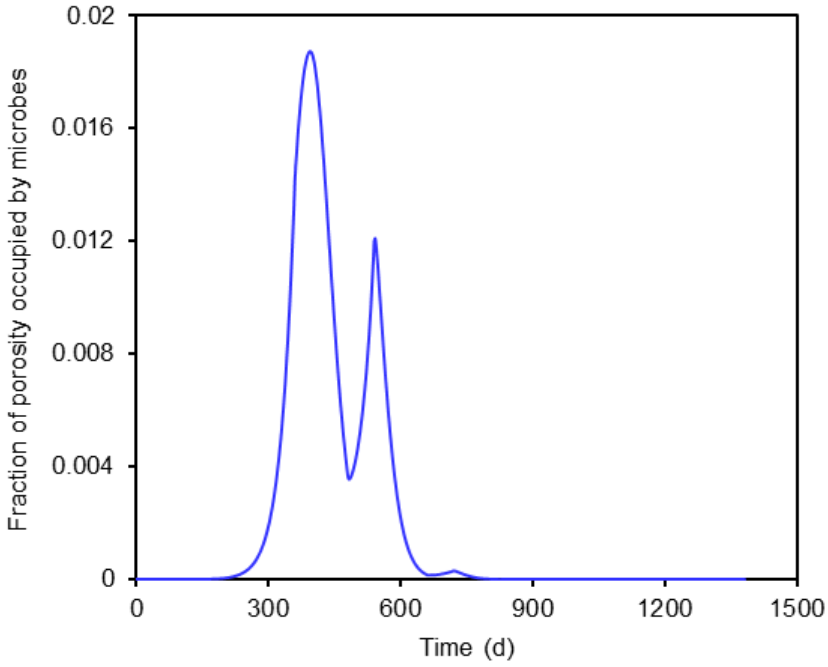

Fig. 4-9 Variation of adsorbed microbe population ($\emptyset_1 + \emptyset_2$) at the observation point during cyclic hydrogen injection and withdrawal.

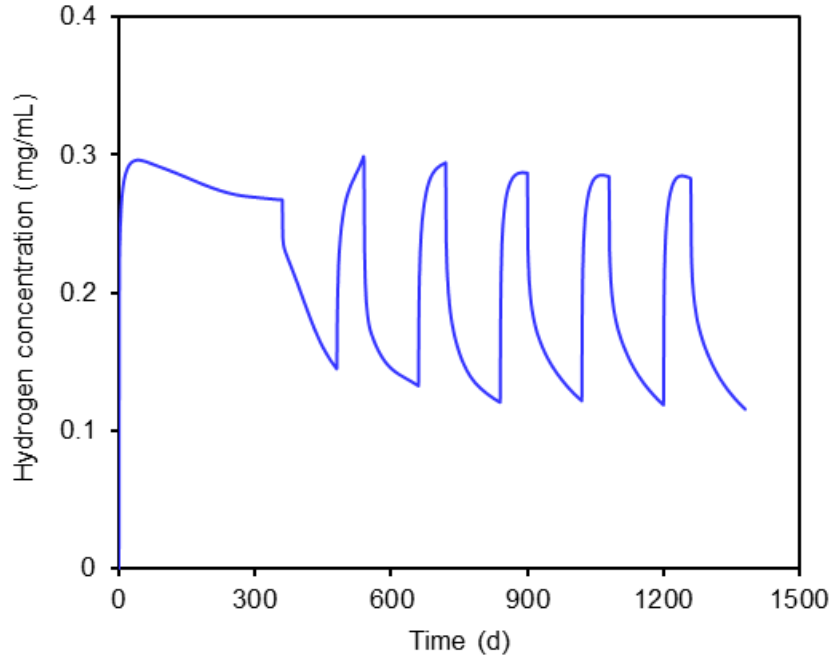

(a)

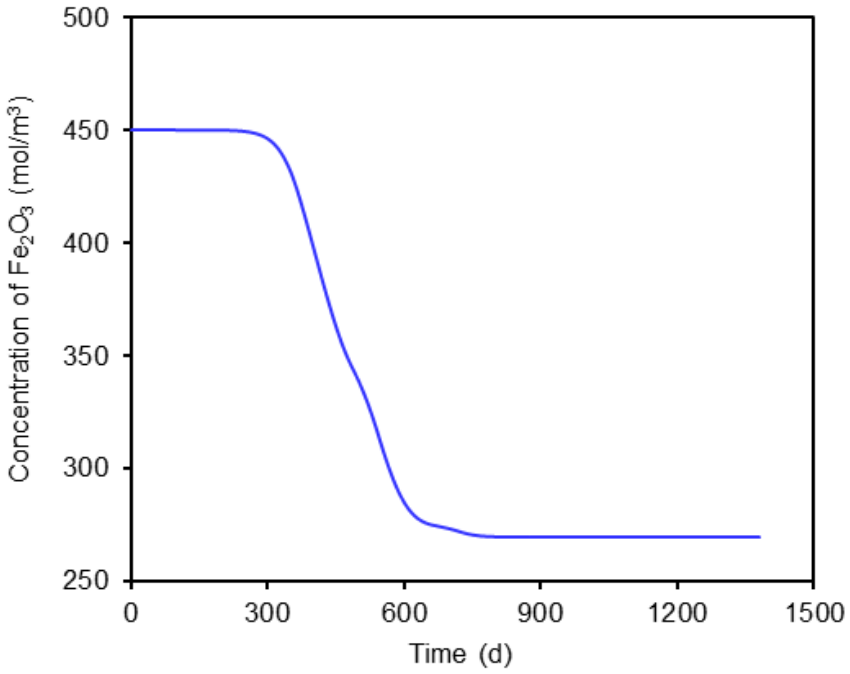

(b)

Fig. 4-10 Simulation results at the observation point: (a) variation of hydrogen concentration in formation water during cyclic hydrogen injection and withdrawal; (b) variation of Fe_2O_3 concentration during cyclic hydrogen injection and withdrawal.

Fig. 4-11 shows the temporal evolution of Fe_2O_3 concentration in porous rock during repeated hydrogen injection and withdrawal cycles. As can be seen, the area where

Fe_2O_3 dissolves gradually enlarges during UHS and this area is consistent with the area where microbes distribute (see Fig. 4-8). Fig. 4-12 shows the variation of Fe_2O_3 and Fe_3O_4 concentrations at the observation point. As iron reduction process leads to Fe_2O_3 dissolution and Fe_3O_4 precipitation, correspondingly the concentration of Fe_2O_3 decreases and the concentration of Fe_3O_4 increases. Fig. 4-13 shows the cumulative hydrogen loss and water production during iron reduction process. The total water production is around 18.5 ton and the total hydrogen loss is around 2.1 ton which is less than 2% of the total hydrogen injected during the six cycles of UHS.

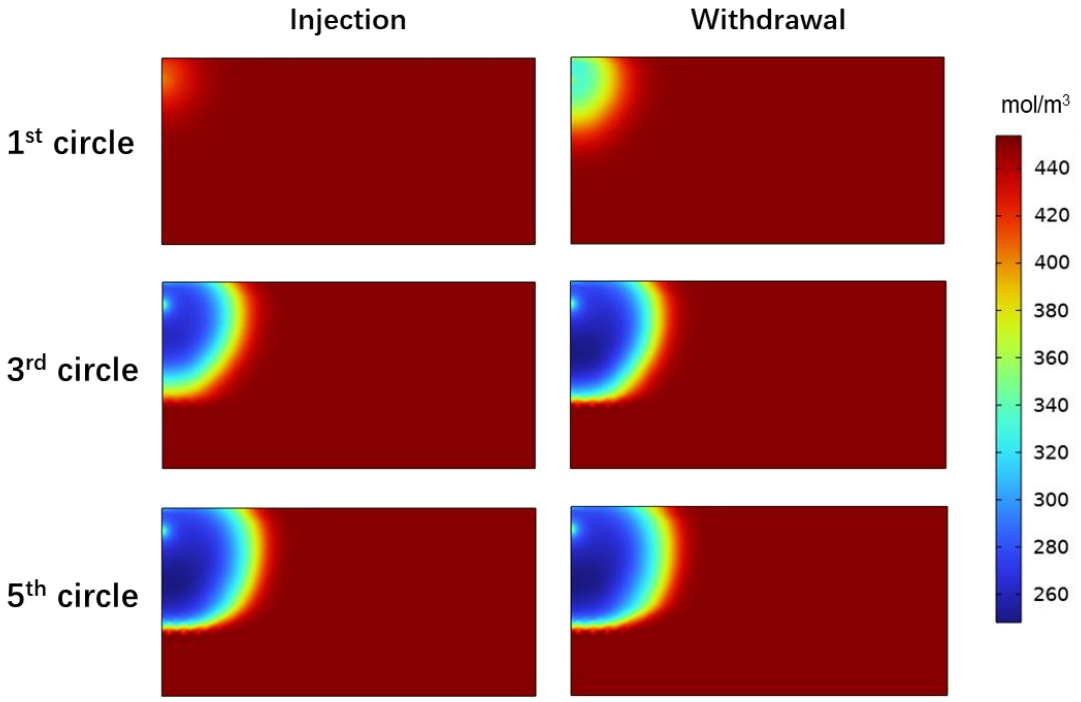

Fig. 4-11 Distribution of Fe_2O_3 concentration in porous rock at the end of different injection and withdrawal cycles.

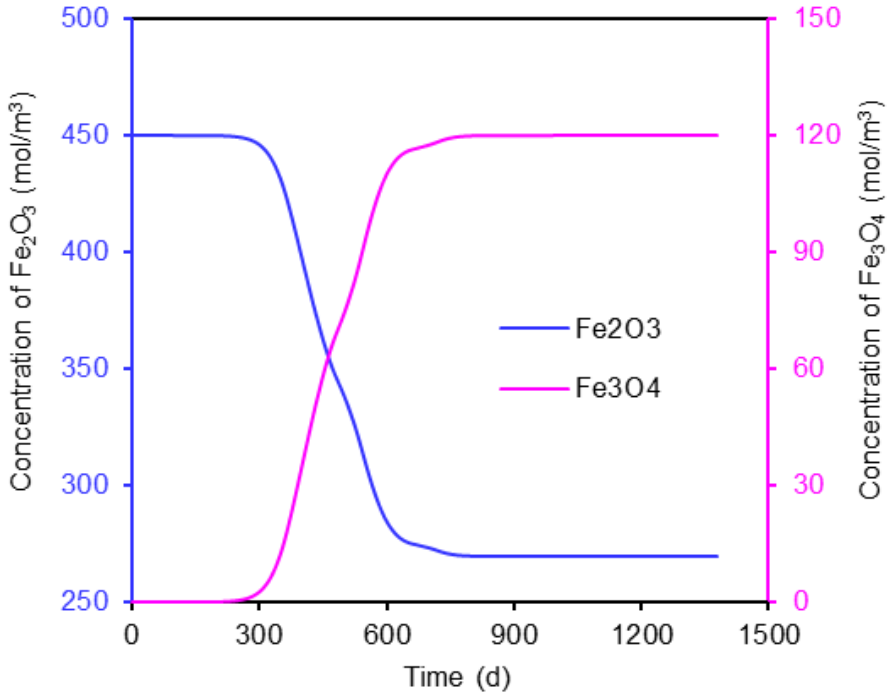

Fig. 4-12 Variation of Fe_2O_3 and Fe_3O_4 concentrations at the observation point during cyclic hydrogen injection and withdrawal.

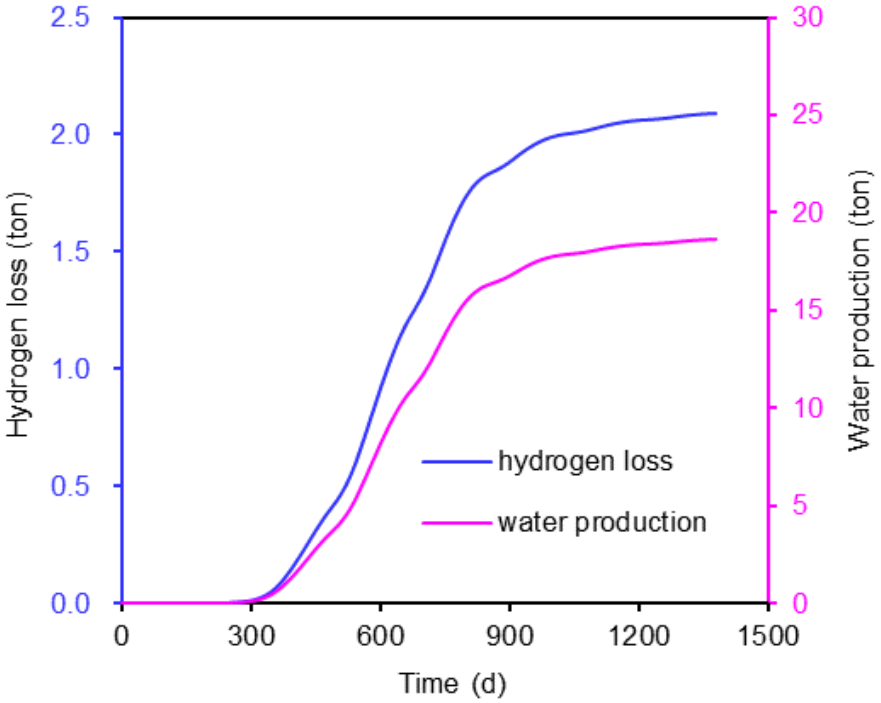

Fig. 4-13 Cumulative hydrogen loss and water production in aquifer during cyclic hydrogen injection and withdrawal.

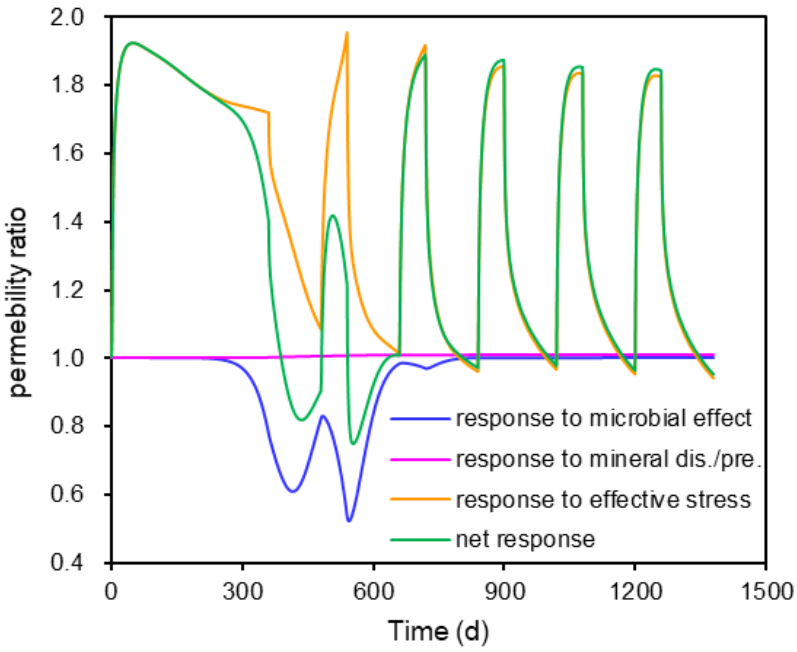

Fig. 4-14 Evolution of rock permeability at the observation point during cyclic hydrogen injection and withdrawal.

Fig. 4-14 shows the rock permeability evolution at the observation point during UHS. In this work, we consider the joint impacts of microbial clogging, mineral dissolution and precipitation, and effective stress change on permeability evolution. As can be seen, microbial clogging leads to permeability decline during UHS and its impact can be ignored after three cycles of hydrogen injection and withdrawal. For mineral dissolution and precipitation, the permeability increase induced by Fe_2O_3 dissolution is nearly counteracted by the permeability decline induced by Fe_3O_4 precipitation. Thus, the impact of mineral dissolution and precipitation can be neglected during UHS. For effective stress, its impact on aquifer permeability is the most significant and lasts during the whole UHS operations.

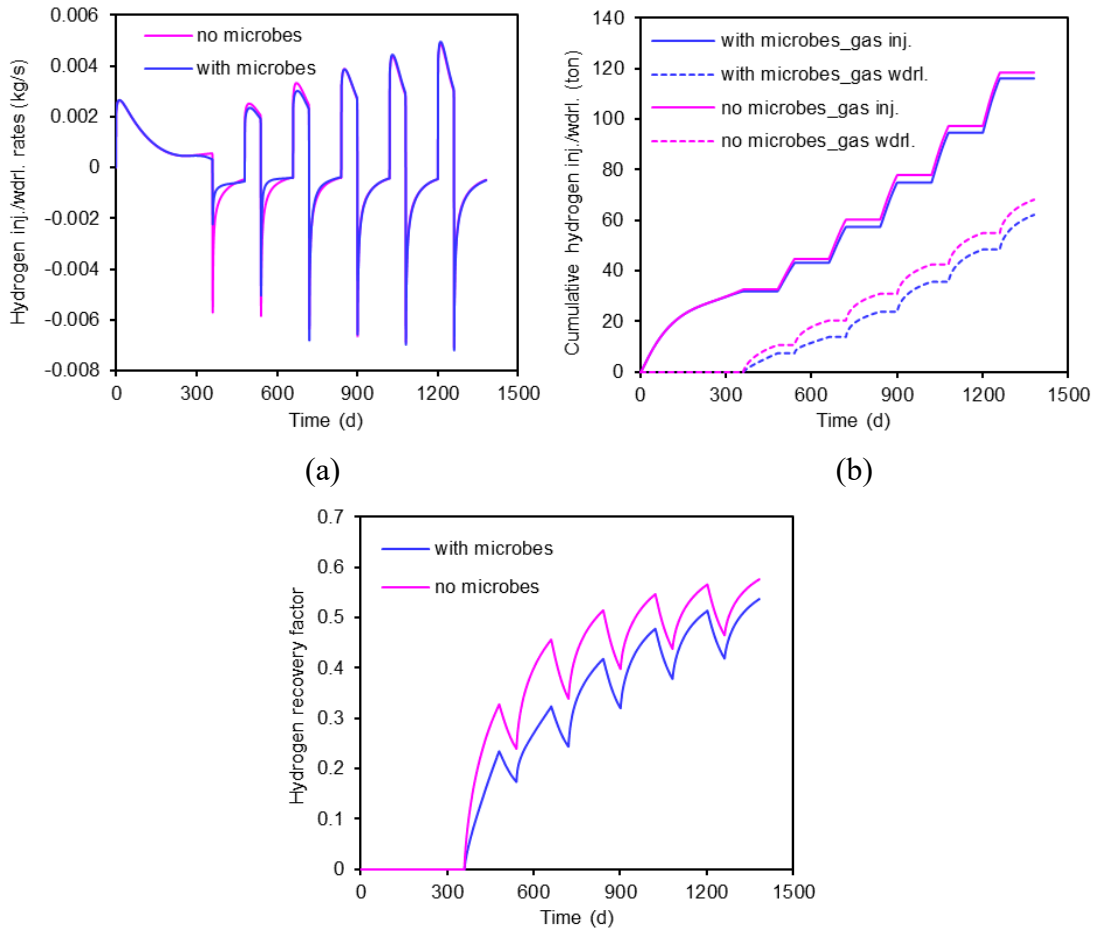

Fig. 4-15 Simulation results: (a) variation of hydrogen injection and withdrawal rates; (b) cumulative hydrogen injected and withdrawn; (c) variation of hydrogen recovery factor.

Fig. 4-15(a) shows the variation of hydrogen injection and withdrawal rates during the six repeated cycles. Notet that the positive value in this figure represents injection rate while the negative value represents withdrawal rate. The results for the case that does not consider the impacts of microbial activities are also presented for a reference. As can be seen, the inclusion of microbial activities leads to the decline of hydrogen injection and withdrawal rates in the first three cycles. This phenomenon can be explained from three aspects. First, microbial clogging results in permeability decline which lowers hydrogen injection and withdrawal rates. Second, water production

during iron reduction process decreases hydrogen saturation and relative permeability, thus leading to the reduction of hydrogen injection and withdrawal rates. Third, the iron reduction process induces permanent hydrogen loss. Fig. 4-15(b) shows the cumulative hydrogen injected and withdrawn. It can be seen that both the amounts of injected and withdrawn hydrogen decrease when the impacts of microbial activities are considered with the amount of hydrogen withdrawn decreasing more than the amount of hydrogen injected. Fig. 4-15(c) shows the variation of hydrogen recovery factor during UHS. The recovery factor is defined as the ratio of cumulative hydrogen withdrawn to cumulative hydrogen injected. As can be seen, hydrogen recovery factor declines when the impacts of microbial activities are considered.

4.5.3 Parametric studies

The investigated five parameters can be classified into two categories. The first category includes microbial growth rate, initial Fe_2O_3 concentration and Fe_2O_3 dissolution rate which are all biochemical parameters. The second category includes injection pressure and withdrawal pressure which are operational parameters. In the following, the impact of each parameter on UHS in aquifers is analyzed.

4.5.3.1 The impact of microbial growth rate

In this subsection, we investigate the impact of microbial growth rate on UHS in aquifers. From Fig. 4-16(a), it can be found that the increase of microbial growth rate leads to more severe bioclogging. When g_1 reaches 0.025 1/h, pore space is fully occupied by microbes. In this case, permeability declines to zero and subsequent hydrogen injection and withdrawal cannot proceed. From Fig. 4-16(b), it can be known that more hydrogen is lost and more water is produced when microbial growth rate increases. As larger microbial growth rate leads to more severe bioclogging, more

hydrogen loss and more water production, the hydrogen injection and withdrawal rates decrease thereby, as shown in Fig. 4-16(c). From Fig. 4-16(d), it can also be known that hydrogen recovery factor declines with the increase of microbial growth rate.

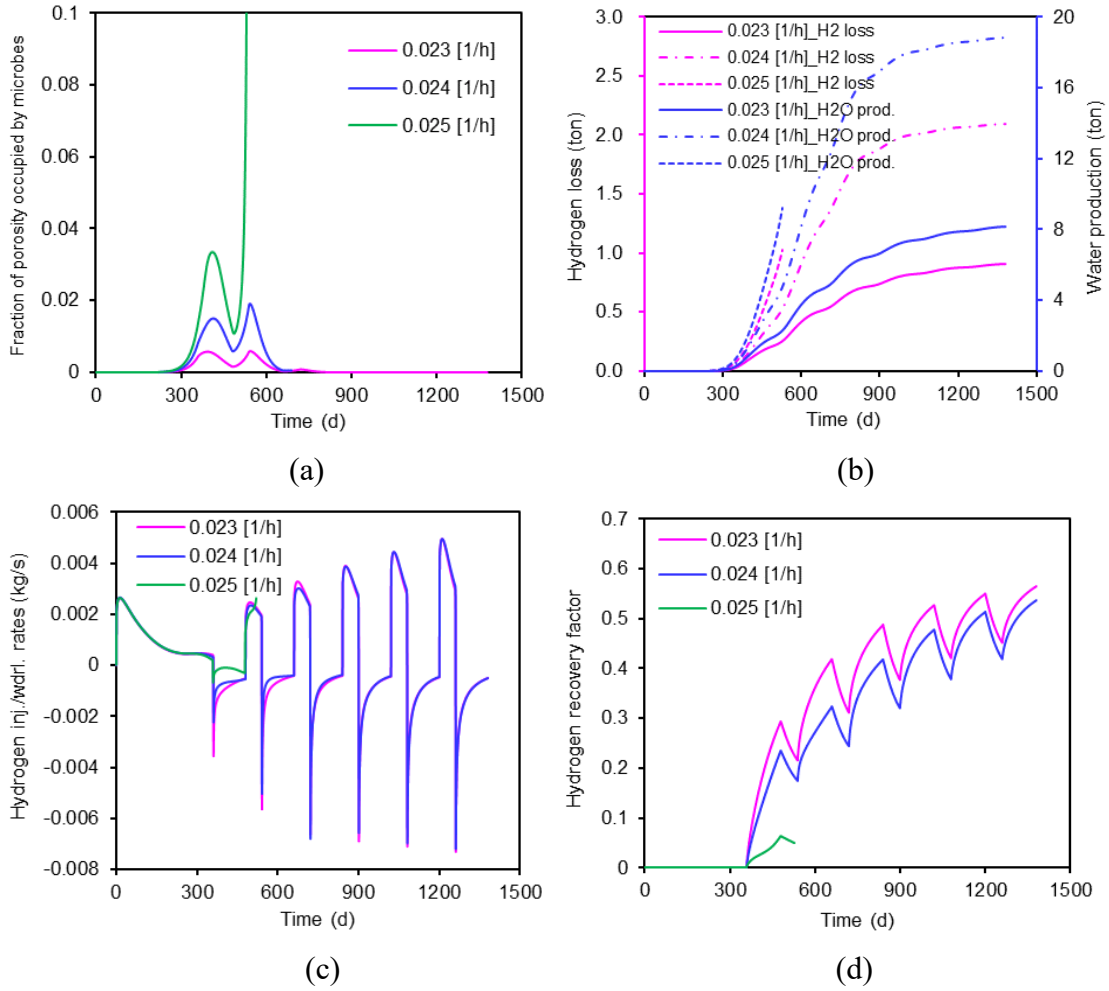

Fig. 4-16 Impact of microbial growth rate on: (a) adsorbed microbe population at the observation point; (b) cumulative hydrogen loss and water production; (c) hydrogen injection and withdrawal rates; and (d) hydrogen recovery factor.

4.5.3.2 The impact of initial Fe_2O_3 concentration

In this subsection, we investigate the impact of initial Fe_2O_3 concentration on UHS in aquifers. According to Eq. (4-22), the larger the Fe_2O_3 concentration, the greater the microbial growth rate. Therefore, it can be found from Fig. 4-17(a) that the increase of initial Fe_2O_3 concentration leads to more severe bioclogging. When initial Fe_2O_3

concentration reaches 470 mol/m^3, pore space is fully clogged by microbes. In this case, subsequent hydrogen injection and withdrawal cannot proceed. From Fig. 4-17(b), the larger initial Fe_2O_3 concentration leads to more hydrogen loss and more water production during iron reduction process. As larger initial Fe_2O_3 concentration leads to more severe bioclogging, more hydrogen loss and more water production, lower hydrogen injection and withdrawal rates are observed thereby, see Fig. 4-17(c). From Fig. 4-17(d), it can be found that hydrogen recovery factor declines with the increase of initial Fe_2O_3 concentration.

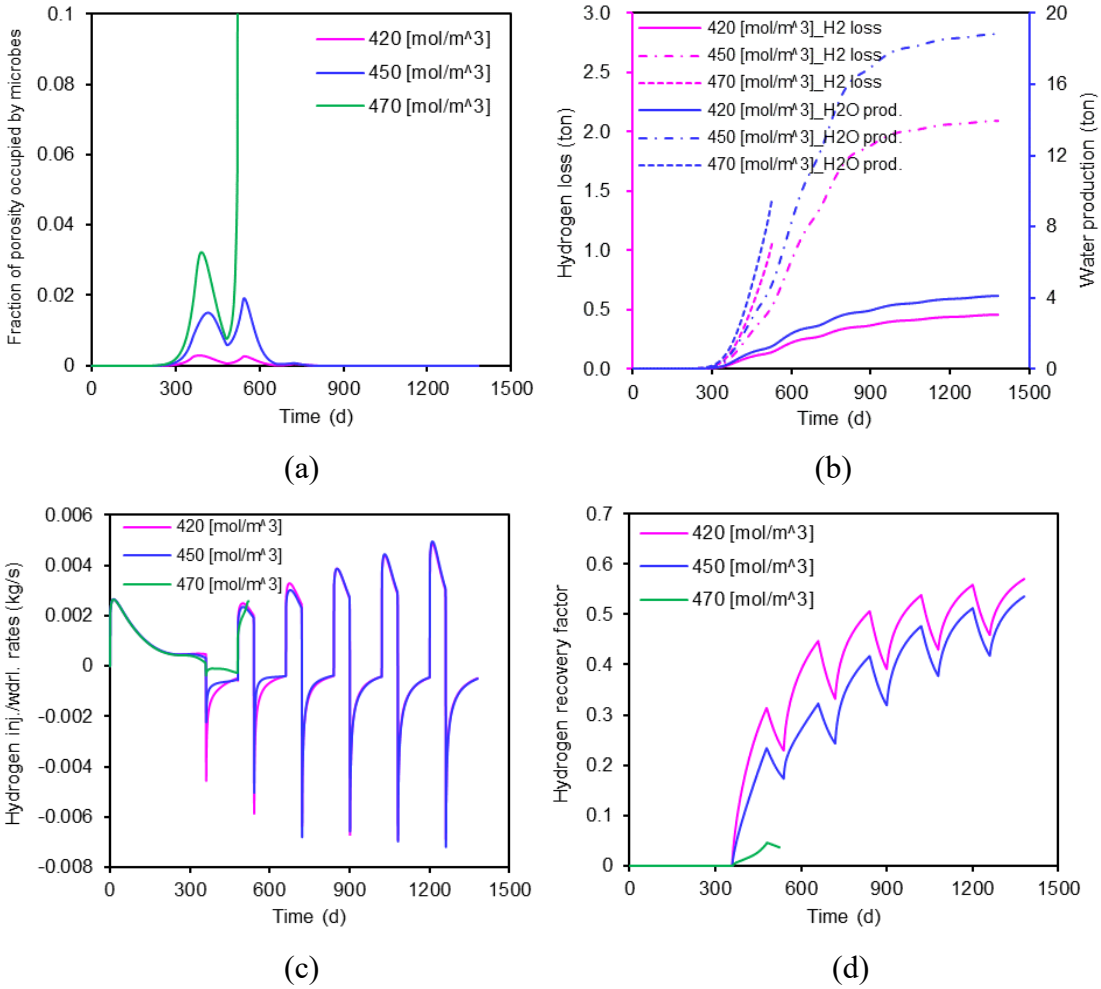

Fig. 4-17 Impact of initial Fe_2O_3 concentration on: (a) adsorbed microbe population at the observation point; (b) cumulative hydrogen loss and water production; (c) hydrogen injection and withdrawal rates; and (d) hydrogen recovery factor.

4.5.3.3 The impact of Fe_2O_3 dissolution rate

In this subsection, we investigate the impact of Fe_2O_3 dissolution rate on UHS in aquifers. The smaller the Fe_2O_3 dissolution rate, the slower the microbial growth rate decreases. Therefore, the bioclogging phenomenon becomes more severe when Fe_2O_3 dissolution rate decreases, as shown in Fig. 4-18(a). When Fe_2O_3 dissolution rate decreases to 0.01 mol/m^3/h, pore space is fully bioclogged which hinders the subsequent hydrogen injection and withdrawal. From Fig. 4-18(b), more hydrogen is lost and more water is produced with the decrease of Fe_2O_3 dissolution rate. As smaller Fe_2O_3 dissolution rate leads to more severe bioclogging and more hydrogen loss and water production, lower hydrogen injection and withdrawal rates are observed thereby, as shown in Fig. 4-18(c). In Fig. 4-18(d), it can be found that hydrogen recovery factor declines with the decrease of Fe_2O_3 dissolution rate.

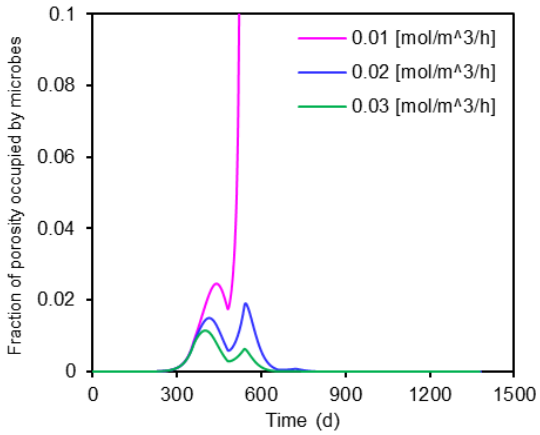

(a)

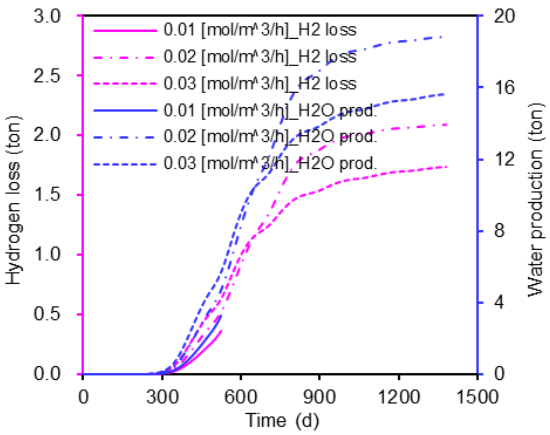

(b)

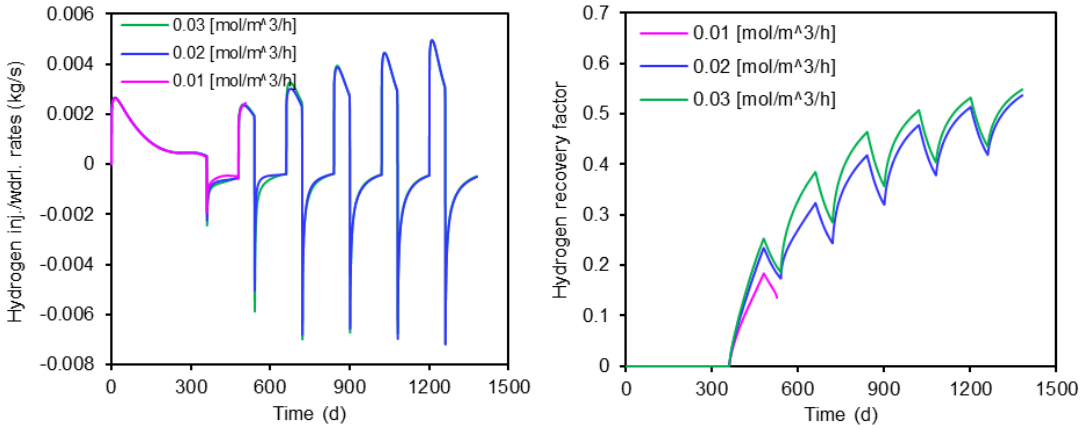

(c) (d)

Fig. 4-18 Impact of Fe_2O_3 dissolution rate on: (a) adsorbed microbe population at the observation point; (b) cumulative hydrogen loss and water production; (c) hydrogen injection and withdrawal rates; and (d) hydrogen recovery factor.

4.5.3.4 The impact of injection pressure

In this subsection, we investigate the impact of injection pressure on UHS in aquifers. According to Eq. (4-22), the microbial growth rate is directly proportional to hydrogen concentration in formation water. As larger injection pressure leads to more hydrogen dissolved in formation water, the microbial growth rate becomes greater with the increase of injection pressure. From Fig. 4-19(a), the bioclogging phenomenon becomes more severe with the increase of injection pressure. When injection pressure reaches 19 MPa, pore space is fully bioclogged (not at the observation point but at the area more close to the wellbore) and hydrogen cannot be further injected and withdrawn in this case. From Fig. 4-19(b), more hydrogen is lost and more water is produced when injection pressure increases. As larger injection pressure leads to more severe bioclogging, more hydrogen loss and more water production, lower hydrogen injection and withdrawal rates are yielded thereby, see Fig. 4-19(c). From Fig. 4-19(d), hydrogen recovery factor decreases when injection pressure increases.

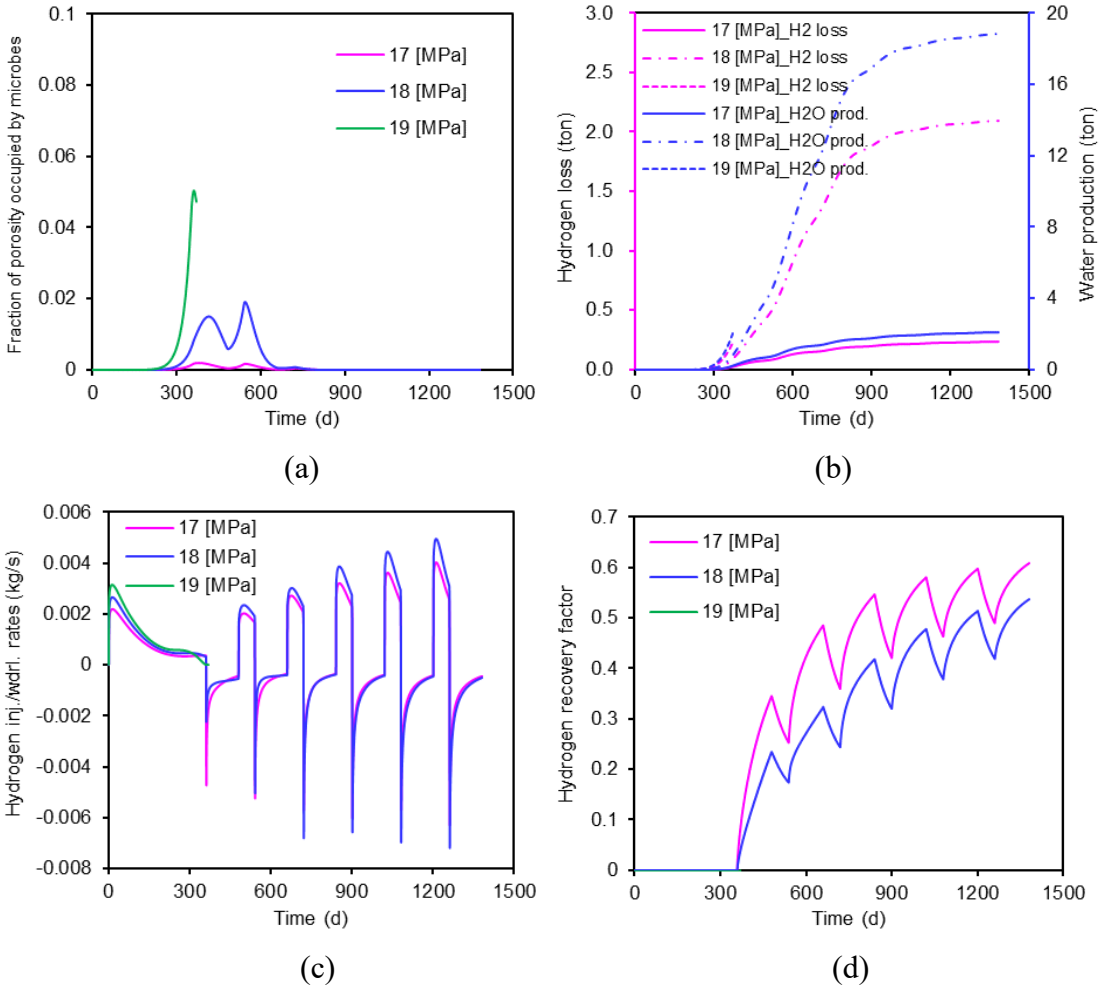

Fig. 4-19 Impact of injection pressure on: (a) adsorbed microbe population at the observation point; (b) cumulative hydrogen loss and water production; (c) hydrogen injection and withdrawal rates; and (d) hydrogen recovery factor.

4.5.3.5 The impact of withdrawal pressure

In this subsection, we investigate the impact of withdrawal pressure on UHS in aquifers. When withdrawal pressure is lowered, more hydrogen will be released from formation water during withdrawal phase which will lead to the decrease of microbial growth rate. Therefore, the greater the withdrawal pressure is, the more severe the bioclogging phenomenon will be, as shown in Fig. 4-20(a). Also, it can be observed from Fig. 4-20(b) that the larger withdrawal pressure leads to more hydrogen loss and more water production during iron reduction process. As larger withdrawal pressure leads to more

severe bioclogging, more hydrogen loss and more water production, hydrogen injection and withdrawal rates are lowered thereby, see Fig. 4-20(c). From Fig. 4-20(d), hydrogen recovery factor decreases with the increase of withdrawal pressure.

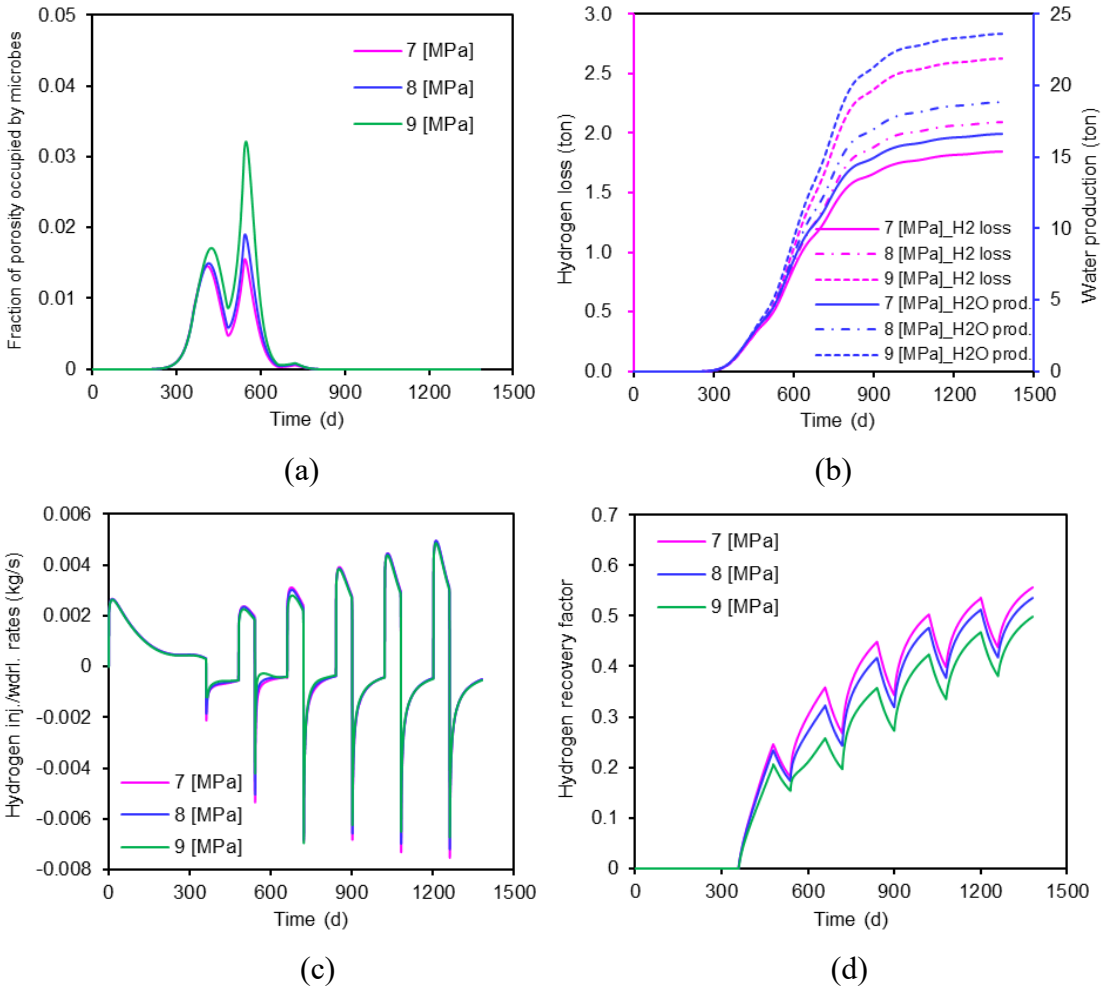

Fig. 4-20 Impact of withdrawal pressure on: (a) adsorbed microbe population at the observation point; (b) cumulative hydrogen loss and water production; (c) hydrogen injection and withdrawal rates; and (d) hydrogen recovery factor.

4.6 Conclusions

In this work, we propose a coupled hydrological-mechanical-chemical-biological multiphysics model to investigate the impacts of IRB activities on UHS in aquifers. This multiphysics model couples (1) rock deformation; (2) water-hydrogen two-phase flow; (3) microbes and dissolved hydrogen transport; (4) mineral

dissolution/precipitation; and (5) microbial adsorption/desorption and growth/decay together. Based on the modelling results, the following conclusions can be drawn:

(1) Although hydrogen saturation at the top surface of the aquifer is the greatest, microbial activities surrounding the injection well is stimulated the most. As a result, the microbially clogged area and biochemical reactions occuring area surround the injection well as well.

(2) Microbial activities influence the initial few cycles of hydrogen injection and withdrawal. When hydrogen is injected into the aquifers, IRB activities are stimulated which catalyze the reaction between hydrogen and the mineral Fe_2O_3 in the hosting rock. In this process, the concentration of Fe_2O_3 in rock decreases and thereby microbial net growth rate declines and be negative until all microbes die out. Once microbes die out, the impacts of microbial activities on UHS operations disappear.

(3) Microbial activities can degrade hydrogen recovery efficiency through microbial clogging of pores, hydrogen consumption and water production. In comparison with hydrogen consumption and water production, microbial clogging affects UHS more significantly as aquifer pore space can be fully clogged by these microbes, in which condition subsequent hydrogen injection and withdrawal operations have to be suspended. Thus, these extreme cases should be avoided when planning UHS projects.

(4) During UHS, aquifer permeability dynamically changes under the joint impacts of microbial clogging, mineral dissolution/precipitation and effective stress. Among these three factors, effective stress plays the dominant role and controls aquifer permeability throughout the UHS operations, while microbial clogging only

influences aquifer permeability in the initial few cycles of hydrogen injection and withdrawal. For mineral dissolution and precipitation, their impacts are counteracted and can be neglected.

Chapter 5 Concluding Remarks

5.1 Main conclusions

In the context of decarbonization and achieving the net-zero emission target, low-carbon gas energy resources like biogenic methane and hydrogen are playing more important roles. Large scale use of these gas energy resources inevitably involves energy extraction/storage in underground formations. However, most of these subsurface environments are not life-free and harbor a variety of microbial communities. The activities of these microbes can be stimulated by the added nutrients/substrates and then have significant impacts on gas energy extraction/storage operations through inducing a series of biochemical reactions in the hosting rock. In this research, we define gas energy extraction/storage operations that involve microbial activities as coupled hydraulic-mechanical-chemical-biological processes. For simplicity, these coupled processes in subsurface formations are called as geo-multiphysics. The individual process, in absence of cross couplings, has already formed the basis of very well-known disciplines such as hydrology, elasticity, chemistry and biology, while the inclusion of cross-couplings between different physical processes implies that one physical process can affect the initiation and progress of another. Therefore, consideration of cross-coupling relations is the key to formulate mathematical equations to quantify the impacts of microbial activities on gas energy extraction/storage.

In chapter 2, a generic geo-multiphysics model is developed. This generic geo-multiphysics model captures various processes including rock deformation, fluid flow, reactive transport, mineral dissolution/precipitation, and various forms of microbial activities such as microbial adsorption/desorption and growth/decay. All these

processes are linked together through rock porosity and permeability models. Commonly, rock porosity and permeability models are defined as a function of effective stress and gas sorption strains. In this work, they are extended to include the impacts of a series of microbe-induced changes such as pore/fracture bioclogging and minerals dissolution/precipitation.

In chapter 3, the generic geo-multiphysics model is tailored to the case of biogenic methane generation and extraction from coal seams with all processes linked through the specific porosity and permeability models. This geo-multiphysics model is verified against laboratory data of biogenic methane generation and microbial transport. The verified model is then applied to simulate biogenic methane generation and extraction under the impact of fracture bioclogging. Based on the simulation results, it can be concluded that:

- Repeated cycles of nutrients alternating water injection can ensure long-term biogenic methane generation and extraction. During nutrients injection, metabolic activities of microbes are stimulated which convert coal to biogenic methane but meanwhile microbial adsorption and growth on fracture surface leads to microbial clogging of the fracture system. In order to release the clogged space, nutrients delivery should be temporally suspended and replaced by water injection. When the clogged fracture space is released, nutrients injection can restart.

- Coal-to-methane bioconversion has the great potential to enhance gas flow capacity in coal seams. During nutrients injection, coal permeability significantly declines due to microbial clogging of fracture. However, coal permeability rebounds and gains net increase after declogging. Therefore, coal permeability and gas flow capacity can be greatly enhanced after multiple cycles of nutrients

alternating water injection.

- In each cycle of nutrients alternating water injection, biogenic methane generation rate exhibits inverted-V shape variation trend while extraction rate exhibits inverted-W shape variation trend. During nutrients injection, biogenic methane generation rate continuously increases due to microbial growth while extraction rate first increases due to the increase of gas generate rate and then decreases due to microbial clogging. During water injection, biogenic methane generation rate continuously decreases due to microbial decay while extraction rate first increases due to fracture space release and then decreases due to of gas generation rate decline.

- Biogenic methane extraction efficiency gradually increases during coal-to-methane bioconversion. When biogenic methane is generated, a fraction of it diffuses into coal matrix, adsorbs on coal grains and becomes adsorbed gas under the pressure difference between fracture and matrix systems. With the progress of coal-to-methane bioconversion, more gas will be extracted instead of becoming adsorbed gas as fracture-matrix pressure difference gradually diminishes. Thus, the extraction efficiency of biogenic methane can be enhanced after multiple cycles of nutrients alternating water injection.

In chapter 4, the generic geo-multiphysics model is tailored to the case of underground hydrogen storage in aquifers with all processes linked through the specific porosity and permeability models. This geo-multiphysics model is verified against laboratory biochemical reaction data and microbial transport data. Then, the verified model is used to investigate the impacts of iron-reduction bacteria activities on hydrogen storage in aquifers. Based on the simulation results, it can be concluded that:

- Microbial activities influence the initial few cycles of hydrogen injection and withdrawal. When hydrogen is injected into the aquifers, iron-reduction bacteria activities are stimulated which catalyze the reaction between hydrogen and the mineral Fe_2O_3 in the hosting rock. In this process, the concentration of Fe_2O_3 in rock decreases and thereby microbial net growth rate declines and be negative until all microbes die out. Once microbes die out, the impacts of microbial activities on hydrogen storage operations disappear.

- Microbial activities can degrade hydrogen recovery efficiency through microbial clogging of pores, hydrogen consumption and water production. In comparison with hydrogen consumption and water production, microbial clogging affects hydrogen storage more significantly as aquifer pore space can be fully clogged by these microbes, in which condition subsequent hydrogen injection and withdrawal operations have to be suspended. Thus, these extreme cases should be avoided when planning hydrogen storage projects.

- During hydrogen storage, aquifer permeability dynamically changes under the joint impacts of microbial clogging, mineral dissolution/precipitation and effective stress. Among these three factors, effective stress plays the dominant role and controls aquifer permeability throughout the hydrogen storage operations, while microbial clogging only influences aquifer permeability in the initial few cycles of hydrogen injection and withdrawal. For mineral dissolution and precipitation, their impacts are counteracted and can be neglected.

The above studies and conclusions suggest that microbial activities can negatively impact the performance of gas energy extraction/storage but can also be utilized to generate energy from underground formations. Thus, more efforts should be done to

minimize the negative impacts induced by microbial activities and meanwhile to maximize the capability of microbes to generate energy that can be extracted.

Here, it is also worthwhile noting that the generic geo-multiphysics model proposed in this thesis has general applicability in various geo-energy development areas. Not only can it be tailored to the cases of biogenic methane extraction and underground hydrogen storage, but also can be tailored to many other cases such as microbially enhanced oil recovery, CO_2 biomethanation, and etc.

5.2 Recommendations for future work

In this thesis, comprehensive study of microbial impacts on gas energy extraction/storage in subsurface formations has been conducted, but further investigations are important and research efforts are still needed from both the theoretical and experimental aspects:

- Although it has been reported in the literatures that microbial growth can be influenced by temperature. However, in this research, all simulations are carried out under the assumptions of isothermal conditions. Thus, the effect of temperature field on microbial activities and gas energy extraction/storage can be studied in the future.
- Underground formations are usually heterogeneous in terms of porosity and permeability. This indicates that pore size in rock changes in a wide range, which can influence microbial transport and distribution and thereby influence gas energy extraction/storage. Thus, the effect of formation heterogeneity on microbial activities and gas energy extraction/storage is an interesting topic to be studied in the future.

- Under the impact of biochemical reactions, rock mechanical properties may change which can further influence rock porosity/permeability and gas energy extraction/storage performance. Thus, dynamic rock mechanical properties may be considered in the future work.

- The numerical studies in this work are based on simple model geometries and boundary conditions which may not represent typical in-situ cases. In the future, more complex well patterns can be used and the 2D numerical model can be extended to 3D numerical model to more realistically study these problems.

- More batch reactor and core flooding experiments should be designed to investigate the impacts of microbial activities on gas energy extraction/storage. During these experiments, the biochemical reactions rates, microbial growth/decay rates, gas generation/consumption rates and many other parameters can be measured as the magnitude of these parameters can aid numerical modelling in the future.

Appendixes

Appendix A

The Peng-Robin equation is used to model hydrogen density (Peng and Robinson, 1976; Jia et al., 2023):

$$p_g = \frac{RT}{V_{mg} - b} - \frac{a}{V_{mg}^2 + 2bV_{mg} - b^2} \tag{6-A1}$$

where T is temperature, V_{mg} is the molar volume of hydrogen, R is the universal gas constant, and a and b are the equation of state parameters. For pure components, a and b are expressed as a function of the critical pressure and temperature:

$$a = 0.45724 \frac{(RT_c)^2}{p_c} \cdot \left| 1 + \kappa \left(1 - \sqrt{\frac{T}{T_c}} \right) \right| \tag{6-A2}$$

$$b = 0.0778 \frac{RT_c}{p_c} \tag{6-A3}$$

$$\kappa = 0.37464 + 1.54226\omega - 0.26992\omega^2 \tag{6-A4}$$

where p_c is critical pressure, T_c is critical temperature, and κ is the acentric factor which can be determined by fitting the equation of state with the experimental hydrogen density data.

Appendix B

The Jossi, Stiel and Thodos equation is used to model hydrogen viscosity (Jia et al., 2023):

$$\left| (\mu_g - \mu^*) \frac{T_c^{\overline{6}}}{M^{\frac{1}{2}} \, \_^{\frac{2}{3}}} + 10^{-4} \right| = a_0 + a_1\rho_r + a_2\rho_r^2 + a_3\rho_r^3 + a_4\rho_r^4 \tag{6-B1}$$

where μ_g is the viscosity of hydrogen, $\rho_r = \rho_g V_c$ is the reduced density, V_c is the critical volume of hydrogen, a_0, a_1, a_2, a_3 and a_4 are the fitting parameters, and μ^* is the low pressure viscosity for pure hydrogen (Stiel and Thodos, 1961):

$$\mu^* \frac{T}{M_{H_2} p_c} = \left(4.610 \frac{T^{0.618}}{T_c} - 2.04 e^{-0.449 \frac{T}{T_c}} + 1.94 e^{-4.058 \frac{T}{T_c}} + 0.1 \right) \times 10^{-4} \quad \text{(6-B2)}$$

Appendix C

The solubility of hydrogen in brine can be calculated by the following equation (Chabab et al., 2020):

$$\ln \left(\frac{x_{H_2}}{x_{H_2}^0} \right) = b_1 m_{NaCl}^2 + b_2 m_{NaCl} \quad \text{(6-C1)}$$

where b_1 and b_2 are the fitting coefficients, m_{NaCl} is the salt concentration of brine, x_{H_2} is the hydrogen solubility in brine, and $x_{H_2}^0$ is the hydrogen solubility in pure water which is defined as a function of temperature and pressure:

$$x_{H_2}^0 = c_1 pT + \frac{c_2 p}{T} + c_3 p + c_4 p^2 \quad \text{(6-C2)}$$

where c_1, c_2, c_3 and c_4 are the fitting coefficients. Here, it should be noted that the Eq. (6-C1) for hydrogen solubility in brine can be reduced to the Eq. (6-C2) for hydrogen solubility in pure water when salt concentration is equal to zero.

Using Eqs. (6-C1) and (6-C2), hydrogen solubility data under different pressure conditions can be calculated. Then, the corrected Henry's constant in Eq. (4-10) can be obtained through fitting the Henry's law with the calculated data.

References

Aftab, A., et al., 2022. Toward a fundamental understanding of geological hydrogen storage. Industrial & Engineering Chemistry Research, 61(9): 3233-3253.

Allen III, M.B., 2021. The mathematics of fluid flow through porous media. John Wiley & Sons.

Amigáň, P., et al., 1990. Methanogenic bacteria as a key factor involved in changes of town gas stored in an underground reservoir. FEMS Microbiology Ecology, 6(3): 221-224.

Amirthan, T., and Perera, M.S.A., 2023. Underground hydrogen storage in Australia: a review on the feasibility of geological sites. International Journal of Hydrogen Energy, 48(11): 4300-4328.

Berryman, J.G., 2002. Extension of poroelastic analysis to double-porosity materials: New technique in microgeomechanics. Journal of Engineering Mechanics, 128(8): 840-847.

Brooks, R.H., and Corey, A.T., 1966. Properties of porous media affecting fluid flow. Journal of the Irrigation and Drainage Division, 92(2).

Caglayan, D.G., et al., 2020. Technical potential of salt caverns for hydrogen storage in Europe. International Journal of Hydrogen Energy, 45(11): 6793-6805.

Cao, P., et al., 2016. A fully coupled multiscale shale deformation-gas transport model for the evaluation of shale gas extraction. Fuel, 178: 103-117.

Cao, P., et al., 2017. A multiscale-multiphase simulation model for the evaluation of shale gas recovery coupled the effect of water flowback. Fuel, 199: 191-205.

Chabab, S., et al., 2020. Measurements and predictive models of high-pressure H_2 solubility in brine (H_2O+NaCl) for underground hydrogen storage application. International Journal of Hydrogen Energy, 45(56): 32206-32220.

Chakraborty, S., et al., 2020. Numerical modeling on the influence of effective porosity, microbial kinetics, and operational parameters on enhanced oil recovery by microbial flooding within a sandstone formation. SPE Journal, 25(06): 2932-2961.

Chen, D., et al., 2016. A unified permeability and effective stress relationship for porous and fractured reservoir rocks. Journal of Natural Gas Science and Engineering, 29: 401-412.

Chen, Z., et al., 2013. Impact of various parameters on the production of coalbed methane. SPE Journal, 18(05): 910-923.

Chong, P., et al., 2019. Effect of pore size on the current produced by 3-dimensional porous microbial anodes: A critical review. Bioresource technology, 289: 121641.

Chowdhury, M.S., et al., 2021. Current trends and prospects of tidal energy technology. Environment, Development and Sustainability, 23: 8179-8194.

Cokar, M., et al., 2013. Reactive reservoir simulation of biogenic shallow shale gas systems enabled by experimentally determined methane generation rates. Energy & Fuels, 27(5): 2413-2421.

Cui, G., et al., 2020. Multidomain two-phase flow model to study the impacts of hydraulic fracturing on shale gas production. Energy & Fuels, 34(4): 4273-4288.

Cui, X., and Bustin, R.M., 2005. Volumetric strain associated with methane desorption and its impact on coalbed gas production from deep coal seams. AAPG Bulletin, 89(9): 1181-1202.

Das, L.M., et al., 2000. A comparative evaluation of the performance characteristics of a spark ignition engine using hydrogen and compressed natural gas as alternative fuels. International Journal of Hydrogen Energy, 25(8): 783-793.

Davis, K.J., et al., 2019. Biogenic coal-to-methane conversion can be enhanced with small additions of algal amendment in field-relevant upflow column reactors. Fuel, 256: 115905.

Davis, K.J., and Gerlach, R., 2018. Transition of biogenic coal-to-methane conversion from the laboratory to the field: A review of important parameters and studies. International Journal of Coal Geology, 185: 33-43.

de Boer, J.H., 1958. The structure and properties of porous materials. In: Proceedings of the 10th Colston Symposium; Everett, D. H., Stone, F.S., Eds.; Butterworths: London, U.K.

Dopffel, N., et al., 2021. Microbial side effects of underground hydrogen storage–Knowledge gaps, risks and opportunities for successful implementation. International Journal of Hydrogen Energy, 46(12): 8594-8606.

Ebigbo, A., et al., 2013. A coupled, pore-scale model for methanogenic microbial activity in underground hydrogen storage. Advances in Water Resources, 61: 74-85.

Eddaoui, N., et al., 2021. Impact of pore clogging by bacteria on underground hydrogen storage. Transport in Porous Media, 139: 89-108.

Fallgren, P.H., et al., 2013. Comparison of coal rank for enhanced biogenic natural gas production. International Journal of Coal Geology, 115: 92-96.

Fernandez, D.M., et al., 2024. A holistic review on wellbore integrity challenges associated with underground hydrogen storage. International Journal of Hydrogen Energy, 57: 240-262.

Fetter, C.W., 2018. Applied Hydrogeology. Waveland Press.

Fuertez, J., et al., 2017. Optimization of biogenic methane production from coal. International Journal of Coal Geology, 183: 14-24.

Gabrielli, P., et al., 2020. Seasonal energy storage for zero-emissions multi-energy systems via underground hydrogen storage. Renewable and Sustainable Energy Reviews, 121: 109629.

Gao, Q., et al., 2021. Effect of shale matrix heterogeneity on gas transport during production: A microscopic investigation. Journal of Petroleum Science and Engineering, 201: 108526.

Gao, Q., et al., 2022. A critical review of coal permeability models. Fuel, 326: 125124.

Gao, Q., et al., 2023. A multiphysics model for biogenic gas extraction from coal seams. Geoenergy Science and Engineering, 228: 212045.

Ginn, T.R., et al., 2002. Processes in microbial transport in the natural subsurface. Advances in Water Resources, 25(8-12): 1017-1042.

Green, M.S., et al., 2008. Characterization of a methanogenic consortium enriched from a coalbed methane well in the Powder River Basin, U.S.A. International Journal of Coal Geology, 76: 34-45.

Guo, H.G., et al., 2021. Feasibility study of enhanced biogenic coalbed methane production by super-critical CO_2 extraction. Energy, 214: 118935.

Gupta, P., and Gupta, A., 2014. Biogas production from coal via anaerobic fermentation. Fuel, 118: 238-242.

Hagemann, B., et al., 2016. Hydrogenization of underground storage of natural gas: Impact of hydrogen on the hydrodynamic and bio-chemical behavior. Computational Geosciences, 20: 595-606.

Hagemann, B., 2018. Numerical and analytical modeling of gas mixing and bio-reactive transport during underground hydrogen storage (Vol. 50). Cuvillier Verlag.

Halim, A., et al., 2014. Experimental study of bacterial penetration into chalk rock: mechanisms and effect on permeability. Transport in porous media, 101: 1-15.

Harris, S.H., et al., 2008. Microbial and chemical factors influencing methane production in laboratory incubations of low-rank subsurface coals. International Journal of Coal Geology, 76: 46-51.

Heidaryan, E., and Aryana, S.A., 2024. Empirical correlations for density, viscosity, and thermal conductivity of pure gaseous hydrogen. Advances in Geo-Energy Research, 11(1): 54-73.

Heinemann, N., et al., 2021. Enabling large-scale hydrogen storage in porous media–the scientific challenges. Energy & Environmental Science, 14(2): 853-864.

Hematpur, H., et al., 2023. Review of underground hydrogen storage: Concepts and challenges. Advances in Geo-Energy Research, 7(2): 111-131.

Hendry, M.J., et al., 1997. The role of sorption in the transport of Klebsiella oxytoca through saturated silica sand. Ground Water, 35(4): 574-584.

Herbert, G.M.J., et al., 2007. A review of wind energy technologies. Renewable and sustainable energy Reviews, 11(6): 1117-1145.

Hoehler, T.M., and Jørgensen, B.B., 2013. Microbial life under extreme energy limitation. Nature Reviews Microbiology, 11(2): 83-94.

Huang, Z.X., et al., 2013. Stimulation of biogenic methane generation in coal samples following chemical treatment with potassium permanganate. Fuel, 111: 813-819.

IPCC Climate Change, 2014. Mitigation of climate change. Contribution of working group III to the fifth assessment report of the intergovernmental panel on climate change, 1454: 147.

Jagger, J., 1983. Physiological effects of near-ultraviolet radiation on bacteria. Photochemical and Photobiological Reviews: Volume 7, 1-75.

Javadpour, F., 2009. Nanopores and apparent permeability of gas flow in mudrocks (shales and siltstone). Journal of Canadian Petroleum Technology, 48(08): 16-21.

Jeong, M.S., et al., 2019. Critical review on the numerical modeling of in-situ microbial

enhanced oil recovery processes. Biochemical Engineering Journal, 150: 107294.

Jia, C., et al., 2023. Numerical studies of hydrogen buoyant flow in storage aquifers. Fuel, 349: 128755.

Kannan, N., and Vakeesan, D., 2016. Solar energy for future world:-A review. Renewable and Sustainable Energy Reviews, 62: 1092-1105.

Kazemi, H., 1969. Pressure transient analysis of naturally fractured reservoirs with uniform fracture distribution. SPE Journal, 9(04): 451-462.

Khajooie, S., et al., 2024. Methanogenic conversion of hydrogen to methane in reservoir rocks: an experimental study of microbial activity in water-filled pore space. International Journal of Hydrogen Energy, 50: 272-290.

Kim, S.B., 2006. Numerical analysis of bacterial transport in saturated porous media. Hydrological Processes: An International Journal, 20(5): 1177-1186.

King, G.R., et al., 1986. Numerical simulation of the transient behavior of coal-seam degasification wells. SPE Formation Evaluation, 1(02): 165-183.

Kumari, W.G.P., and Ranjith, P.G., 2023. An overview of underground hydrogen storage with prospects and challenges for the Australian context. Geoenergy Science and Engineering, 231: 212354.

Le, T.D., et al., 2020. Multiscale model for flow and transport in CO2-enhanced coalbed methane recovery incorporating gas mixture adsorption effects. Advances in Water Resources, 144: 103706.

Li, J., et al., 2011. Interactions of microbial-enhanced oil recovery processes. Transport in porous media, 87: 77-104.

Li, W., et al., 2022. A fully coupled multidomain and multiphysics model considering stimulation patterns and thermal effects for evaluation of coalbed methane (CBM) extraction. Journal of Petroleum Science and Engineering, 214: 110506.

Lim, K.T., and Aziz, K., 1995. Matrix-fracture transfer shape factors for dual-porosity simulators. Journal of Petroleum Science and Engineering, 13: 169-178.

Liu, H.H., and Rutqvist, J., 2010. A new coal-permeability model: internal swelling stress and fracture–matrix interaction. Transport in Porous Media, 82: 157-171.

Liu, J., et al., 2011. Interactions of multiple processes during CBM extraction: a critical review. International Journal of Coal Geology, 87(3-4): 175-189.

Liu, N., et al., 2023. Pore-scale study of microbial hydrogen consumption and wettability alteration during underground hydrogen storage. Frontiers in Energy Research, 11: 1124621.

Lupton, N., et al., 2020. Enhancing biogenic methane generation in coalbed methane reservoirs–Core flooding experiments on coals at in-situ conditions. International Journal of Coal Geology, 219: 103377.

MacQuarrie, K.T., and Mayer, K.U., 2005. Reactive transport modeling in fractured rock: A state-of-the-science review. Earth-Science Reviews, 72(3-4): 189-227.

Mahdi, D.S., et al., 2021. Hydrogen underground storage efficiency in a heterogeneous sandstone reservoir. Advances in Geo-Energy Research, 5(4): 437-443.

Maier, R.M., et al., 2009. Environmental microbiology (Vol. 397). Academic press.

Malik, A.Y., et al., 2020. Coal biomethanation potential of various ranks from Pakistan: A possible alternative energy source. Journal of Cleaner Production, 255: 120177.

Margaux, M., et al., 2016. Design of a small-scale high-pressure reactor system to study microbial bioconversion of coal to methane. In: Presented at the GSA Annual Meeting in Denver, Colorado, USA.

Masum, S.A., and Thomas, H.R., 2018. Modelling coupled microbial processes in the subsurface: model development, verification, evaluation and application. Advances in water resources, 116: 1-17.

Mehrabian, A., and Abousleiman, Y.N., 2015. Gassmann equations and the constitutive relations for multiple-porosity and multiple-permeability poroelasticity with applications to oil and gas shale. International Journal for Numerical and Analytical Methods in Geomechanics, 39(14): 1547-1569.

Moestedt, J., et al., 2016. Effects of trace element addition on process stability during anaerobic co-digestion of OFMSW and slaughterhouse waste. Waste Management, 47: 11-20.

Okoroafor, E.R., et al., 2022. Toward underground hydrogen storage in porous media: Reservoir engineering insights. International Journal of Hydrogen Energy, 47(79): 33781-33802.

Pandey, R., and Harpalani, S., 2019. Evaluation of dynamic flow and production behavior of biogenic methane reservoirs. In: Presented at the 53rd US Rock Mechanics/Geomechanics Symposium held in New York, NY, USA.

Papendick, S.L., et al., 2011. Biogenic methane potential for Surat Basin, Queensland coal seams. International Journal of Coal Geology, 88: 123-134.

Paris Agreement, 2015. In report of the conference of the parties to the United Nations framework convention on climate change (21st session, 2015: Paris).

Park, S.Y., & Liang, Y., 2016. Biogenic methane production from coal: A review on recent research and development on microbially enhanced coalbed methane (MECBM). Fuel, 166: 258-267.

Parker, N., et al., 2016. Microbiology. ISBN-13: 978-0-9986257-0-6.

Payler, S.J., et al., 2019. An ionic limit to life in the deep subsurface. Frontiers in microbiology, 10: 435620.

Pedersen, K., 2000. Exploration of deep intraterrestrial microbial life: Current perspectives. FEMS Microbiology Letters, 185(1): 9-16.

Pedrós-Alió, C., and Manrubia, S., 2016. The vast unknown microbial biosphere. Proceedings of the National Academy of Sciences, 113(24): 6585-6587.

Peng, D.Y., and Robinson, D.B., 1976. A new two-constant equation of state. Industrial & Engineering Chemistry Fundamentals, 15(1): 59-64.

Peng, Y., et al., 2014. Why coal permeability changes under free swellings: New insights. International Journal of Coal Geology, 133: 35-46.

Pérez, A., et al., 2016. Patagonia wind-hydrogen project: Underground storage and methanation. In: 21st world hydrogen energy conference.

Pichler, M., 2019. Underground sun storage results and outlook. In: EAGE/DGMK joint workshop on underground storage of hydrogen. European Association of Geoscientists & Engineers, 2019(1): 1-4.

Ponnudurai, V., et al., 2022a. Investigation on future perspectives of ex-situ biogenic methane generation from solid waste coal and coal washery rejects. Fuel, 318: 123497.

Ponnudurai, V., et al., 2022b. Investigation on the utilization of coal washery rejects by different microbial sources for biogenic methane production. Chemosphere, 287: 132165.

Raad, S.M.J., et al., 2022. Hydrogen storage in saline aquifers: Opportunities and challenges. Renewable and Sustainable Energy Reviews, 168: 112846.

Ratkowsky, D.A., et al., 1983. Model for bacterial culture growth rate throughout the entire biokinetic temperature range. Journal of Bacteriology, 154(3): 1222-1226.

Rice, D.D., and Claypool, G.E., 1981. Generation, accumulation, and resource potential of biogenic gas. AAPG Bulletin, 65(1): 5-25.

Ritter, D., et al., 2015. Enhanced microbial coalbed methane generation: a review of research, commercial activity, and remaining challenges. International Journal of Coal Geology, 146: 28-41.

Rittmann, B.E., 1993. The significance of biofilms in porous media. Water Resources Research, 29(7): 2195-2202.

Rittmann, B.E., and McCarty, P.L., 2001. Environmental biotechnology: Principles and Applications.

Robbins, S.J., et al., 2016. The effect of coal rank on biogenic methane potential and microbial composition. International Journal of Coal Geology, 154-155: 205-212.

Rockhold, M.L., et al., 2004. Coupled microbial and transport processes in soils. Vadose Zone Journal, 3(2): 368-383.

Sainz-Garcia, A., et al., 2017. Assessment of feasible strategies for seasonal underground hydrogen storage in a saline aquifer. International Journal of Hydrogen Energy, 42(26): 16657-16666.

Saurabh, S., and Harpalani, S., 2018. Modeling of microbial methane generation from coal and assessment of its impact on flow behavior. Fuel, 216: 274-283.

Scott, A.R., 1999. Improving coal gas recovery with microbially enhanced coalbed methane. In: Mastalerz, M., Glikson, M., Golding, S.D. (eds) Coalbed Methane: Scientific, Environmental and Economic Evaluation. Springer, Dordrecht.

Senthamaraikkannan, G., et al., 2016a. Kinetic Modeling of the Biogenic Production of Coalbed Methane. Energy & Fuels, 30: 871-883.

Senthamaraikkannan, G., et al., 2016b. Development of a multiscale microbial kinetics coupled gas transport model for the simulation of biogenic coalbed methane production. Fuel, 167: 188-198.

Senthamaraikkannan, G., et al., 2016c. Multiphase reactive-transport simulations for estimation and robust optimization of the field scale production of microbially enhanced coalbed methane. Chemical Engineering Science, 149: 63-77.

Sharma, A., et al., 2018. Modeling framework for biogenic methane formation from coal. Energy & Fuels, 32(8): 8453-8461.

Shojaee, A., et al., 2024. Interplay between microbial activity and geochemical reactions during underground hydrogen storage in a seawater-rich formation. International Journal of Hydrogen Energy, 50: 1529-1541.

Sivasankar, P., and Kumar, G.S., 2014. Numerical modelling of enhanced oil recovery by microbial flooding under non-isothermal conditions. Journal of Petroleum Science and Engineering, 124: 161-172.

Sivasankar, P., and Kumar, G.S., 2019. Influence of bio-clogging induced formation damage on performance of microbial enhanced oil recovery processes. Fuel, 236: 100-109.

Steefel, C.I., et al., 2005. Reactive transport modeling: An essential tool and a new research approach for the Earth sciences. Earth and Planetary Science Letters, 240(3-4): 539-558.

Stephen, A., et al., 2014. Bioconversion of coal: new insights from a core flooding study. RSC Advances, 4: 22779-22791.

Stiel, L.I., and Thodos, G., 1961. The viscosity of nonpolar gases at normal pressures. AIChE Journal, 7(4): 611-615.

Stocker, T., et al., 2014. IPCC climate change 2013: the physical science basis-findings and lessons learned. In: EGU general assembly conference abstracts.

Strapoc, D., et al., 2011. Biogeochemistry of microbial coal-bed methane. Annual Review of Earth and Planetary Sciences, 39: 617-656.

Strobel, G., et al., 2023. Coupled model for microbial growth and phase mass transfer in pressurized batch reactors in the context of underground hydrogen storage. Frontiers in Microbiology, 14: 1150102.

Szymkiewicz, A., 2012. Modelling water flow in unsaturated porous media: accounting for nonlinear permeability and material heterogeneity. Springer Science & Business Media.

Tamamura, S., et al., 2016. Reaction of lignite with dilute hydrogen peroxide to produce substrates for methanogens at in situ subsurface temperatures. International Journal of Coal Geology, 167: 230-237.

Tan, Y., et al., 2019. Laboratory characterisation of fracture compressibility for coal and shale gas reservoir rocks: A review. International Journal of Coal Geology, 204: 1-17.

Tarafa, M., et al., 1987. Sediment slumps in the middle and lower eocene of deep sea drilling project holes 605 and 613: Chemical detection by pyrolysis techniques.

Taylor, S.W., and Jaffé, P.R., 1990. Substrate and biomass transport in a porous medium. Water Resources Research, 26(9): 2181-2194.

Taylor, S.W., et al., 1990. Biofilm growth and the related changes in the physical properties of a porous medium: 2. Permeability. Water Resources Research, 26(9): 2161-2169.

Thaysen, E.M., et al., 2021. Estimating microbial growth and hydrogen consumption in hydrogen storage in porous media. Renewable and Sustainable Energy Reviews, 151: 111481.

Tian, J., et al., 2022. Linking fractal theory to a fully coupled coal deformation and two-phase flow multiphysics: The role of fractal dimensions. Energy & Fuels, 36(20): 12591-12605.

Tufenkji, N., 2007. Modeling microbial transport in porous media: Traditional approaches and recent developments. Advances in water resources, 30(6-7): 1455-1469.

Vandevivere, P., and Baveye, P., 1992. Saturated hydraulic conductivity reduction caused by aerobic bacteria in sand columns. Soil Science Society of America Journal, 56(1): 1-13.

Varjani, S.J., and Gnansounou, E., 2017. Microbial dynamics in petroleum oilfields and their relationship with physiological properties of petroleum oil reservoirs. Bioresource technology, 245: 1258-1265.

Wallace, R.L., et al., 2021. Utility-scale subsurface hydrogen storage: UK perspectives and technology. International Journal of Hydrogen Energy, 46(49): 25137-25159.

Wang, G., et al., 2024. Bioreaction coupled flow simulations: Impacts of methanogenesis on seasonal underground hydrogen storage. International Journal of Hydrogen Energy, 55: 921-931.

Wang, S., and Jaffe, P.R., 2004. Dissolution of a mineral phase in potable aquifers due to CO2 releases from deep formations; effect of dissolution kinetics. Energy conversion and management, 45(18-19): 2833-2848.

Ward, J.P., et al., 2001. Mathematical modelling of quorum sensing in bacteria.

Mathematical Medicine and Biology, 18(3): 263-292.

Warren, J.E., and Root, P.J., 1963. The behavior of naturally fractured reservoirs. SPE Journal, 3(03): 245-255.

Whelan, J.K., et al., 1986. Maturity of organic matter and migration of hydrocarbons in two Alaskan North Slope wells. Organic geochemistry, 10(1-3): 207-219.

Yang, Y., and Liu, S., 2020. Review of shale gas sorption and its models. Energy & Fuels, 34(12): 15502-15524.

Yu, W., et al., 2015. Numerical study of the effect of uneven proppant distribution between multiple fractures on shale gas well performance. Fuel, 142: 189-198.

Zeng, L., et al., 2023. Role of geochemical reactions on caprock integrity during underground hydrogen storage. Journal of Energy Storage, 65: 107414.

Zhang, H., et al., 2008. How sorption-induced matrix deformation affects gas flow in coal seams: a new FE model. International Journal of Rock Mechanics and Mining Sciences, 45(8): 1226-1236.

Zhang, J., et al., 2016a. Optimization of methane production from bituminous coal through biogasification. Applied Energy, 183: 31-42.

Zhang, J., et al., 2016b. Finding cost-effective nutrient solutions and evaluating environmental conditions for biogasifying bituminous coal to methane ex situ. Applied Energy, 165: 559-568.

Zhao, Q., et al., 2024. Numerical simulation of the impact of different cushion gases on underground hydrogen storage in aquifers based on an experimentally-benchmarked equation-of-state. International Journal of Hydrogen Energy, 50: 495-511.

Zhi, S., et al., 2018. Hydraulic fracturing for improved nutrient delivery in microbially-enhanced coalbed-methane (MECBM) production. Journal of Natural Gas Science and Engineering, 60: 294-311.

Zhu, Y., et al., 2020. Quantifying the impact of capillary trapping on coal seam gas recovery. Journal of Natural Gas Science and Engineering, 83: 103588.

Zysset, A., et al., 1994. Modeling of reactive groundwater transport governed by biodegradation. Water Resources Research, 30(8): 2423-2434.